SYNTHESIS AND CHARACTERIZATION OF ALKALINE EARTH OXIDE ADDED BOROSILICATE GLASSES FOR HIGH TEMPERATURE SEALANT APPLICATION

Thesis

Submitted in partial fulfilment of the requirements for the degree

of

DOCTOR OF PHILOSOPHY

by

SOUMALYA BHATTACHARYA

DEPARTMENT OF PHYSICS

NATIONAL INSTITUTE OF TECHNOLOGY KARNATAKA

SURATHKAL, MANGALORE – 575025

05th June 2020

D E C L A R A T I O N

by the Ph.D. Research Scholar

I hereby *declare* that the Research Thesis/Synopsis entitled **"SYNTHESIS AND CHARACTERIZATION OF ALKALINE EARTH OXIDE ADDED BOROSILICATE GLASSES FOR HIGH TEMPERATURE SEALANT APPLICATION",** which is being submitted to the National Institute of Technology Karnataka, Surathkal in partial fulfilment of the requirements for the award of the Degree of Doctor of Philosophy in **PHYSICS** is a *bonafide report of the research work carried out by me*. The material contained in this Research Thesis/Synopsis has not been submitted to any University or Institution for the award of any degree.

Soumalya Bhattacharya
(Register No.: 123007PH12F05)
Department of Physics
National Institute of Technology Karnataka, Surathkal.

Place: NITK – Surathkal
Date: 05-06-2020

C E R T I F I C A T E

This is to certify that the Research Thesis entitled **"SYNTHESIS AND CHARACTERIZATION OF ALKALINE EARTH OXIDE ADDED BOROSILICATE GLASSES FOR HIGH TEMPERATURE SEALANT APPLICATION",** submitted by **SOUMALYA BHATTACHARYA** (Register Number: *123007PH12F05*) as the record of the research work carried out by him, is *accepted* as the *Research Thesis submission* in partial fulfilment of the requirements for the award of degree of Doctor of Philosophy.

Dr. H. D. Shashikala

Research Supervisor (Professor)

Department of Physics

NITK Surathkal – 575025

Chairman - DRPC

(Signature with Date and Seal)

Dedicated to my beloved grandparents

Late Dhirendra Chandra Bhattacharjee & Late Sudharani Bhattacharjee

and

Late Chitta Ranjan Bhattacharjee & Smt. Basana Bhattacharjee

ACKNOLEDGEMENT

ABSTRACT

BaO-CaO-Al$_2$O$_3$-SiO$_2$ (BCAS) glass and their derivatives have gained extreme importance for their high endurance to elevated temperatures and being suitable for various high temperature applications. Two glass systems, BaO-CaO-B$_2$O$_3$-SiO$_2$-Al$_2$O$_3$ (BCBSA) and another without Al$_2$O$_3$ (BCBS) were synthesized using melt quenching technique in the present work. Addition of ZnO and MgO as flux helped in melting them at 1300 $^{\circ}$C which is much lower than the usual melting temperature of these glasses. Density of the quenched glasses was measured by Archimedes method and structural bond vibrations were confirmed through FTIR. UV Visible spectroscopy was used to determine band gap energy and confirm the insulating nature of the synthesized glasses. Annealed glass powders were isothermally heated at 700 $^{\circ}$C, 800 $^{\circ}$C for 50 hours and at 900 $^{\circ}$C for 50 and 100 hours duration in air to observe their devitrification behaviour, which were then analysed by X-ray diffraction to identify the developed phases. The growth of detrimental monocelsian phase could be avoided by removing Al$_2$O$_3$ from the composition. The BCBS glasses with low BaO concentrations were found to be most promising for high temperature sealing. Reducing BaO concentrations improved the coefficient of thermal expansion (CTE) and other characteristic temperatures of glasses. Compacted glass pellets show maximum shrinkage at 700 $^{\circ}$C. Dilatometric analysis conducted on these glass compacts showing maximum shrinkage, exhibited CTE more than the bulk glasses. Glasses with low BaO concentrations exhibited excellent mechanical properties. The optimized glass composition 00B was screen printed and sandwiched between two Crofer22APU plates forming Crofer22APU – Glass – Crofer22APU (CGC) sandwiches and heat treated for repeated thermal cycles from RT to 800 $^{\circ}$C. Microscopic images of the CGC interface, XRD analysis of the internal surface of the broken sandwich and DC resistivity measurements of the glass under sandwiched conditions between two Crofer22APU plates, at RT and at elevated temperatures up to 800 $^{\circ}$C were carried out, to determine its compatibility with Crofer22APU at high temperatures. The CGC sandwiches showed good adherence and compatible structural and thermal properties after repeated thermal cycles. It also exhibited sufficiently high specific resistance at room and elevated temperatures.

CONTENTS

LIST OF FIGURES

LIST OF TABLES

CHAPTER 1

INTRODUCTION

1.1.Glass, an amorphous solid

Glass is any material, (inorganic, organic or metallic) formed by any technique, which exhibits glass transformation behaviour (J E Shelby 2005). Glasses are traditionally formed by cooling from a melt, fast enough to prevent crystallization. All glasses share two common characteristics. First, no glass has a long range, periodic atomic arrangement and secondly, every glass exhibits a time-dependent glass transformation behaviour (J E Shelby 2005).

The traditional view is that glass is a solid obtained by super cooling a liquid and that it has amorphous structure. Additionally a glass, when heated, should also exhibit a thermal characteristic known as the "glass transition" or "glass transformation" at a temperature, T_g. At T_g, second derivative thermodynamic properties, namely heat capacity, thermal expansion coefficient and compressibility undergo abrupt changes. Therefore all amorphous materials are not necessarily glasses. The glassy state is governed by the unique glass transition or transformation (Rao 2002).

When a glass forming melt is cooled to the glass transition temperature, an already metastable super cooled liquid transforms into a metastable solid. At this temperature the rate of volume shrinkage with decreasing temperature drops suddenly. Hence a bend is observed in the Volume – Temperature plot. The initiation of the bend is marked T_{g1} and the end as T_{g2}. The area between T_{g1} and T_{g2} is called glass transformation region. Heat capacity of glassy materials changes abruptly and increases at the glass transition region as compared to crystalline materials (Rao 2002).

1.2.Kinetic theory of glass formation

According to the earliest theory of glass formation, stated by Goldschmidt, only the melts containing cations arranged in a tetrahedral coordination, can form glasses on rapid cooling. This observation was purely empirical, with no explanation to why tetrahedral coordination is so important for glass formation (J E Shelby 2005). In later years, Zachariasen extended the ideas of Goldschmidt and explained why certain

coordination numbers help in glass formation (J E Shelby 2005). This new approach to glass formation is known as the *Kinetic Theory of Glass Formation*. This has become the basis for the most widely used models for glass structures. Zachariasen noted that the silicate crystals which readily form glasses instead of re-crystallizing after melting and cooling, have a network, which consist of tetrahedron connected at all four corners, just as in the corresponding crystals, but not in a periodic and symmetrical arrangement (J E Shelby 2005). These networks extend in all three dimensions such that the average behaviour in all directions is the same. This means that the properties of glasses are isotropic. Zachariasen concluded that the ability to form such networks thus provides the ultimate condition for glass formation (J E Shelby 2005). He referred to such a glass structure as a "vitreous network".
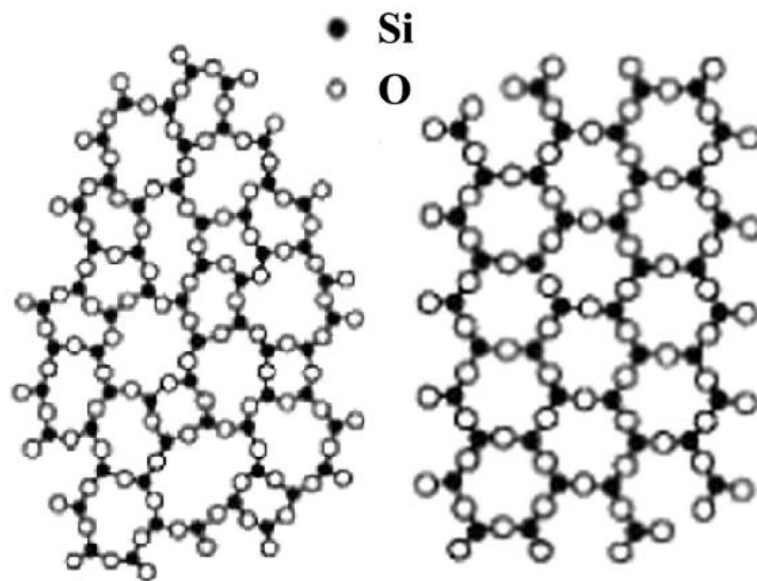
Figure 1.1: Random/vitreous and crystalline arrangements of silicate structure (Cao et al. 2014)

1.3. Glass components

In 1950 Stanworth quantified the mixed bond concept by using partial ionic character of Pauling model. He classified oxides into three groups on the basis of the electronegativity of the cation. Since the anion is oxygen in every case, this approach is effectively identical to grouping by fractional ionic character of the cation-anion bond. Cations which form bonds with oxygen with a fractional ionic character near 50% should act as *network formers* (group 1), and produce good glasses. Cations with

slightly lower electronegativities (group 2), which form slightly more ionic bonds with oxygen, cannot form glasses by themselves, but can partially replace cations from the first group. Since these ions behave in a manner which is intermediate between that of cations which do form glasses and those which never form glasses, they are known as *intermediates*. Finally, cations which have very low electronegativities (group 3), and therefore form highly ionic bonds with oxygen, never act as network formers. Since these ions only serve to modify the network structure created by the network forming oxides, they are termed as *glass network modifiers* (J E Shelby 2005).

1.4.Classification of glass

Silica is not a necessarily required component of glass. But up to 1900 AD mankind used only silica based glasses for all purposes (J E Shelby 2005). In recent years, many non-silicate glasses got recognition, and their various properties are being investigated by glass scientists. Polymers, metals, various non-oxide, inorganic and organic compositions have been made into glass in past few decades. In fact, it is now realized that virtually any material can be used to make glass (J E Shelby 2005). According to the compositions there are three major classifications of glasses, Chalcogenide glasses, Halide and Oxy-Halide glasses and Oxide glasses.

1.4.1. Chalcogenide glasses

Chalcogenide glasses have a tendency for their atoms to link together to form chain. These are obtained from the chalcogen elements viz. Sulphur, Selenium and Tellurium along with As, Sb, Sn, Ge, Si, Ga, In, etc. in an oxygen free atmosphere. In oxide and halide glasses ionic bond will be existing but in case of Chalcogenide glasses covalent bond exists. These glasses are attracting much importance due to its sensor applications and they exhibit phenomena like photoluminescence, photoconduction, photo darkening, memory switch etc.

1.4.2. Halide and Oxy-Halide glasses

The fluoroberyllate glasses and the flourozirconate glasses are the two main types of glasses that can be categorized under fluoride glasses. The fluoroberyllate glass shows the least distortion for a high intensity optical beam due to its very low nonlinear

refractive index. Its practical application is limited due to its high toxicity and hygroscopic nature, whereas fluorozirconate multicomponent glasses are neither toxic nor hygroscopic and these glasses are ionic in nature. This glass shows good transparency in the infrared region, because of which it is used in various optical applications.

Oxyhalide glasses are the glasses prepared from the batch mixture of oxides and halides. The fluorophosphate glasses which belong to this system show low dispersion and a low nonlinear refractive index, and are used as host materials for high-power laser systems. Other oxy-halide glasses like PbF_2-SnF_2-P_2O_5 show very low glass transition temperature and have fair chemical durability.

1.4.3. *Oxide glasses*

The oxide glasses can be further classified in to three subcategories borate glasses, phosphate glasses and silicate glasses.

a. Phosphate glasses

These glasses, prepared using P_2O_5 as network former, are important due to their special nature like low refractive index and high absorption cross section. Hence, they are used in optical applications. But the disadvantages arise due to their poor chemical durability, which limits their extensive practical applications. Figure 1.2 shows different phosphate tetrahedral units that can be expected in these glasses.
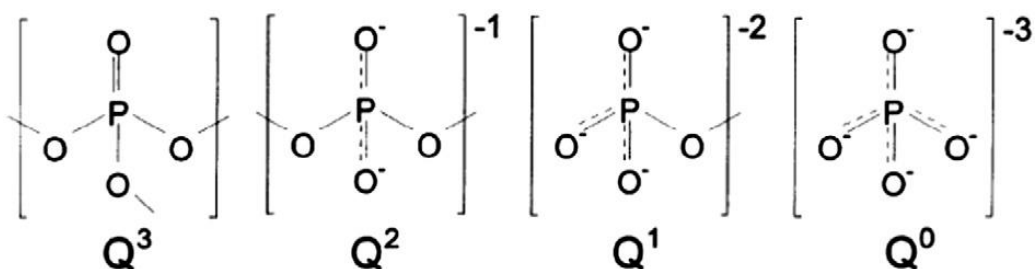
Figure 1.2: Structures of different possible phosphate tetrahedral units (Fu and Mauro 2013)

b. Borate glasses

Borate glasses consist of BO_3 triangles and BO_4 tetrahedron which are formed by combining with alkali, alkaline earth oxides, etc. They show high compatibility with rare-earth elements, which is the most important feature of borate glasses for application in optical and opto-electronic fields. Borate glasses have also been used widely as solder glasses for glass-to-glass and glass-to-ceramic bonding because of their low softening point. Figure 1.3 shows the structures of BO_3 triangles and BO_4 tetrahedra.
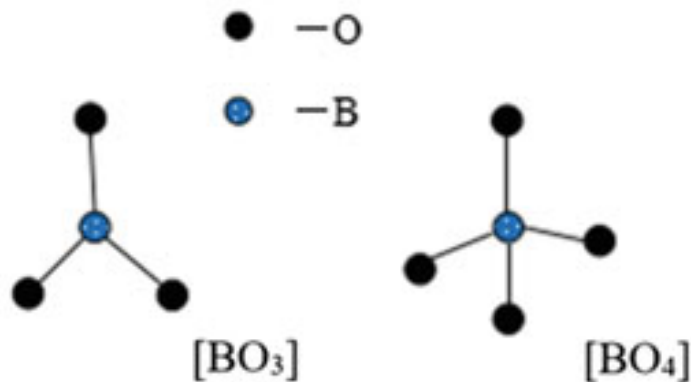
Figure 1.3: Structure of borate triangle and tetrahedron (Q. Xu and Xu 2018)

c. Silicate glasses

In oxide glass system silicate glasses are commercially very important and extensively studied. In silicate glasses SiO_2 is the glass former. These glasses are having plenty of applications in the field of semiconductor industry, photolithography and in opto-electronic devices due to their chemical and weathering stability. Figure 1.4 shows the silicate tetrahedron and how it accommodates added ions in the matrix. The present work will be on silicate glasses.
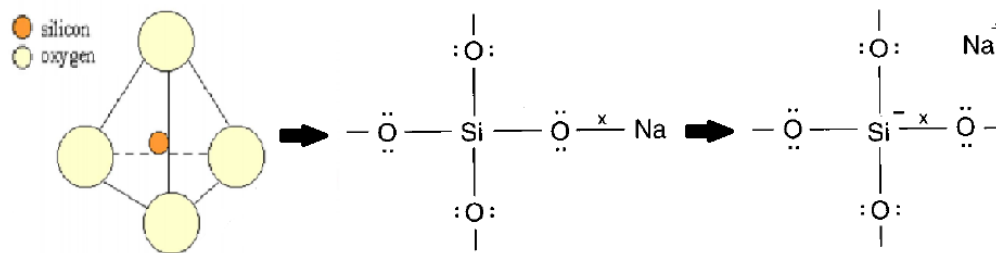
Figure 1.4: Silicate tetrahedral structure with added Na ions (Jain 1996)

1.4.4. Special glasses

One of the important properties of glasses is their unique ability to accommodate various types of dopants, such as rare earth ions, transition metal ions, metal nanoparticles, etc. A foreign atom can easily find a place to occupy inside the glass because of its random network structure. The flexibility of chemical composition of glass enables the doping of active elements for the development of special properties like colour, high nonlinear susceptibility, emission of fluorescent light, etc. Even two glass formers can be mixed to effectively produce a composition which may be useful for a particular application. Glass is one of the most promising and developing technical material whose properties can be tailored to meet and suit the present day requirements for various applications.

1.5. Introduction to solid oxide fuel cell (SOFC) and high temperature sealants

1.5.1. Solid Oxide Fuel Cell

Solid oxide fuel cells (SOFCs) are devices which convert chemical energy into electrical energy through chemical reactions with higher efficiency than conventional thermal energy conversion systems (Grema 2018). SOFCs have a self-reformation ability coupled with fuel flexibility (Ghosh, Sharma, et al. 2008; S. F. Wang et al. 2009), such as the use of hydrocarbon and municipal waste (Grema 2018) and are environment friendly (Grema 2018). They are therefore an option to help to achieve reduced CO_2 emitting applications (Grema 2018). There are two popular designs named according to the cell stacking arrangement, planar and tubular (Grema 2018). Planar SOFCs are preferred over tubular ones due to a simpler manufacturing process and higher current outputs as planar SOFCs have a shorter current path, though they require hermetic sealing (Grema 2018).

In case of Hydrogen fuel cell, at the anode H_2O splits through the reaction

$$2H_2O \longrightarrow 2H^{2+} + 2e^-$$
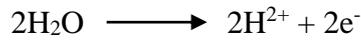
The H_2 ions pass through the membrane which does not allow the electrons to pass because it is electrically an insulator. Hence the electrons require an external circuit to reach the cathode. At the cathode they recombine to give

$$2H^{2+} + 2e^- + O^{2-} \longrightarrow 2H_2O$$

Fuel cells do not store any reactants inside themselves. Instead the reactants are stored outside in fuel tanks. Once the entire tank is used up, somebody needs to replace the tank i.e. refuelling. Thus according to theory the fuel cell has an infinite lifetime. The schematic diagram of a fuel cell is shown in figure 1.5.
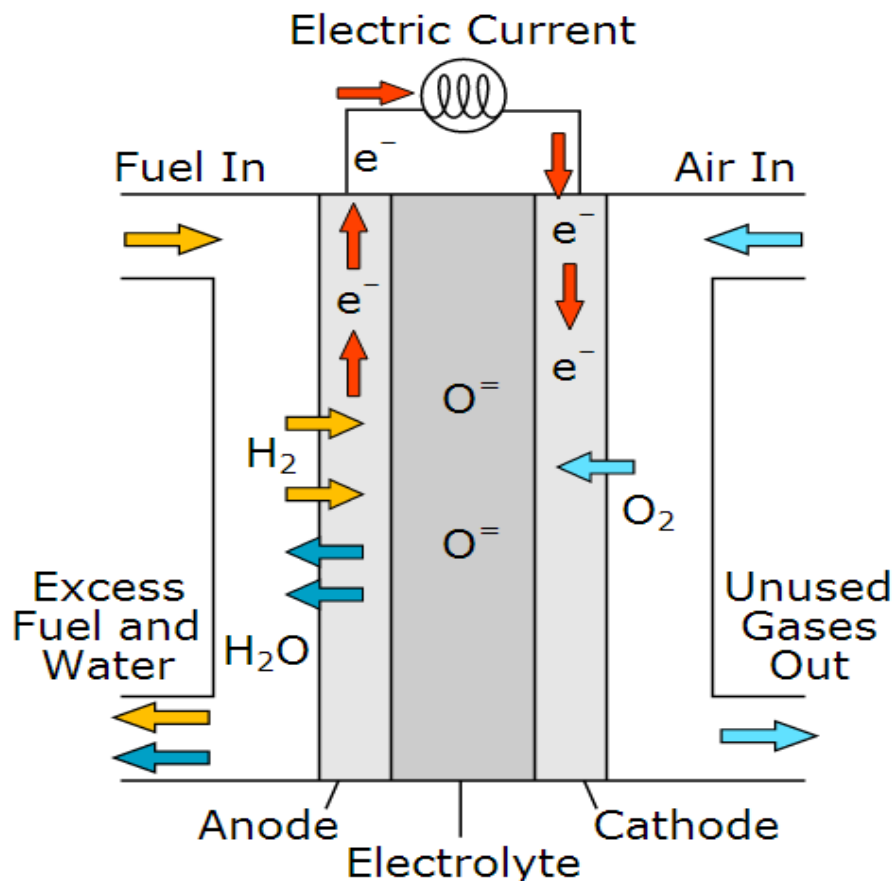
Figure 1.5: Schematic diagram of a Solid Oxide Fuel Cell

A fuel cell works at an elevated operating temperature near 800 °C to 1000 °C (Mukhopadhyay et al. 2009; Ghosh, Sharma, et al. 2008). It mainly consists of three essential components, anode, cathode and an electrolyte. The cathode is generally made of Lanthanum Strontium Manganite (Ghosh, Kundu, et al. 2008). The anode is commonly a composite of nickel and yttria stabilized zirconia (Ni-YSZ cermet) and the electrolyte is generally made of 8 mol% yttria stabilized zirconia (8-YSZ) (Ghosh, Kundu, et al. 2008). Conventionally several cells are stacked together to achieve higher power output. Stacking can be tubular or planer, among which most researchers prefer the anode supported planer design. This is mainly because it can be operated at an intermediate range of temperature between 700 °C to 800 °C. This allows the usage of metallic interconnects instead of ceramic components. Such a fuel cell is called Intermediate Temperature – SOFC (IT-SOFC) (Ghosh, Das Sharma, et al. 2008). One of the most important challenges for the development of intermediate temperature planar anode-supported solid oxide fuel cell (IT-SOFC) is the development of a proper sealant that separates the cathode and anode chambers and maintains the gas-tightness of the total system at elevated operating temperatures near 700 °C to 800 °C (Ghosh, Sharma, et al. 2008; Ghosh, Das Sharma, et al. 2008). The construction of an IT-SOFC is shown in figure 1.6. It clearly shows that seals are generally applied to the cell edges between ceramic electrolytes and metallic interconnects (Ghosh, Kundu, et al. 2008; Ghosh, Das Sharma, et al. 2008).

The operation and performance of a SOFC stack depends on having robust gas-tight seals that prevent the mixing of the fuel and oxidizer gas streams. The presence of leaks, due to flaws formed during stack manufacture or as a result of component degradation during stack operation, lead to reduced system performance, lower power generation efficiency and poor fuel utilization. They can also cause local hot spots or worse. It may also spread internal combustion in the stack, which accelerates degradation of the device. The most challenging limitation of an IT-SOFC is fabrication of this stack ensuring long term hermetic sealing (Meinhardt et al. 2008).
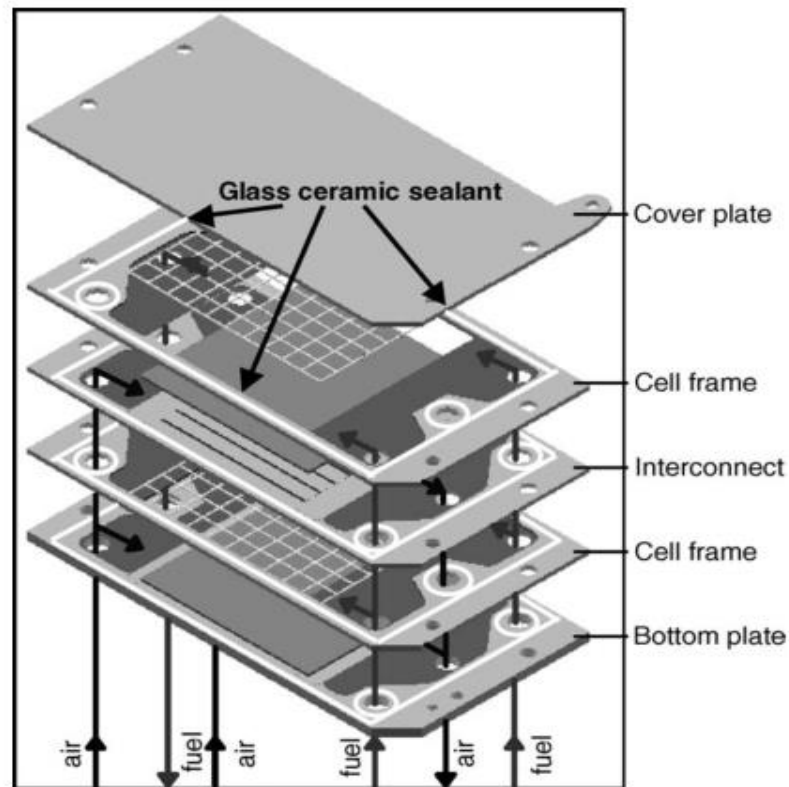
Figure 1.6: Construction of intermediate temperature planar anode-supported solid oxide fuel cell

1.5.2. *High temperature sealants*

Planar solid oxide fuel cells (SOFCs) provide higher power density but require high-temperature sealants. Both rigid and compressive seals are being developed for SOFCs. A major advantage of compressive seals is that the seals are not rigidly fixed to the other SOFC components, so an exact match of thermal expansion is not required. However, maintenance of a gas-tight seal without attaching the components requires the constant application of pressure during operation. Rigid seals, on the other hand, do not require this applied pressure, but have more stringent requirements for adherence, cracking and thermal expansion matching. The most common sealants for SOFCs are glass or glass–ceramic materials, which have been found by many people to operate in fuel cells for more than 1000 h with no significant degradation. A glass or glass-ceramic sealant is a viscous fluid at the cell operating temperature which can provide a mechanism for CTE-mismatch tolerance. The glass must have a glass-transition temperature below the cell operating temperature. Then, as the structure cools to room

temperature, significant stresses begin to develop only when the temperature drops below T_g. Consequently, the total stresses due to thermal expansion mismatch are considerably less than if the stresses would have begun to develop at the elevated operating temperatures.

Typical conditions under which these seals are expected to function efficiently at elevated temperatures are continuous exposure to oxidation reaction on cathode side and simultaneous exposure to redox reactions to the anode side for a long time under repeated thermal cycles of thousands of hours. The reason for using glasses and glass ceramics, of all other materials available, are some intrinsic features of glasses like (Meinhardt et al. 2008), they

      a) tend to display acceptable stability in the reducing and oxidizing atmospheres of the stack.

      b) are generally inexpensive.

      c) can be readily applied to the sealing surfaces as a powder dispersed in a paste or a tape cast sheet.

      d) typically exhibit good wetting behaviour on both sealing surfaces.

      e) are electrically insulating.

      f) can be engineered to exhibit a coefficient of thermal expansion (CTE) matching with other SOFC components.

These sealant glasses are generally screen printed on the metallic components of the cell (Ghosh, Das Sharma, et al. 2008). Screen printing, which prints the mixture of coating materials and binders onto the substrate through the screen, enables to achieve control over the surface morphology which is beneficial for its further development and application (Q. Xu and Xu 2018). Screen printing also enables accurate control of the dimensions and borders of the printed matter. Thus it enables one, to print the cell edges masking certain required areas.

1.6. Introduction to BCAS glasses

Many glass compositions were experimented upon by various researchers around the globe to decide an optimum composition to be used for high temperature sealing. In 2002 K. D. Meinhardt et. al. published a patent that claims that a $M_AO\text{-}M_BO_Y\text{-}SiO_2$ based glass system is a potential seal material for both tubular and planer solid oxide

fuel cell (SOFC), oxygen electrolyzers, commodity chemicals and other products, requiring high temperature sealing. This is because this system has matching thermal expansion coefficient of solid electrolytes used in these applications (Meinhardt K D Morin et al. 2002). BaO was used as M_AO and Al_2O_3 was used as M_BO_Y, hence forming a $BaO-Al_2O_3-SiO_2$ based system, which was later modified with CaO and B_2O_3 in 2008(Meinhardt et al. 2008; Meinhardt K D Morin et al. 2002). Thus $BaO-CaO-Al_2O_3-SiO_2$ glass system termed as BCAS glasses came in to existence and was extensively studied for the past decade as potential high temperature sealing materials.

CaO helps to reduce glass transition temperature (T_g) and softening temperature (T_d) and raise the coefficient of thermal expansion (CTE). B_2O_3 can be used to reduce T_g, T_d, CTE and viscosity and improve wetting (Meinhardt et al. 2008; S. F. Wang et al. 2017). BaO itself contributes in raising the CTE of the glass (Ghosh, Kundu, et al. 2008). Raising BaO content to more than 50 wt% does improve the transition temperatures and other characteristic temperatures but it also leads to development of a detrimental crystal phase called celsian ($BaAl_2Si_2O_8$) bearing a monoclinic form and a very low CTE of 2.2×10^{-6} K^{-1} (M. Kaur et al. 2017; X. Xu et al. 2018). Presence of BaO, also affects the metal-glass interface, once sealed together at high temperatures, barium from BaO and chromium from Crofer22APU electrode react in the presence of oxygen to form a $BaCrO_4$ phase bearing high CTE (~16-18 $\times 10^{-6}$ K^{-1}) (Mukhopadhyay et al. 2009). BaO was substituted by SrO by many researchers, but that leads to formation of $SrCrO_4$, which again has CTE in the range of $16 – 22 \times 10^{-6}$ K^{-1}, which is very high for sealing applications (S. F. Wang et al. 2017).

1.7. Thermal requirements of BCAS glasses as potential SOFC sealants

The CTE of the glass must match to that of the other cell components for high temperature functioning. The most commonly used electrolyte 8mol% Yttria stabilized Zirconia (8-YSZ) bears the CTE of $10 – 13 \times 10^{-6}$ K^{-1} (Meinhardt et al. 2008; Mukhopadhyay et al. 2009; Hao et al. 2012; Heydari et al. 2013; Wu et al. 2015; M. Kaur et al. 2017). The interconnect material is generally a Chromium rich steel called Crofer22APU bearing CTE $11.8 – 12.5 \times 10^{-6}$ K^{-1} (Meinhardt et al. 2008; Ghosh, Kundu, et al. 2008; Mukhopadhyay et al. 2009; Wu et al. 2015; M. Kaur et al. 2017). The cathode and the anode used in such devices generally bear the CTE around 12.5 $\times 10^{-6}$ K^{-1} and around $10 – 14 \times 10^{-6}$ K^{-1} respectively (Heydari et al. 2013). Hence it is

necessary that the CTE of the sealing glass be in the range of $11.5 - 13 \times 10^{-6}$ $K^{-1} \times 10^{-6}$ K^{-1} for best functioning. Some commonly used sealant glasses are listed in table 1.1.

Table 1.1: Various Sealant glasses

Glass Name	Basic Composition	Opt Temp (°C)	Melted at (°C)	T_g (°C)	Ref
Diopside ($CaMgSi_2O_6$) glasses	SrO-CaO-MgO-Al_2O_3- B_2O_3- La_2O_3- Bi_2O_3-SiO_2	800 – 1000	1550	520 – 550	(Ashutosh Goel and Pascual 2010)
Magnesium-Lanthanum-Aluminium-Borosilicate Glass	MgO-BaO- Al_2O_3- B_2O_3- La_2O_3-SiO_2	750 – 800	1350 – 1500	560 – 680	(Mukhopadhyay et al. 2009)
BaO/SrO-MgO-B_2O_3-SiO_2	BaO/SrO-MgO-B_2O_3-SiO_2	800	1550	650 – 675	(Rodríguez-López et al. 2017)
Bilayer glass ceramics	MgO-CaO-SrO-SiO_2- Al_2O_3-B_2O_3- Gd_2O_3 (La_2O_3-NiO-BaO)	850	---	744 – 770	(Amarnath et al. 2014)
Bismuth containing seal glass	CaO-SrO- B_2O_3- Al_2O_3-SiO_2-BiO_2-ZnO	700	1300 – 1350	650 – 680	(Zhang et al. 2015)
Lithium Silicate glasses	Li_2O-K_2O- Al_2O_3- B_2O_3-SiO_2	≤ 800	1550	500	(Gaddam et al. 2016)
Melilite glass ceramics	CaO-MgO-SrO-Al_2O_3-La_2O_3-SiO_2- B_2O_3- Bi_2O_3-ZrO_2	700 – 800	---	---	(Reddy et al. 2013)
Ba-free alkaline earth borosilicate glasses	SrO-CaO-ZnO- B_2O_3- La_2O_3-SiO_2	700 – 1000	1500	650 – 700	(Sasmal et al. 2014)
Lanthanide containing glasses	CaO-MgO-SrO- Al_2O_3-Ln_2O_3-SiO_2- B_2O_3	800 – 1000	1580	---	(Mafra et al. 2014)
BCAS	BaO-CaO- Al_2O_3-SiO_2	700 – 800	1450	600 – 670	(Ghosh, Das Sharma, et al. 2008)

K D Meinhardt et. al. (2002) reported that the critical thermal parameters, T_g and T_d for the glasses lie in the range of 650 °C – 800 °C. The onset of crystallization temperature T_c, which is generally determined using Differential Scanning Calorimeter (DSC) was reported by many people over the last decade all of which lie in the range of nearly 700 °C – 800 °C (Ghosh, Das Sharma, et al. 2008; Ghosh, Kundu, et al. 2008; Mukhopadhyay et al. 2009; Hao et al. 2012; Puig et al. 2017; Schilm et al. 2018; Kurama and Saydam 2017). All these characteristic temperatures would help in determining the Glass Forming Tendency (GFT) or working temperature of glass (Mukhopadhyay et al. 2009).

Another important consideration is the shrinkage behaviour of the glasses. These sealing glasses are going to be granulated and applied on the fuel cell electrode materials using some organic carrier. Typical grain or particle size, selection of organic binder, process of applying the paste on the metal, etc. needs to be optimized for efficient functioning. Basu et. al. (2008) reported that a large particle size of the glasses leads to increase in porosity of the glasses when exposed to high temperature atmospheres (Ghosh, Sharma, et al. 2008). A Goel et. al. (2008) reported that 10 vol% aqueous polyvinyl alcohol (PVA) can be used as a binder to make pellets with fine glass powders. A Goel et al (2008) reported shrinkage by measuring dimensions or density of pellets before and after heat treatments. A Goel et al (2010) reported usage of hot stage microscopy for the same purpose. They reported 5% to 17% shrinkage in the temperature range of 900 ˚C to 1100 ˚C in multiple articles during 2008 to 2010 and reported those glasses to be suitable for SOFC applications (A. Goel et al. 2008; Ferrari et al. 2010). Basu et al (2008) reported volume shrinkage from 10% to 45% in the temperature range of 700 ˚C to 850 ˚C for BCAS glasses. M J Pascual et al (2010) reported that the glasses with particle size 45 μm – 53 μm, achieved a maximum T_x – T_g value of 145 °C, which means a wide working temperature range for glass (Reis et al. 2010). Puig et al (2015) reported maximum shrinkage in the temperature range of 690 ˚C to 725 ˚C (Puig et al. 2016). Bakal et al (2016) reported that shrinkages of all samples start at sintering temperatures and all samples start to expand at softening temperatures. They also reported that a glass ceramic body could resist the mechanical force caused by shrinkage on reaching up to 20% of maximum shrinkage. They reported a maximum shrinkage of 20 vol%. It was also reported that Al_2O_3 has negligible effect on shrinkage at sintering temperature but at softening temperature, shrinkage is high for low Al_2O_3 content, which drops with rise in Al_2O_3 content (Ozgur Colpan, Ibrahim, and Feridun 2008). Z X Li et al (2018) conducted a detailed shrinkage study on BCAS glass system and reported 8% to 16% shrinkage in their glasses (Li et al. 2018). They explained how slow heating rates are important for steady densification of powder compacts. Faster heating rates can deform the sample causing it to hamper the integrity of the device. Javed et al (2018) reported maximum shrinkage in the range of 775 ˚C to 875 ˚C for borosilicate based glasses. Shrinkage has to be completed before

crystallization starts, which means the maximum shrinkage temperature must be less than the crystallization onset temperature, for efficient operation (Javed et al. 2018).

1.8. Physical and Structural properties of BCAS glasses

BaO-CaO-Al$_2$O$_3$-SiO$_2$ (BCAS) based systems are found to be most suitable for high temperature applications like SOFC sealants due to their highly suitable thermal properties (Mukhopadhyay et al. 2009). However these glasses have some limitations to offer. In general these glasses, having high melting points, mostly above 1500 °C, are coated on chromium rich alloys like Crofer22APU.

The formation of BaCr$_2$O$_4$ (barium-chromate) phase due to reaction between barium and chromium in Crofer22APU affects the integration of the coatings causing degradation due to development of interfacial defects (M. J. Da Silva et al. 2016; Rodríguez-López et al. 2017; Sasmal et al. 2014; Sabato et al. 2016). M J Pascual et. al. (2016) reported that incorporation of B$_2$O$_3$ in the glass matrix helps in reducing the overall crystallization and retards the growth of chromate phase (Cr$_2$O$_3$) (L. D. Silva et al. 2017). But B$_2$O$_3$ is also responsible for reduction of viscosity, transition temperature (T$_g$), softening temperature (T$_d$) and glass stability. Reduction of viscosity is favourable for glass melting but high concentration of B$_2$O$_3$ at elevated operation temperature may lead to formation of volatile materials like gaseous HBO$_2$ on reacting with water. Formation of such volatile compounds results in breaking of the glass network.

Incorporation of ZnO and MgO in small quantities, in the glass matrix acts as a flux and helps to reduce melting temperature (Shao, Wang, and Zhang 2009). Addition of Al$_2$O$_3$ lowers the rate of crystallization of the samples, but high concentration of Al$_2$O$_3$ is also harmful for glass-metal integrity (Kim, Choi, and Yang 2015).

The most significant issue in development of BCAS glass, is the formation of BaAl$_2$Si$_2$O$_8$ (celsian) phase in the glass matrix at elevated operation temperatures. BaO dominantly contributes to crystallization if its concentration is more than 30 mol%, in the glass matrix (Mukhopadhyay et al. 2009). The hexa-celsian phase was reported on heating the glasses at 800 °C. This phase, which is a polymorph of the celsian phase has a relatively lower CTE, 8×10^{-6} K^{-1}. Though the CTE value of this phase is in the acceptable range, on prolonged heat treatment hexa-celsian, which is stable only in the temperature range of 1590 °C-1760 °C, is found to get converted in to mono-celsian phase which is thermodynamically stable below 1590°C. This phase has a very low

CTE 2.29×10^{-6} K^{-1} and hence is detrimental for applications where integration with high temperature alloys are important (A. Goel et al. 2008; Ghosh, Sharma, et al. 2008; Puig et al. 2017; Kurama and Saydam 2017). $BaSiO_3$, $CaSiO_3$ were reported along with the other identified phases. $BaSiO_3$ has a CTE of $10\text{-}14 \times 10^{-6}$ K^{-1}, causes no harm to the glass-metal integrity and $CaSiO_3$ helps in improving thermal properties of the sample (M. J. Da Silva et al. 2016; L. D. Silva et al. 2017; Sabato et al. 2016).

So it can be concluded that there is a requirement to find a glass ceramic sealant on BCAS which does not give rise to barium chromate or monocelsian phase after coating on Crofer22APU.

1.9. Mechanical properties of high temperature sealants

Due to consecutive thermal cycles and repeated expansions and contractions, a significant amount of mechanical stress develops within the material (L. D. Silva et al. 2017; Rodríguez-López et al. 2017). In order to ensure the robustness of the seal, mechanical properties of the sealant glass must be investigated. Mechanical hardness of the samples must be determined to ensure that the seal is capable of bearing this stress. Indentation techniques are generally employed under varying loads to determine the hardness of glasses. In 1972 A Makishima and J D Mackenzie reported a model for calculation of Young's Modulus (E) from Vicker's hardness data for glasses (Rodríguez-López et al. 2017; Makishima and Mackenzie 1973; Kožušníková 2009; Kruzic et al. 2009; Soares et al. 2014; Venkateswara Rao and Shashikala 2014). Glasses with more BaO content show low hardness properties (Rodríguez-López et al. 2017). Hardness values of BCAS glasses were reported to lie in the range of 7.1 to 7.7 GPa and Young's modulus for BAS glasses were reported to be near 790 kBar (Rodríguez-López et al. 2017). The Young's modulus of BCAS glasses lie in the range of 61 GPa to 91 GPa and fracture toughness values are considered good if they are near 1 MPa.m$^{1/2}$ (Rodríguez-López et al. 2017).

1.10. Structural and electrical compatibility between glass sealant and Crofer22APU, metallic interconnect

A sealant material is expected to be capable of integrating with the other SOFC components such as the anode, cathode or metallic interconnects like the most commonly reported Crofer22APU. They must be chemically and thermally stable at

elevated operating temperatures (Meinhardt et al. 2008). Formation of monoclinic-celsian phase with low coefficient of thermal expansion (CTE), after prolonged exposure of these BCAS glasses to high temperatures, causes CTE mismatch between the glass and the metal. This leads to formation of cracks and leaks and degrades cell performance (Bhattacharya and Shashikala 2019, 2018). Electrical resistivity of the glasses must be greater or equal to 10^4 Ω-cm at 800 °C (Grema 2018). Due to the presence of BaO in the BCAS glasses, and chromium in Crofer22APU the formation of Barium Chromate ($BaCrO_4$) with high CTE and electrical conductivity, after long term operation at elevated temperatures are common flaws of the BCAS glasses (Mukhopadhyay et al. 2009; Bhattacharya and Shashikala 2019).

1.11.   *Scope of the work*

BaO-CaO-Al_2O_3-SiO_2 (BCAS) based systems are considered to be most suitable for high temperature applications like SOFC sealants due to their highly suitable thermal properties (Mukhopadhyay et al. 2009). However these glasses have three important limitations to offer. Firstly BCAS glasses are having high melting points, mostly above 1500 °C which makes it difficult to synthesise. The second issue involves the compatibility of these glasses when they are coated on chromium rich interconnect alloys like Crofer22APU bearing composition 20-24wt%Cr-0.03C-0.3-0.8Mn-0.5Si-0.5Cu-0.5Al-0.02S-0.05P-0.03-0.2Ti-0.04-0.2La. These coated samples where together glass and Crofer22APU as a single unit, must be exposed to high temperatures in the presence of ambient atmosphere, to observe their mutual compatibility under SOFC operating conditions. At high temperatures, barium in the glass is found to react with chromium forming a layer of $BaCr_2O_4$ (barium-chromate) phase on the surface of Crofer22APU. This newly developed barium chromate phase has a very high coefficient of thermal expansion (CTE) of $16 - 18 \times 10^{-6}$ K^{-1}, as compared to that of Crofer22APU which has CTE of 12×10^{-6} K^{-1}. This affects the integration of the coatings causing degradation of the cell due to development of interfacial defects (L. D. Silva et al. 2017; Rodríguez-López et al. 2017; Javed et al. 2018). Lastly and the most significant issue in development of BCAS glasses, is the formation of $BaAl_2Si_2O_8$ (celsian) phase in the glass matrix at elevated operation temperatures. The mono-celsian phase which is thermodynamically stable below

1590°C, has a very low CTE 2.29×10^{-6} K^{-1} and hence is detrimental for high temperature sealing applications (Kurama and Saydam 2017; Ferreira et al. 2008; A. Goel et al. 2008; Puig et al. 2017; Sasmal et al. 2014). This monocelsian phase if present in the glass system tends to reduce the CTE of the entire system, which effects the glass-metal integrity at a later stage. It is also very important that these glass – metal joints are stable and functional after multiple heating cycles. Efforts are still going on to find a suitable glass, with compatible thermal, electrical and mechanical properties, optimum for high temperature sealing applications, for operations in the 800 °C to 900 °C temperature range.

1.12. Objectives of the present work

The primary objective of the present work is to synthesize derivatives of 40 mol% $SiO_2 – 10B_2O_3 – xBaO – (45-x)$ CaO $– 5Al_2O_3$ (BCBSA glass system) with varying BaO and Al_2O_3 concentrations, and study their properties. The main objectives of the work include:

- ❖ Optimization of composition, synthesis parameters like calcination and melting time and temperatures for the BCBSA glasses and their derivatives.
- ❖ To study the structural properties of the synthesized glasses and make sure the mono celsian phase do not occur on prolonged heat treatment and barium chromate phase do not develop at a later stage, when in contact with Crofer22APU.
- ❖ To investigate the Thermal Properties of the synthesized glasses employing dilatometry. To observe the shrinkage behaviour of the pelletized glass compacts and ensure that the required CTE is maintained even after sintering.
- ❖ To determine the DC electrical resistivity at different temperatures from room temperature to 800 °C and ensure that the glasses have resistivity $\geq 10^4$ Ωcm.
- ❖ To coat the thermally and mechanically optimized glass on Crofer22APU metallic interconnect using screen printing technique and to check the compatibility of the glass with the metallic interconnect material, Crofer22APU under metal-glass-metal sandwiched condition.

1.13. Organization of the thesis

The present work is organised as described below:

- In an attempt to understand the need and requirements of high temperature sealing, a brief introduction and literature review of the past few years, on glass, glass ceramics and SOFCs in general and on BCAS glasses in particular, are explained in **Chapter 1**.

- **Chapter 2** accounts for all the materials used for synthesis of the reported glasses. This chapter also explains the methodology and techniques used to prepare samples studied in the present work. It lists all the characterization technique used and discusses their working.

- The conversion of H_3BO_3 to B_2O_3, in the raw batch mixtures before melting of the glasses require optimum heat treatment, to allow the conversion reactions to occur. The details of this optimisation of the calcination parameters before melting of the glasses are discussed in **Chapter 3**.

- Physical optical and structural properties of the glasses are important aspects of consideration. **Chapter 4** explains all these properties in detail. This chapter discusses the density, molar volume, optical band gap energy and Urbach tail energy of all the glasses and their variation with varying concentrations of alkaline earth oxides in the glass matrix. This chapter also deals with the devitrification behaviour of the glasses at elevated temperatures like 800 °C – 900 °C after 50 and 100 hours of heating.

- The thermal behaviour of all glasses are discussed in **Chapter 5**. This chapter shows the dilatometric, T_g, T_d and CTE of the bulk glasses, which were then sintered at various temperature to observe their shrinkage behaviour. The observed maximum shrinkage for the samples and comparison between their respective T_g, T_d and CTE before and after sintering are explained in this chapter. The mechanical properties of the prepared glasses like their microhardness, Young's modulus and fracture toughness are also discussed.

- **Chapter 6** deals with the compatibility of the glass ceramic 00B with the metallic interconnect Crofer22APU. This chapter discusses screen printing technique, preparation of CGC sandwich and determination of dc electrical resistivity at elevated temperatures using two-probe method.

- **Chapter 7** summarises the important findings of the present work along with the conclusions. This chapter also discusses the scope of the future work.

CHAPTER 2

EXPERIMENTAL METHODS

2.1. Materials and Synthesis of Glasses

Two series of glasses were prepared and their detailed analysis were conducted in this work. Five glass compositions of 40 mol% $SiO_2 - 10B_2O_3 - xBaO - (45-x)$ CaO $- 5Al_2O_3$ were termed as BCBSA glasses. The details of the batch compositions of these BCBSA glasses are listed in table 2.1. Five other samples, termed as BCBS glasses containing 40 mol% $SiO_2 - 10B_2O_3 - xBaO - (45-x)$ CaO were prepared without Al_2O_3. Details of the batch compositions of these BCBS glasses are also listed in table 2.1. 6wt% of ZnO and MgO were added to all the compositions, with or without Al_2O_3, as a flux to reduce their melting temperatures.

BaO (purity 98%, reagent grade, Rolex), CaO (90%, Merck), Al_2O_3 (99.997%, Alfa Aesar), SiO_2 (99.5%, Alfa Aesar), H_3BO_3 (99.5%, AR grade, Loba Chemie), ZnO (99.5%, reagent grade, Nice) and MgO (98%, reagent grade, Nice) were used as starting materials for preparation of samples. All the compounds were accurately weighed in calculated molar proportions (J E Shelby 2005) using Contech analytical balance with an accuracy of 0.1 mg and mixed in an agate mortar using a pestle. All glasses were synthesized using melt quenching technique.

The thoroughly mixed powders were first subjected to calcination. This is a pre-melting process followed to ensure the conversion of H_3BO_3 used as the starting material to B_2O_3 which is actually required in the matrix. All the samples from both the glass series were calcined at 350 °C for 7 hours. The temperature and time of calcination were experimentally optimized and is discussed elaborately in chapter 3.

The samples in the BCBSA series were initially melted in a high temperature programmable muffle furnace, without ZnO and MgO at 1100 °C, 1200 °C and 1300 °C for 1, 2 and 3 hours. But none of the samples could be melted and only a molten slag was obtained even after heating the batch compositions to 1300 °C. The addition of 6 wt% ZnO and MgO helped in reduction of melting temperature of the glasses at 1200 °C and 1300 °C. All samples could easily be melted at 1300 °C, after soaking for

one hour. Hence this temperature was considered optimum and all samples in this work including the BCBS glasses, were melted at 1300 ^{O}C for 1 hour.

The glasses in molten state were quenched in two parts. The first part between two stainless steel slabs at room temperature in air. They were annealed at 550 ^{O}C for 3 hours immediately after quenching to eliminate any developed thermal stresses. This process helps obtaining bulk glasses. The second half was directly quenched in ice water held in stainless steel containers, to obtain glass frits. These frits were dried at 80 ^{O}C for 24 hours, using an incubator. This helps in obtaining glass frits which were then further ground and sieved to fine powders with particle size $\leq$ 40 μm.

Table 2.1: Composition of all prepared glasses

Sl. No	Glass system	Sample	Composition (mol%)					Flux (wt%)	
			SiO$_2$	B$_2$O$_3$	BaO	CaO	Al$_2$O$_3$	ZnO	MgO
1		40B-A	40	10	40	05	5	6	6
2		35B-A	40	10	35	10	5	6	6
3	**BCBSA**	30B-A	40	10	30	15	5	6	6
4		25B-A	40	10	25	20	5	6	6
5		20B-A	40	10	20	25	5	6	6
6		35B	40	10	35	15	---	6	6
7		30B	40	10	30	20	---	6	6
8	**BCBS**	20B	40	10	20	30	---	6	6
9		10B	40	10	10	40	---	6	6
10		00B	40	10	00	50	---	6	6

2.2. Methodology

The synthesized samples were used in five forms, which are bulk flat glasses, bulk cubic glasses, bulk glasses powdered by grinding, glass frits powdered and sieved through a 40 μm mesh and compacted glass pellets. The methodology followed and the characterizations conducted on these prepared samples are explained in figure 2.1. The characterization methods used include, X-ray diffraction (XRD), Fourier transformed infrared spectroscopy (FTIR), measurement of density and calculation of molar volume

from the obtained data, U V Visible Spectroscopy, measurement of refractive index (RI) using Abbe Refractometer and calculation of metalicity factor (M). Devitrification studies were carried out through prolonged isothermal heat treatment up to 100 hours, followed by XRD to determine the crystalline phases, determination of shrinkage by sintering pelletized glasses, dilatometric studies from room temperature (RT) to 700 °C
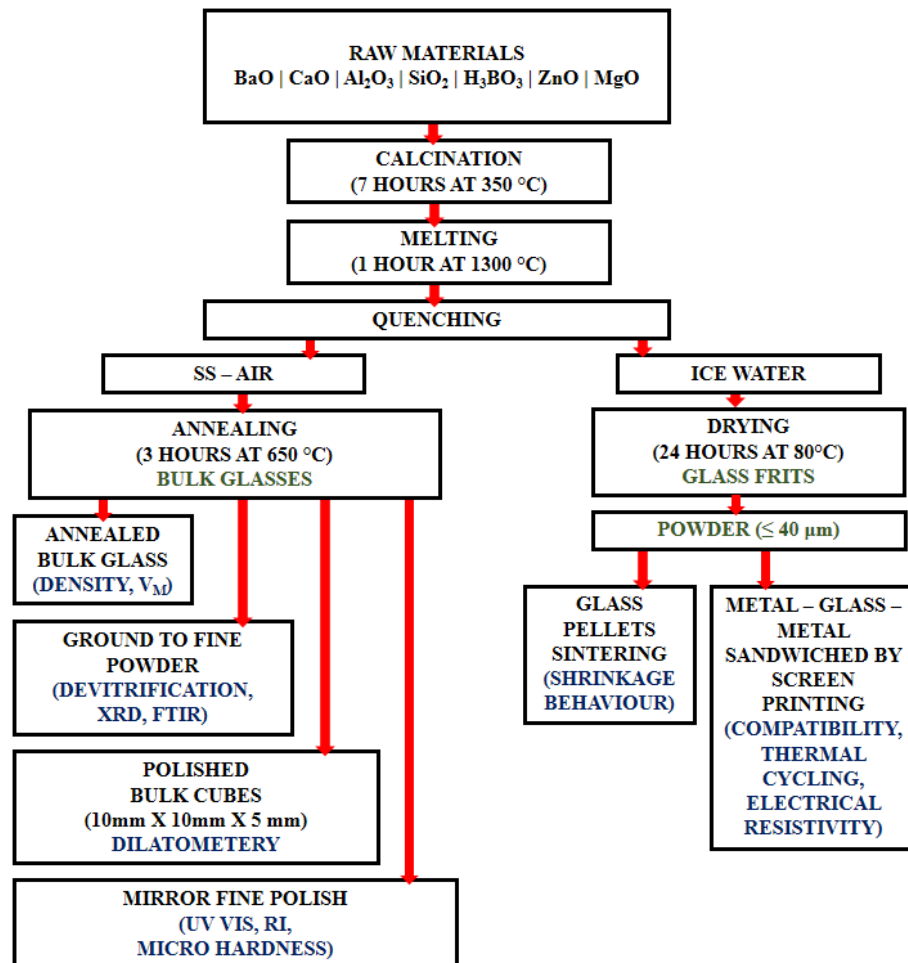
Figure 2.1: Process flow of the work done

on both cubic bulk glasses and sintered pelletized glasses. Mechanical properties studied include measurement of Vickers hardness and calculation of a various parameters from the obtained data. Usefulness of the glasses at high temperature was verified through repeated thermal cycling and dc resistivity measurements under sandwiched conditions between metals. Apart from this the compatibility of the glasses with Crofer22APU and SS304 under metal – glass – metal sandwiched assembly at

elevated temperatures were also considered and studied. In this chapter the methods mentioned above are explained in detail.

Figure 2.2 exhibits the different forms of samples prepared during the study. Sample 00B was chosen to form metal – glass – metal sandwiches.
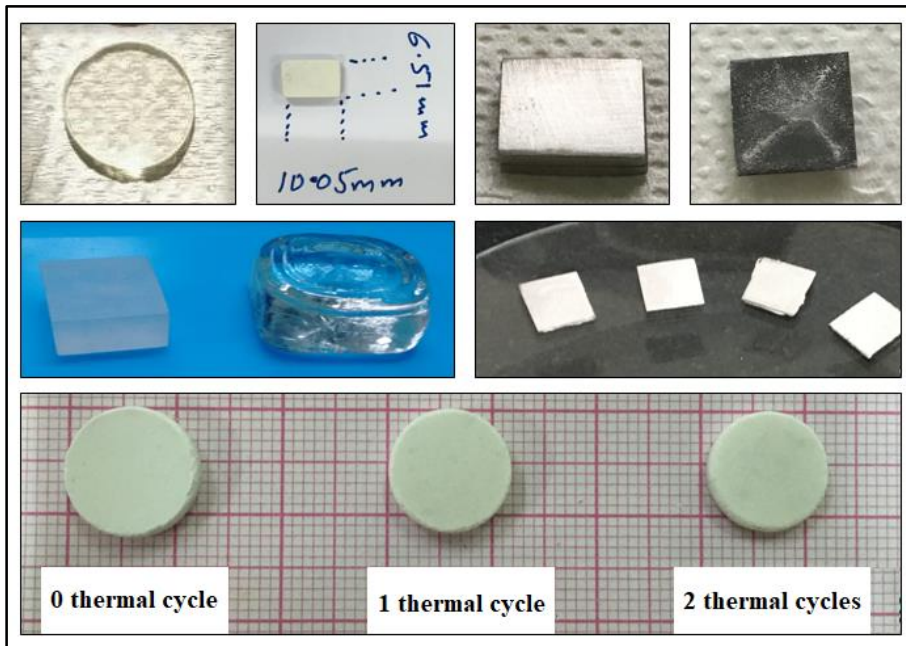
Figure 2.2: Various forms of sample 00B prepared for the present study

2.3. Characterization techniques

2.3.1. X-ray Diffraction

In the present study XRD has been used for three purposes.

i. The pre-melted batch mixtures that were used to optimize the calcination time and temperature were subjected to XRD analysis. XRD data was recorded both before and after calcination of the mixtures. This helped in determining presence of H_3BO_3 or B_2O_3 or both in the glasses and hence infer about the conversion of H_3BO_3 or B_2O_3.

ii. The amorphous nature of the as prepared samples were determined using XRD.

iii. The crystalline phases developed in the samples after isothermal heat treatment at elevated temperatures were also identified through XRD.

The scans were conducted using a Rigaku Miniflex 600 X-ray diffractometer. All the samples or mixtures considered for any of the analysis mentioned above, were

scanned with 1.54 Å Cu-K$_\alpha$ radiation through 2θ ranging from 20° to 80° at a scan rate of 1°min^{-1}.

2.3.2. *Fourier Transformed Infra-Red Spectroscopy*

Fourier Transformed Infra-Red spectroscopy (FTIR) is a technique used to obtain an infra-red spectrum of absorption or emission of a solid, liquid or gas. The FTIR spectrometer collects high resolution data simultaneously over a wide spectral range. A Fourier transformation is required to convert the raw data to the actual spectrum. Hence this process is called Fourier Transformed Infra-red spectroscopy.

Figure 2.3: FTIR Spectrometer

In this study, FTIR was used to identify and confirm the presence of structural bands in the glass network. The transmission spectra of all the samples were recorded

using Bruker ALPHA-200952 Spectrometer. The samples were studied in the wave number range from 400-1500 cm^{-1} using KBr pellet method.

2.3.3. Determination of Density and Molar Volume

Density (ρ) was measured using Archimedes' liquid displacement method using Contech analytical balance and density kit. Ortho-Xylene (O-Xylene) (C_8H_{10}, 99%-Alfa Aesar) was used as the immersion medium. Molar volume (V_m) was calculated from the measured density data using equation 2.2 (J E Shelby 2005). Densities of at least three samples for each composition, were measured and the average value of the recorded densities were considered, along with the error calculated using standard deviation of mean (SDOM).

$$V_m = \frac{M.Wt}{\rho} \qquad \qquad \text{... (2.2)}$$

where, V_m is the molar volume, M.Wt is the molecular weight of the glass composition and ρ is the measured density of the glass.

2.3.4. U V Visible Spectroscopy

U V Visible (UV-Vis) absorption spectroscopy is a measurement of the attenuation of a beam of light after it passes through a sample or after reflection from the surface of a sample. Measurements can be conducted on a single wavelength or over an extended spectral range. Light is illuminated on a sample, which matches the energy difference between a possible electronic transitions within the molecule, such that the electron is promoted to the higher energy state. The degree of absorption for different wavelengths is recorded by the spectrometer and wavelength versus absorption spectrum graph can be plotted.

In this study the fine polished bulk flat glasses were subjected to ultraviolet and visible radiation using Ocean Optics U V Visible Spectrometer shown in figure 2.6 and their absorption patterns were recorded. The absorption edge for all samples were identified using the absorbance versus wavelength (λ) plots. These observed λ values were used to calculate the band gap energy using the Davis-Mott relation (El-nahass et al. 2005; Hassanien and Akl 2015)

$$\alpha = \frac{B}{h\upsilon}\left(h\upsilon - E_g\right)^n \qquad \qquad \text{... (2.3)}$$

where, α = absorption coefficient, $h\upsilon$ = incident photon energy, E_g = band gap energy, B is a constant and n represents the type of transition like n = 1/2, 2, 3/2 and 3 for direct allowed, indirect allowed, direct forbidden and indirect forbidden respectively. Considering n = 2, for indirect allowed transitions, and taking square root both sides, equation 2.3 can be reframed as:

$$(\alpha h\upsilon)^{1/2} = B^{1/2} (h\upsilon - E_g) \qquad \text{... (2.4)}$$

Equation 2.4 represents the equation of a straight line whose x-intercept gives the optical band gap energy. Hence the extrapolation of the straight line region of the graph to x axis at y = 0 gives the band gap energy, E_g, of the samples.

In materials with poor crystalline nature, due to the disorder in the material there exists a number of localised electron states extending in to the band gap and is seen as an exponential tail called Urbach Tail, defined by Urbach empirical rule as stated in equation 2.5 (Hassanien and Akl 2015),

$$\alpha = \alpha_0 \exp(\frac{h\upsilon}{E_u}) \qquad \text{... (2.5)}$$

where, α_0 is a constant and E_u is the Urbach energy. Taking natural logarithm on both sides of equation 2.5 we arrive at equation 2.6,

$$Ln\ \alpha = \left(\frac{1}{E_u}\right) h\upsilon + Ln\ \alpha_0 \qquad \text{... (2.6)}$$

which is again in the gradient form of a straight line. The reciprocal of the slopes of the linear region of this graph is the Urbach Energy E_u (El-nahass et al. 2005; Hassanien and Akl 2015).

2.3.5. Abbe Refractometer

An Abbe refractometer is a bench-top device for the high-precision measurement of an index of refraction. Working principle of an Abbe refractometer is based on critical angle. Sample is put between two prisms - measuring and illuminating. Light enters sample from the illuminating prism, gets refracted at critical angle at the bottom surface of measuring prism, and then a telescope is used to measure position of the border between bright and light areas. Telescope reverts the image, so the dark area is seen at

the bottom, even if we expect it to be in the upper part of the field of view. Knowing the angle and refractive index of the measuring prism, the refractive index of the sample can be calculated. Surface of the illuminating prism is matted, so that the light enters the sample at all possible angles, including those almost parallel to the surface.

Figure 2.4: Abbe Refractometer

In this study, the refractive indices 'n' of all the samples were measured using the Abbe Refractometer shown in figure 2.4.

In order to evaluate the metallization tendency of the samples the Lorentz Lorenz equation (Dimitrov and Komatsu 2010) given as equation 2.7 was used,

$$\frac{R_m}{V_m} = \frac{n^2-1}{n^2+2} \qquad \qquad \text{... (2.7)}$$

where, R_m is the molar refraction, V_m is the molar volume and n is the refractive index of the glasses.

According to Herzfeld theory of metallization (Dimitrov and Komatsu 2010; Herzfeld 1927), if one starts with a material of very high refractive index, in gaseous state and keep condensing it till it gets solidified and density increases such that R_m/V_m

approaches unity, then the right hand side of the equation 2.7 becomes $(n^2 - 1) = (n^2 + 2)$. This can only be possible when the value of n becomes infinite. This condition is called polarization catastrophe (Dimitrov and Komatsu 2010). This means the valence electrons that were quasi-elastically bound to their atoms in the gaseous state, are now free to move in the condensed state turning the solidified material into a metallic conductor. On the basis of this theory an estimation of metallic or insulating behaviour of the material can be drawn. The difference given in equation 2.8 is called the metallization criterion (Dimitrov and Komatsu 2010).

$$M = 1 - \frac{R_m}{V_m} \qquad \qquad ... (2.8)$$

For materials with M close to zero, width of both valance and conduction bands become large resulting in a narrow band gap. Materials with the value of M nearing one are typical insulators (Dimitrov and Komatsu 2010).

2.3.6. Thermo Gravimetric Analysis

Thermo Gravimetric Analysis (TGA) was conducted to measure the amount of weight change of a material and hence understand the stability of the premelted glass mixtures. The pre-melted batch mixtures were characterized with a Perkin Elmer TGA 4000 thermal analyzer in a temperature range of 50 °C to 900 °C at a heating rate of 1 °C min⁻¹ in air. The weight loss of the batch mixtures were recorded at different temperatures for samples calcined under different conditions. This along with XRD analysis helped in understanding the conversion of H_3BO_3 to B_2O_3 for all glasses.

2.3.7. Dilatometer

A dilatometer is a precision instrument for the measurement of dimensional changes in material as a function of temperature. It provides measurements of various properties that include linear thermal expansion, coefficient of thermal expansion, phase transitions, change in density, softening point and decomposition temperature, glass transition temperature, etc. In a dilatometer the sample is placed in a special holder inside a moveable furnace. A push-rod placed directly against the sample transmits length change to a linear variable displacement transducer (LVDT). As the length of the sample changes with changing temperature, the LVDT core is moved, and an output

signal proportional to the displacement is recorded. The temperature program is normally controlled using a thermocouple located next to the heating element or the sample.

The samples used for dilatometric analysis were quenched in 10 mm × 10 mm × 5 mm stainless steel moulds to obtain bulk samples. These samples were then polished using SiC papers of grit size 80 and 180 to exact dimensions of 10 mm × 10 mm × 5 mm. The polished samples were then subjected to heating in a TA DIL802 Differential Dilatometer from room temperature to 700 °C at the rate of 5 °C min^{-1} in air.

Figure 2.5: TA DIL802 differential dilatometer

The compacted glass pellets that exhibited maximum shrinkage after sintering, were also subjected to dilatometric analysis. The shrunk pellets were polished using SiC papers, to the dimensions of 10 mm × 6 mm × 2 mm. The dilatometer study on these glass pellets were carried out using the same instrument, following exactly the same parameters used for the analysis of the bulk glasses explained above for comparative analysis between them.

2.3.8. Field Effect Scanning Electron Microscope (FESEM)

In this work, a Carl Zeiss Sigma - Field Effect Scanning Electron Microscope (FESEM) was used to view the surface of the fine polished glasses that were subjected to microhardness test as will be explained in the next section. The main purpose was to view the indentations or the developed cracks on the surface of the samples and measure

the lengths of these cracks. Since the present study deals with only glasses, all samples were first sputtered with gold, to ensure surface electron conduction.

2.3.9. Microhardness test by Vicker's Indentation Technique

The fine polished bulk flat glasses were used to determine the micro-hardness of all the samples using Vicker's indentation technique with a Clemex computer controlled micro-hardness tester. Each sample was tested under four different loads of 0.25 N, 0.49 N, 0.98 N and 1.96 N. The average of hardness corresponding to ten indentations at each load were considered for microhardness measurements. The Young's Modulus (E), for all samples were calculated using Makishima-Mackenzie method. The Young's Modulus (E) is given by (Makishima and Mackenzie 1973)

$$E = 83.6 \, V_t \, \sum G_i X_i \qquad \qquad \dots (2.9)$$

where, G_i is the Dislocation Energy per unit volume of oxides, X_i is the Mole Fraction of the component i and V_t is given as (Makishima and Mackenzie 1973),

$$V_t = \frac{\rho}{M} \sum_i V_i X_i \qquad \qquad \dots (2.10)$$

where, V_t is the Packing Density, ρ is the Density of the glasses, M is the Molar Mass and V_i is the Packing Fraction.

The fracture toughness (K_{IC}) is calculated using the formula (Kruzic et al. 2009)

$$K_{IC} = \alpha \, (\frac{E}{H_V})^{1/2} \, \frac{P}{C^{3/2}} \qquad \qquad \dots (2.11)$$

where, K_{IC} is the Fracture Toughness, α is the calibration constant generally taken as 0.016 ± 0.004, E is the Young's Modulus, H_v is the Vicker's Hardness, P is the Applied Load, C is the Crack length from centre of the indent.

The brittleness (B) can be calculated using the formula (Venkateswara Rao and Shashikala 2014)

$$B = \frac{H_V}{K_{IC}} \qquad \qquad \dots (2.12)$$

where, B is the Brittleness, H_v is the Vicker's Hardness and K_{IC} is the Fracture Toughness.

2.4. *Isothermal Heat Treatment*

The annealed bulk samples were crushed in to fine powders using a mortar and pestle to carry out the isothermal heat treatment. The crushed samples were filled in alumina crucibles and introduced in a muffle furnace. They were heated separately from room temperature to 700 $^{\circ}$C and 800 $^{\circ}$C at 5 $^{\circ}$C min^{-1}, and held at those temperatures for 50 hours. After this soaking period, the samples were again cooled to room temperature using the same rate of cooling. Similarly, the samples were heat treated at 900 $^{\circ}$C at the same rate and held for 50 and 100 hours and cooled to room temperature, to observe their devitrification behaviour. The developed phases were identified by XRD.

2.5. *Determination of Shrinkage Behaviour*

2.5.1. *Preparation of Glass Pellets*

In order to determine the shrinkage behaviour, the glass frits prepared by quenching in ice water, were used. The glass samples used in this study are 00B, 10B and 30B-A. The reason for selecting these samples is as follows.

Sample 30B-A was the primary composition of this work, from which other derivatives were prepared by varying the concentration of the constituents. 10B and 00B are the samples with less than 20 mol% BaO concentration, which were found to be useful for high temperature sealing applications.

The three selected compositions 30B-A, 10B and 00B were ground in an agate mortar using a pestle and the powdered glasses were sieved through a mesh of grit size 40 μm to obtain samples with particle size ≤ 40 μm. These fine crushed powders were used to prepare pellets.

Polyvinyl alcohol (PVA) was the organic binder used to make pellets of these glasses. 10 vol% aqueous solution of PVA was freshly prepared in a beaker using distilled water, and continuously stirred using a magnetic stirrer. The fine crushed glass powder (≤ 40 μm) and the prepared aqueous PVA solution in the ratio of 97.5 wt%

glass and 2.5 wt% aqueous PVA were mixed thoroughly using a mortar and pestle. This mixture was then transferred in to a mould with a diameter of 12 mm, and a uniaxial pressure of 500 MPa was applied for 1.5 minutes, using a hydraulic press. Thus, cylindrical pellets with a diameter of 12 mm and height 2 mm were prepared.

2.5.2. Shrinkage Behaviour of Glasses

The dimensions of the pellets made from the glass as explained in the earlier section, were measured using a micrometre screw gauge. The mass of each pellet was determined using a Contech analytical weighing balance with an accuracy of 0.1 mg. These pellets were then sintered from room temperature to 650 ˚C and allowed to dwell at that temperature for one hour. After that, they were cooled back to room temperature. Both heating and cooling rates were kept low and constant at 2 ˚C min^{-1} to avoid deformation of samples. Post cooling the dimensions of the sintered samples were again measured. The linear and volume shrinkages were determined using equation 2.13 and 2.14 respectively.

$$Linear\ Shrinkage = \frac{L_f - L_i}{L_i} \times 100 \qquad \qquad \dots (2.13)$$

$$Volume\ Shrinkage = \frac{V_f - V_i}{V_i} \times 100 \qquad \qquad \dots (2.14)$$

where, L_i and L_f are initial and final lengths, V_i and V_f are initial and final volumes of the pellets, before and after sintering respectively. Both mass and density of the sintered samples were determined using Contech analytical balance and density kit using O-Xylene as an immersion medium. This process was repeated for five pellets of each composition to check the reproducibility of the data and the average value of all the trials were considered for analysis. This process was also repeated for 700 ˚C, 800 ˚C and 900 ˚C temperatures. The pellets of 00B, 10B and 30B-A were re-sintered at 700 ˚C for one more hour, at the same heating rate. This second cycle of sintering was repeated for three samples and the average results were considered for further analysis. The second cycle of heat treatment was conducted to confirm that the samples do not expand on repeated heating and that they do not show any deformation on repeated temperature cycling.

2.6. Preparation and Thermal Cycling of CGC sandwich

The glass composition 00B containing 50mol% CaO – 10 B_2O_3 – 40 SiO_2, the glass without BaO and Al_2O_3, which exhibited most promising mechanical, thermal and structural properties, amongst the other synthesized glasses was ground using a mortar and a pestle and sieved to obtain uniform glass powder with particle size $\leq$ 40 μm. These finely crushed powders were then screen printed on the 10 mm × 10 mm × 2 mm polished Crofer22APU substrates. For screen printing, nylon mesh with 300 pores per square-inch was commercially obtained and stretched across a wooden frame. The tension of the mesh, was maintained at 5 N/cm and was measured with a HT-6510N Screen tension meter. Toluene ($C_6H_5CH_3$ = 92.14, Rectified, 99%, NICE), Ethanol (99.9%, AR grade) and Ethyl Cellulose (90-110mPa.s TCI) were obtained commercially. Toluene and ethanol were mixed in 80:20 ratio using a magnetic stirrer. 5 wt% Ethyl Cellulose was slowly added to the mixture, while being stirred. This mixture was stirred for 24 hours at room temperature in air to form an organic binder solution. The sieved 00B glass powders and the prepared organic binder solution were mixed in a 60:40 ratio to form a viscous paste, which was screen printed on the Crofer22APU substrates.

The glass coated Crofer22APU substrates were joined together so as to form a metal – glass – metal sandwich. This arrangement was then heated from room temperature to 800 °C at a rate of 2 °C min^{-1} under an applied load of 100 g. They were allowed to soak at that temperature for 1 hour. The samples were then allowed to cool overnight. These sandwiches formed are then subjected to multiple heating cycles following the same heating rate, but without any applied load. They were subjected to 1, 3 and 5 cycles of heating and cooling.

The cross sections of each sample prepared were observed under an optical microscope with a 100X zoom, to determine the thickness of the sandwiched glass-ceramic layer. The sandwiches were broken and the XRD patterns for the glass coated metal surfaces were recorded using a Rigaku Miniflex 600 X-ray Diffractometer with a 1.54 Å Cu-K_α radiation from a 2θ value of 20° to 80° at a scanning rate of 1°min^{-1}.

2.7. Electrical Characterization

Electrical resistivity of the sandwiched samples was determined by two probe technique built with pressure contacts, perpendicular on either side of the sample, using a Keithley 2400 source meter. The measurements were conducted with a constant applied current of 1A and sweeping voltage of -10 V to +10 V, at room temperature and at elevated temperatures from 600 °C to 800 °C. The voltage readings were noted at an interval of every 50 °C. The electrical resistance was calculated from which the electrical resistivity at a particular temperature was evaluated.

2.8. Surface Polishing

All samples requiring polishing were polished using Chennai Metco made semiautomatic polishing machine. The thickness of all the samples were first reduced to 2.0 mm. Emery sheets of grit size 80, 180, 400, 600, 800 and 1000 were used for this purpose. Regular tap water was used as a cooling liquid to prevent change in internal structures due to frictional heating. Each side of the samples were polished approximately for 30 minutes. Following this the samples were polished with finer emery papers bearing grit size 1500 and 2000 without using any cooling liquid. Each sides of the glasses were polished for approximately 2 hours with these papers. Final polishing of surfaces was carried out with a silk cloth and alumina powder suspension with alumina powder particle size of 0.05 μm. Each of the samples were polished with alumina suspension for approximately 3 to 3.5 hours on each side.

For dilatometric analysis the thickness of the bulk samples were adjusted by polishing to approximately 5 mm and with length and breadth of 10 mm using emery sheets of grit size 80 and 180. Each sample was polished for required amount of time to achieve the final dimensions, and the dimensions were frequently measured with a micrometre screw gauge. Finally the samples were polished with the emery paper of grit size 1000 for approximately 30 minutes on each side.

The glass compacts or pellets after sintering have undergone shrinkage. The shrunk pellets were polished using emery sheets of grit size 180 and 400 for

approximately 30 minutes on each side to obtain samples of dimensions 10 mm $\times$ 6.5 mm $\times$ 2 mm for dilatometric studies. Apart from this the Crofer22APU and SS304 substrates were also polished for short durations using either 80 or 180 grit emery papers before coating to obtain a rough and oxide free surface.

2.9. Error Analysis

Scientific studies, no matter how carefully conducted, are always associated with inevitable uncertainties and errors. These errors can be of human origin or due to aging of the instrument and sometimes even due to limitations of ease of recording the readings. In the present case multiple number of readings were considered in evaluation of many properties like density, microhardness, shrinkage etc. The error in all the measured quantities were estimated by taking the standard deviation of the mean (SDOM) of all measurements.

2.9.1. Calculation of Standard Deviation of the Mean

If "N" measurements of a quantity made using same instrument and procedure are $x_1, x_2,....., x_N$, then the best estimate for the quantity x is obtained by taking average or mean $\bar{x}$ of $x_1, x_2,....., x_N$. Here $\bar{x}$ is calculated as

$$\bar{x} = \frac{x_1 + x_2 + \cdots + x_N}{N} = \frac{\sum_i x_i}{N} \qquad \dots (2.15)$$

Uncertainty in $\bar{x}$ is estimated by taking the standard deviation of the mean (SDOM) or standard error of the N measurements and is given by the equation

$$\sigma_{\bar{x}} = \frac{\sigma_x}{\sqrt{N}} \qquad \dots (2.16)$$

where, $\sigma_{\bar{x}}$ is standard deviation of the mean and σ_x is standard deviation, which measures average uncertainty of N measurement. Standard deviation (σ_x) is given by the relation

$$\sigma_x = \sqrt{\frac{1}{N-1}\sum_i d_i^2} = \sqrt{\frac{1}{N-1}\sum_i (x_i - \bar{x})^2} \qquad \dots (2.17)$$

where, difference $x_i - \bar{x} = d_i$ gives the deviation of ith measurement x_i from mean value $\bar{x}$. If these deviations are very small then measurement carried out will be precise. Some deviations may be positive and some may be negative, so averaging the deviations may not give reliable uncertainty in the measurements. Thus, deviations are squared first to obtain a set of positive numbers and then square root of the average of set of positive

numbers are obtained to get a quantity having same unit as the measurements. This root mean square (RMS) deviation of the measurements is known as standard deviation, σ_x, which is found to be useful in characterizing reliability of measurements.

Standard deviation of the mean ($\sigma_{\bar{x}}$) is preferred over standard deviation (σ_x) to obtain uncertainty in the $\bar{x}$. Because, as the number of measurements increases, σ_x will give more reliable uncertainty in the final result due to the presence of factor $\sqrt{N}$ in the denominator. But, σ_x will not change appreciably with increase in number of measurements. Final result (X) of N number of measurements is represented as

$$X = \bar{x} + \delta x = \bar{x} + \frac{\sigma_x}{\sqrt{N}} \qquad \qquad \dots (2.18).$$

CHAPTER 3

EFFECT OF CALCINATION TEMPERATURE AND TIME ON SYNTHESIS OF BaO-CaO-Al$_2$O$_3$-SiO$_2$ GLASS

This chapter presents the work done to optimize the time and temperature of calcination before preparation of glasses, in order to ensure conversion of all starting materials in to required ingredients. Batch mixture of composition 30 mol% BaO – 15 CaO – 05 Al$_2$O$_3$ – 40 SiO$_2$ – 10 B$_2$O$_3$ was calcined at different temperatures, from 300 °C to 400 °C for varying number of hours, from 0 to 7 hrs. H$_3$BO$_3$ was used as a starting material to obtain the required B$_2$O$_3$. The samples considered for this study to ensure the conversion of H$_3$BO$_3$ to B$_2$O$_3$ are listed in table 3.1. X Ray Diffraction (XRD) and Thermo Gravimetric Analysis (TGA) studies were conducted on these raw mixtures before and after calcination. XRD of non calcined batch mixture contained H$_3$BO$_3$ phase in addition to other oxide phases. Conversion of H$_3$BO$_3$ to B$_2$O$_3$ was observed from XRD studies after calcination and increase in thermal stability was confirmed by thermal analysis.

Table 3.1. Details of the batch mixture considered to optimize the calcination temperature and time

Composition: 30mol%BaO-15CaO-05Al$_2$O$_3$-40SiO$_2$-10B$_2$O$_3$ (6wt%ZnO 6%MgO)		
Sample Code	**Calcination**	
	Time (hrs)	**Temperature (^{0}C)**
P-0	0	non-calcined
P-1	2	300
P-2	4	300
P-3	2	350
P-4	4	350
P-5	2	400
P-6	6	350
P-7	7	350

3.1. Results and Discussion

Calcination time and temperature required to allow the reaction for conversion of the H_3BO_3, used as starting material, to B_2O_3, was optimized as discussed below.

3.2. X-Ray Diffraction

X-ray diffraction studies were carried out on all calcined and non-calcined glass batch mixed powders. Figure 3.1 represents the X-ray diffraction data for the samples calcined by varying the temperature for a constant time interval of 2 hrs. The two peaks observed at 20.8° and 26.6° are assigned to SiO_2 crystal according to ICDD File No. 46-1045. The peaks observed at 34.3°, 36.2°, 47.5° and 56.5° belong to ZnO crystals (ICDD File No. 79-1045). Rest of the peaks corresponding to 31.7°, 39.4°, 50.1° and 68.0° are found to match with H_3BO_3 phase (ICDD File No. 73-2158) for sample P-0. The peak intensity of H_3BO_3 is observed to reduce as the temperature was raised from 300 °C to 350 °C. This is due to the conversion of H_3BO_3 phase to B_2O_3 at that temperature. On further increasing the temperature, the B_2O_3 phase starts developing. The observed B_2O_3 phase was compared with ICDD File No. 76-1655.

When boric acid is heated slowly it converts to HBO_2-III (orthorhombic metaboric acid) (Sevim et al. 2006). When the temperature is below 150 °C boric acid is always found in the metaboric form. But above 150 °C boric acid loses all its water content and turns in to boron oxide B_2O_3. Amorphous boron oxide starts to soften only at 325 °C and crystalline B_2O_3 has a melting point of 450 °C (Sevim et al. 2006). The increase in peak intensity of the borate phase on increasing the temperature from 350 °C to 400 °C may hence be due to the increase in B_2O_3 phase. When the samples were calcined for 4 hrs at 300 °C and 350 °C, as shown in figure 3.2, the peak intensities were found to reduce for samples calcined at 350 °C similar to that observed for 2 hrs. Samples P-1 and P-2 were calcined at 300 °C for 2 hrs and 4 hrs respectively and are shown in figure 3.3. With increasing time, the H_3BO_3 phase has shown considerable growth at 300 °C, but on calcination for 4 hrs the peak intensities were found to reduce as shown in figure 3.2. This indicates that conversion of H_3BO_3 to B_2O_3 may not be complete at 300 °C. Hence 350 °C was considered as optimum temperature for calcination and all samples were then calcined at 350 °C for longer durations.
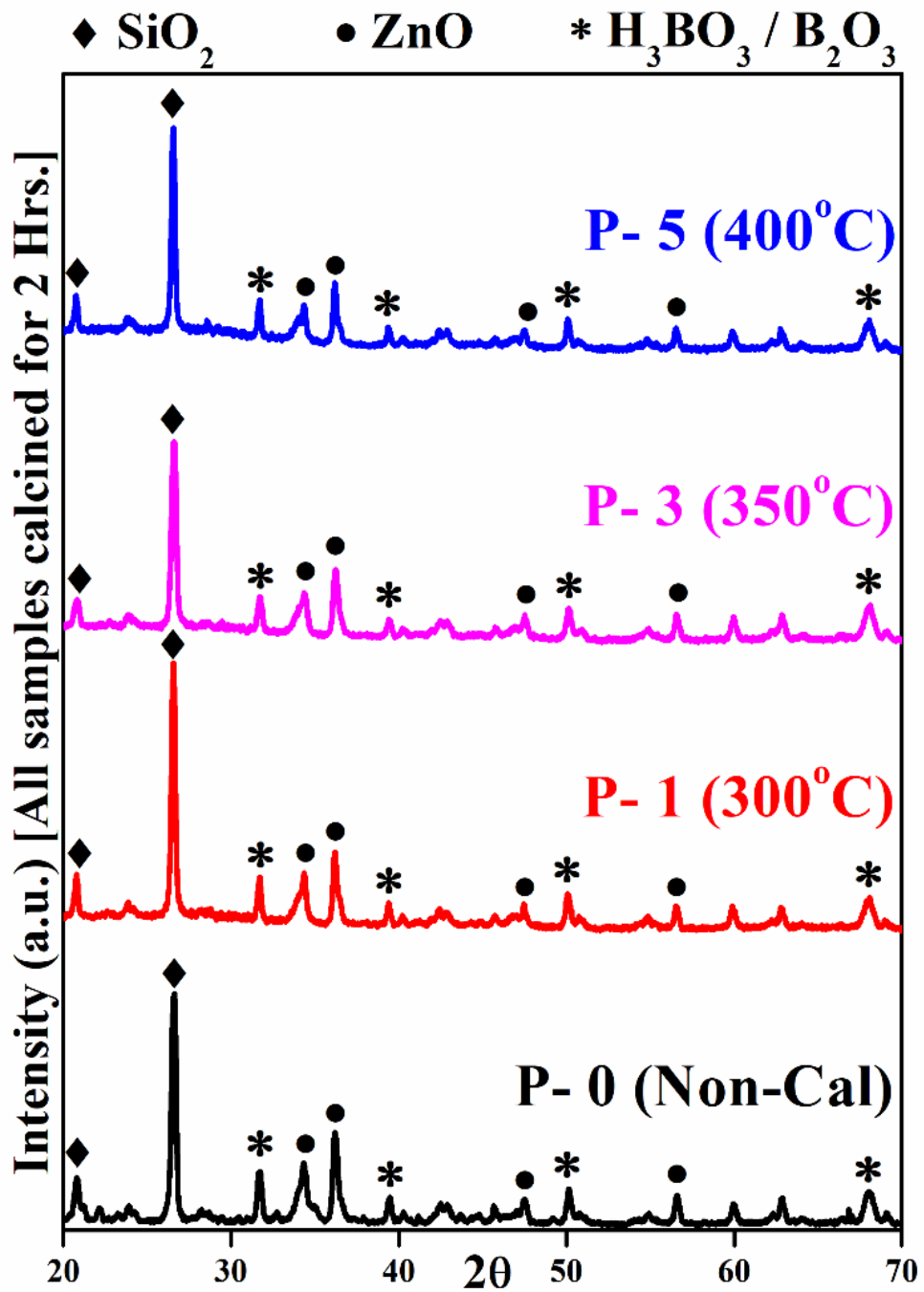
Figure 3.1. Comparison between XRD data of non calcined samples and samples calcined at different temperatures for 2 hours
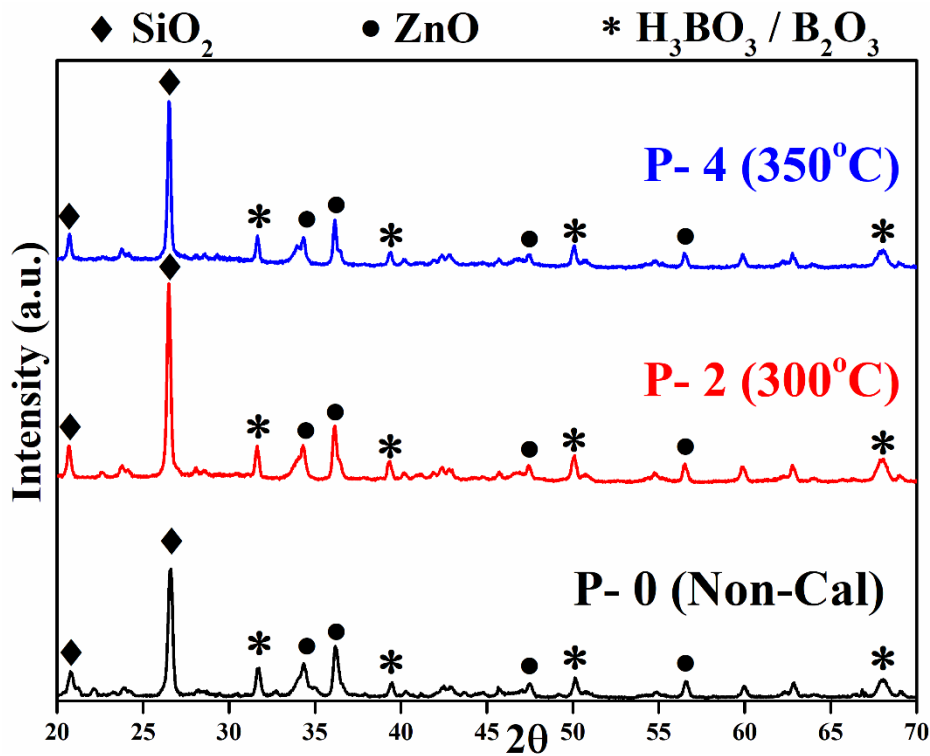
Figure 3.2. Comparison between XRD data of non calcined samples and samples calcined at different temperatures for 4 hours
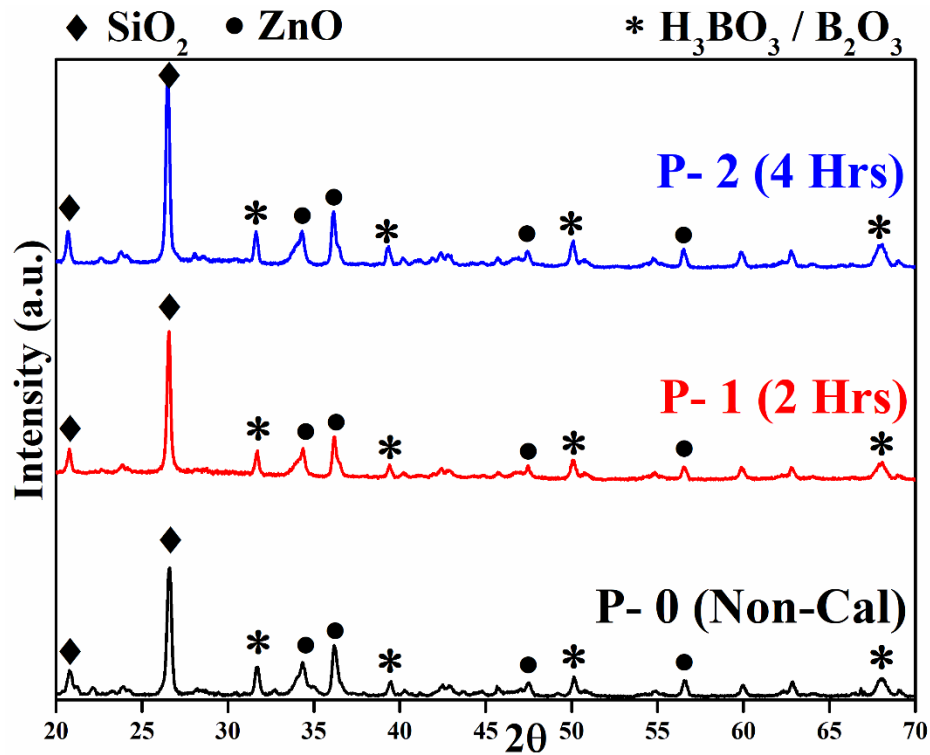
Figure 3.3. Comparison between XRD data of non calcined samples and samples calcined at 300°C for different durations

3.3. Thermo Gravimetric Analysis

Figure 3.4 shows the thermo-gravimetric data for the non calcined sample P-0. The samples were found to exhibit tremendous weight loss at very low temperatures like 132 °C and was found to lose 83% weight, by the time the temperature reaches around 283 °C. But from Figure 3.6 it is evident that the TGA data of the samples calcined at 300 °C for 2 hrs and 4hrs, show minimal weight reduction. For samples P-1 and P-2 the weight does not fall below 98% up to 289 °C and 315 °C respectively. This is due to the reduction of H_3BO_3 and its conversion to B_2O_3 releasing H_2O (Sevim et al. 2006). As temperature was increased from 300 °C to 350 °C the region of stability was found to increase up to 365 °C for sample P-3 as shown in Figure 3.6. Hence the samples were calcined at 350 °C for better conversion results.

On increase in the duration of calcination at 350°C, the stability temperature increased further. This can be observed from the thermo-gravimetric data for sample P-3, P-4, P-6 and P-7 which were calcined at 350°C for 2, 4, 6 and 7 hours respectively, and is shown in figure 3.7. As calcination time increased the samples were found to be stable up to as high as 380°C for sample P-7, as shown in figure 3.7. Calcination at 350°C for 7 hours seems to give the most stable sample with a weight loss of less than 2% up to 380 °C.
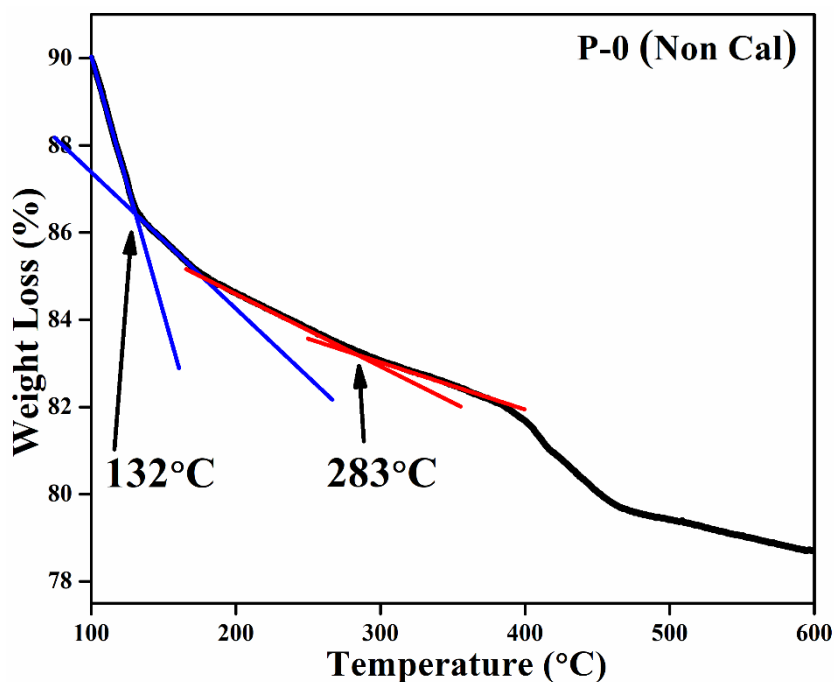
Figure 3.4. TGA for sample P-0
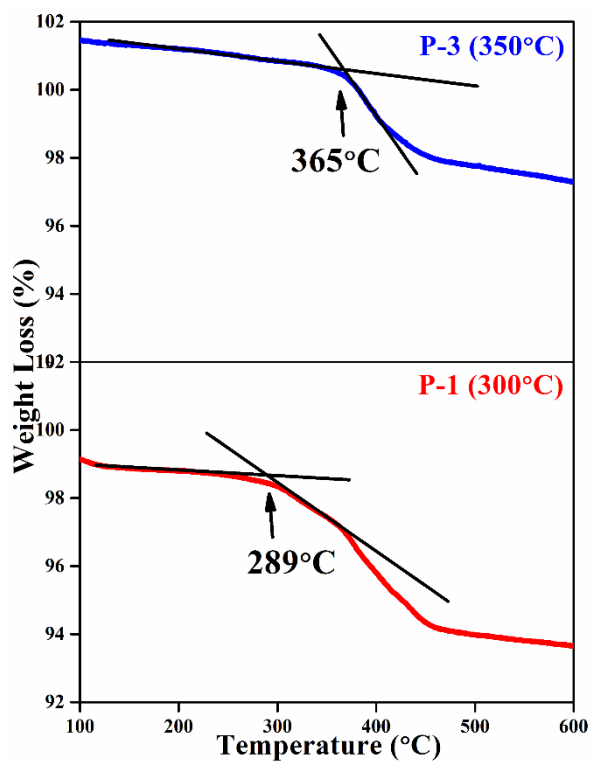
Figure 3.5. TGA for samples calcined at different temperatures for 2 hours
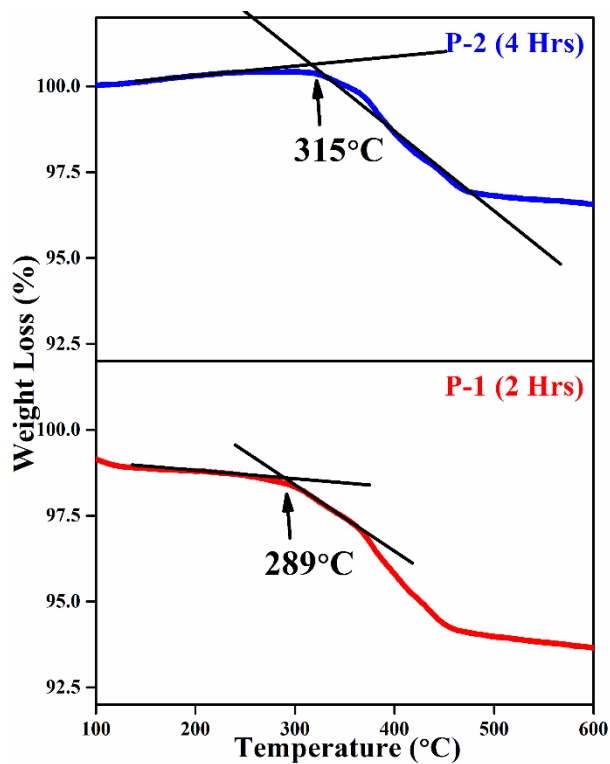
Figure 3.6. TGA for samples calcined at 300 °C for different durations
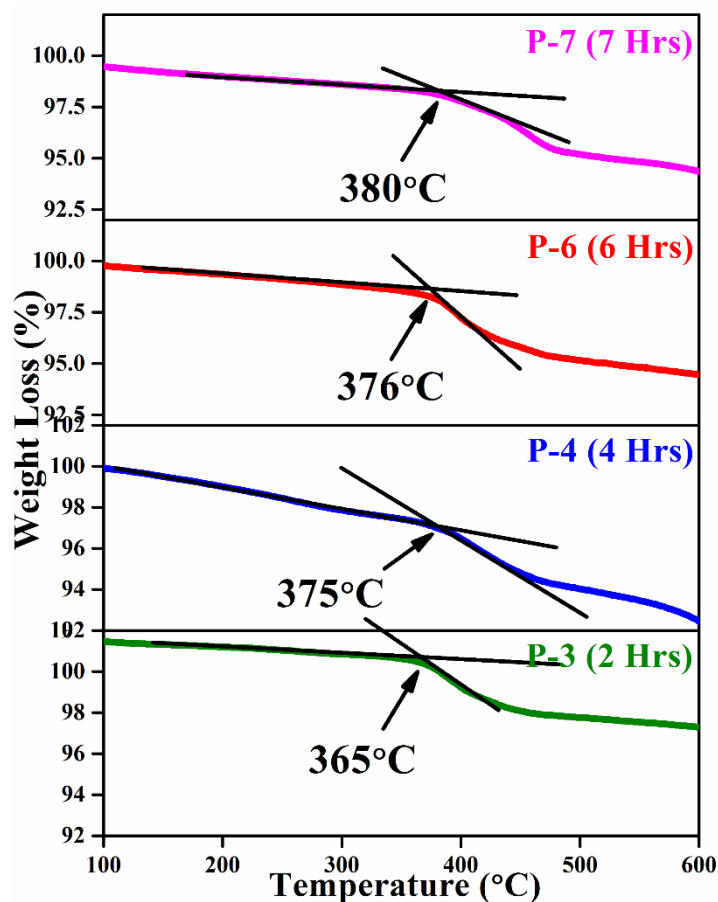
Figure 3.7. TGA for samples calcined at 350 °C for different durations

3.4. Summary

In this chapter the conversion reaction of H_3BO_3 to B_2O_3 in the glass mixture, was monitored with X-ray diffraction and thermo gravimetric analysis. From XRD data the temperature of 350 °C was optimized while from the TGA studies optimum calcination conditions were confirmed and concluded to be 350 °C for a duration of 7 hours. For all samples prepared in this work, these optimum calcination conditions were applied here after.

CHAPTER 4

OPTICAL AND STRUCTURAL PROPERTIES OF BCBS GLASS SYSTEM WITH AND WITHOUT ALUMINA

BaO-CaO-Al$_2$O$_3$-SiO$_2$ (BCAS) glass and their derivatives have gained extreme importance for their high endurance at elevated temperatures and being suitable for various electrochemical applications. Two glass systems, one being 40mol% SiO$_2$-10B$_2$O$_3$-xBaO-(45-x)CaO-5Al$_2$O$_3$ called as BCBSA and another without Al$_2$O$_3$ termed as BCBS were synthesized using melt quenching technique in the present work. Addition of ZnO and MgO as flux helped in melting them at 1300 ^{O}C which is much lower than the usual melting temperature of these glasses (Lara et al. 2004; M. J. Da Silva et al. 2016; Rodríguez-López et al. 2017; Kurama and Saydam 2017). *Density of the quenched glasses was measured by Archimedes method and structural bond vibrations were confirmed through FTIR. UV Visible spectroscopy was used to determine band gap energy and confirm the insulating nature of the synthesized glasses. The samples were isothermally heated at 700 ^{O}C, 800 ^{O}C for 50 hours and at 900 ^{O}C for 50 and 100 hours duration in air to allow the devitrification process to take place. The heat treated samples were analysed by X-ray diffraction to identify the developed phases. Five Al$_2$O$_3$ free samples synthesized at 1300 ^{O}C by regular melt quenching technique were found to be devoid of the monocelsian phase. This is a detrimental phase for high temperature sealant applications as it has a very low coefficient of thermal expansion (CTE). Al$_2$O$_3$ free BCBS glasses, properties of which were investigated for the first time and glasses with low BaO concentrations were found to meet the requirements for high temperature applications as sealants in Solid Oxide Fuel Cell (SOFC).*

4.1. Results and Discussion

Physical, optical and structural properties of the prepared glasses were investigated and the detailed analysis is discussed in this chapter.

4.2. Phase confirmation

XRD data was collected on powdered annealed glasses. Figure 4.1a and 4.1b represent the XRD data of the prepared samples. No crystalline peaks were detected and amorphous phase was observed from X-ray diffractograms of all samples. The

hump observed near 30° is due to the short range order of glass network and typical to all silicate glasses (J E Shelby 2005). The annealed glasses were completely amorphous in nature.
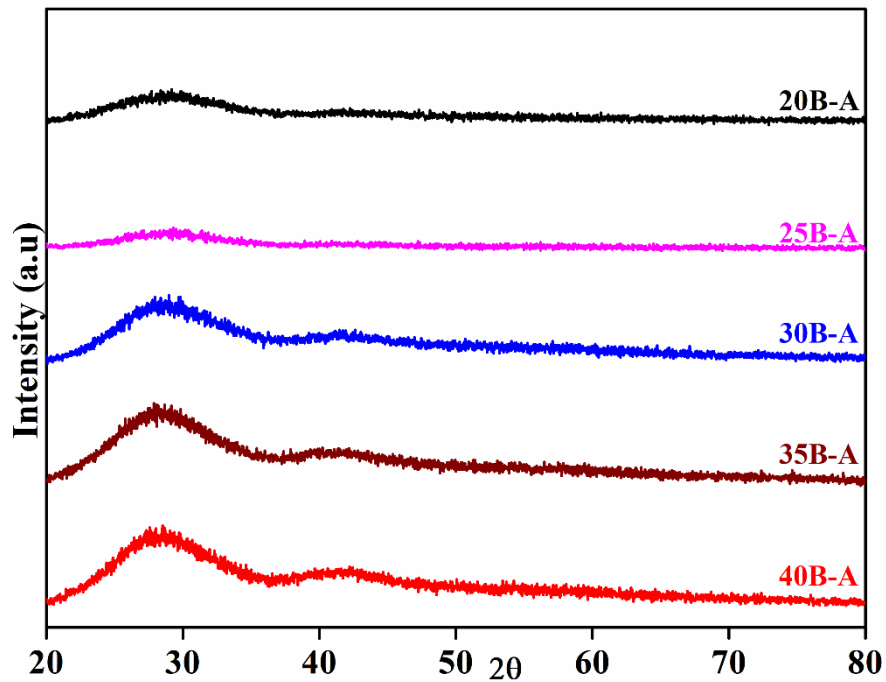
Figure 4.1a. XRD of BCBSA glasses after annealing
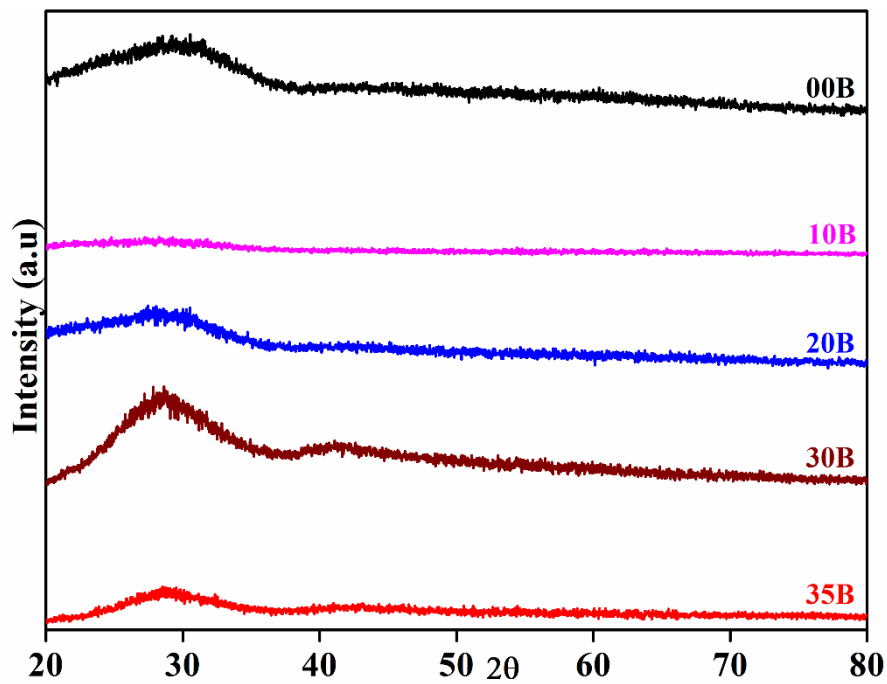
Figure 4.1b. XRD of BCBS glasses after annealing

4.3.Density and molar volume of annealed glasses

Density of the annealed bulk glasses were measured by weighing them in air and immersed in O-Xylene. Density of the samples was found to increase with increase in BaO content in the glass matrix. As shown in table 4.1 sample 40B-A with maximum molar content of BaO (40 mol%) has the maximum density of 3.51 gcm^{-3}. Sample 20B-A with the least BaO content (20 mol%) exhibits the minimum density of 3.18 gcm^{-3} among the samples containing Al_2O_3. Density was observed to depend on concentration of BaO even for the Al_2O_3 free samples. 30B and 30B-A, the glasses with and without Al_2O_3 having equal BaO content showed similar densities (3.36 gcm^{-3} and 3.33 gcm^{-3} respectively) as observed for 35B and 35B-A (3.47 gcm^{-3} and 3.43 gcm^{-3} respectively). This leads to the conclusion that Al_2O_3 is not affecting the density of these glasses. In case of sample 20B, 10B and 00B, the densities were found to drop significantly and become minimum for the BaO free sample 00B (2.89 gcm^{-3}). These trends are clearly evident from Figure 4.2a and 4.2b representing the density and molar volume of the prepared glasses as a function of BaO concentration. The measured densities, molar volumes and molecular weights of the glasses are listed in table 4.1.

Table 4.1. Physical properties of the prepared glasses

Sl. No.	Sample	Molecular Wt. (gmol^{-1})	Density (ρ) (gcm^{-3})	Molar Volume (V_m) (cm^{3}mol^{-1})
1	40B-A	100.23	3.5077 ($\pm$0.0034)	28.573
2	35B-A	95.36	3.4273 ($\pm$0.0054)	27.825
3	30B-A	90.49	3.3292 ($\pm$0.0047)	27.181
4	25B-A	85.64	3.2602 ($\pm$0.0035)	26.268
5	20B-A	80.78	3.1782 ($\pm$0.0041)	25.416
6	35B	93.07	3.4652 ($\pm$0.0036)	26.858
7	30B	88.21	3.3639 ($\pm$0.0022)	26.222
8	20B	78.48	3.2276 ($\pm$0.0025)	24.317
9	10B	68.76	3.0571 ($\pm$0.0001)	22.492
10	00B	59.03	2.8929 ($\pm$0.0003)	20.407

BaO is a heavy alkaline earth metal with molar mass 153.32 gmol^{-1}. It has the highest ionic radius among all other alkaline earth metals. When alkaline earth metals are introduced in to the glass network, it breaks the bond between oxygen atoms and other network formers like silicon or borate groups. This increases the number of non-bridging oxygens (NBO) in the glass network (J E Shelby 2005; S. F. Wang et al. 2017). But introduction of such a large and heavy alkaline earth metal ion increases the mass and thereby the density of the material significantly. In case of the Al_2O_3 free samples also, similar variation in density is observed with increasing BaO content. This indicates that Al_2O_3 has negligible effect on the density of the system. It can be stated that Al_2O_3 has insignificant effect on the density of the sample and it is dominated by alkaline earth metals. Densities exhibited by these samples are in acceptable range of data reported by earlier researchers for SOFC application (S. F. Wang et al. 2009, 2017; M. Kaur et al. 2017).
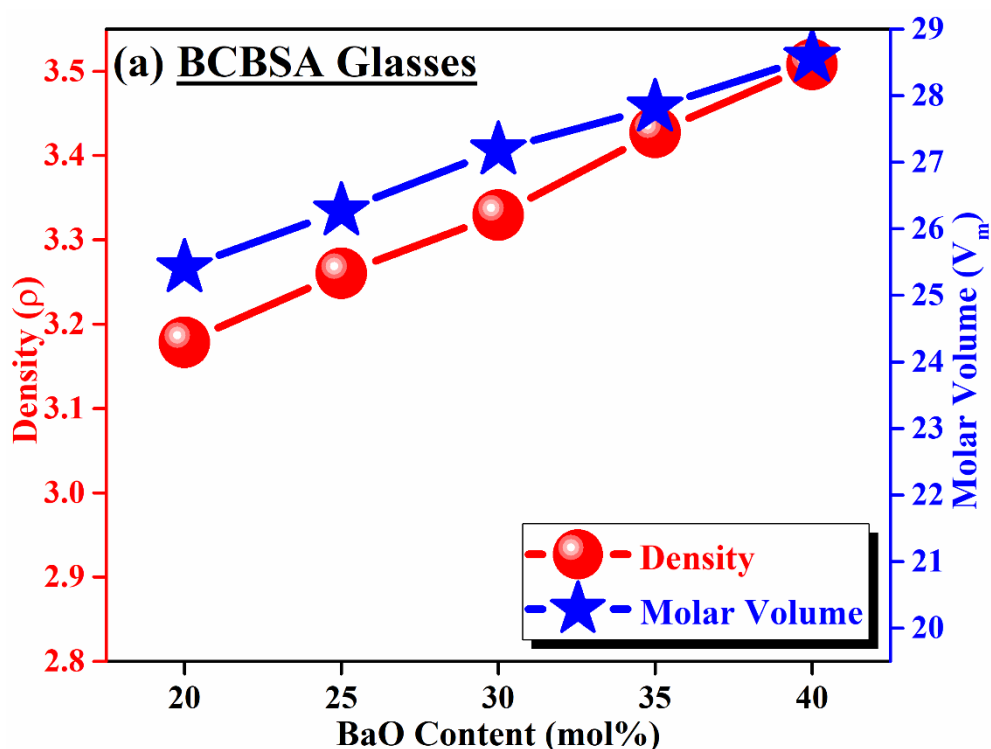
Figure 4.2a. Density and molar volume as a function of BaO concentration in BCBSA glasses
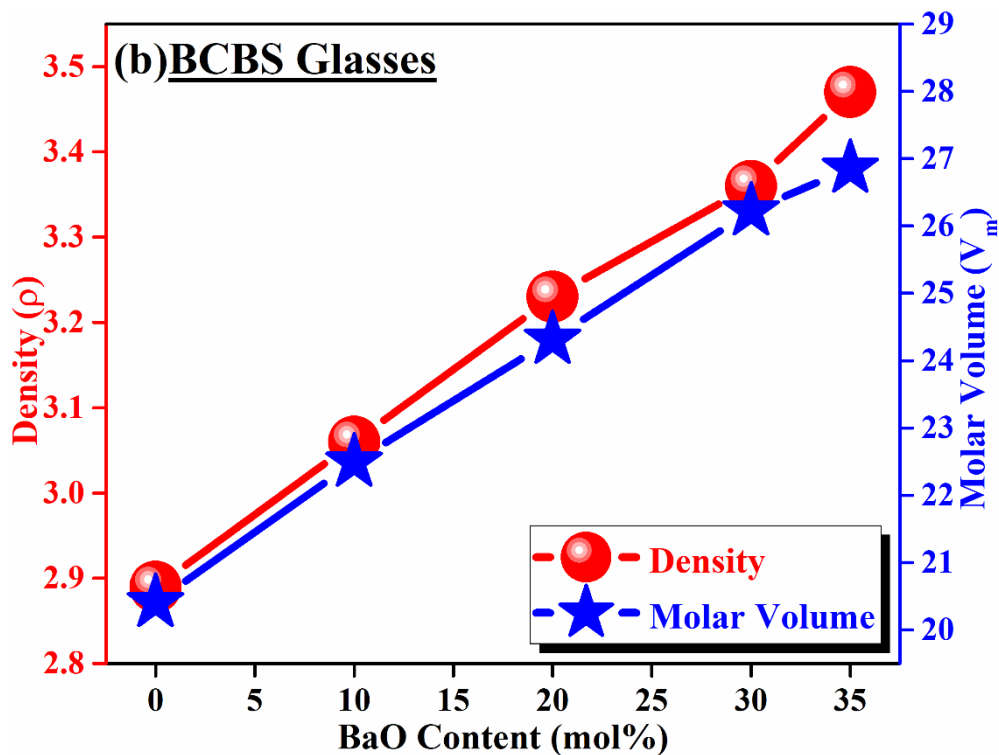
Figure 4.2b. Density and molar volume as a function of BaO concentration in BCBS glasses

Since BaO is a heavy metal with high molecular weight, increasing content of BaO must increase the molar volume of the glass. This is also clearly evident from Figure 4.2a and 4.2b. The molar volume was found to increase with increase in concentration of BaO in the glasses with and without Al_2O_3.

4.4. Fourier Transformed Infra-Red (FTIR) Spectra

FTIR transmission spectra of all the prepared samples were collected in the wave number range of 400-1500 cm^{-1}. The FTIR spectra of all the samples are shown in figures 4.3a and 4.3b. None of the samples are found to exhibit sharp well defined features which indicates that the general disorder in the network is due to the wide distribution of Q^n units, where n denotes the number of bridging oxygens (A. Goel et al. 2008; Hong et al. 2008; Tulyaganov 2016). Formation of more Q^n units with lower order of n, leads to increase in the disorder in the matrix and hence causes reduction in transmission (J E Shelby 2005; Tulyaganov 2016).

The spectrum can be divided into five bands. The first band observed in the present work, around 400-600 cm^{-1} (centred at 510 cm^{-1}) represents bending vibrations of Si-O-Si and Si-O-Al linkages (Sasmal et al. 2014; A A Reddy, Tulyaganov 2013). For the samples containing Al_2O_3 in the network (Figure 4.3a) this band at 510 cm^{-1}, was found to shift towards the lower wave number. This indicates the formation of Q^1 and Q^2 units (A. Goel et al. 2008). The short band in the range of 600-800 cm^{-1} (centred at 705 cm^{-1}) represents Al-O stretching vibrations in four-fold tetrahedral coordination and B-O stretching vibrations in BO_4 structural units (Sasmal et al. 2014; Hong et al. 2008). The wide band that lies in the 800 – 1200 cm^{-1} range (centred at 985 cm^{-1}) represents stretching vibrations of silica in SiO_4 tetrahedron with varying number of bridging oxygen (A A Reddy, Tulyaganov 2013). The band in the range 1300 – 1500 cm^{-1} represents borate vibrations. In the present study two distinct transmissions were observed in this range one centred at 1245 cm^{-1} and the other centred at 1405 cm^{-1}. These bands represent the B-O stretching vibrations in BO_3 triangles and in BO_4 tetrahedral coordination (Sasmal et al. 2014; Ferreira et al. 2008; Ferrari et al. 2010; Science, Rutgers, and Spanish 2013; Hong et al. 2008). Since concentration of B_2O_3 was not varied in the system, these bands show weak but relatively uniform transmissions for all the BCBSA glasses.

For the BCBS glasses the band centred at 510 cm^{-1} shows the similar shift towards lower wave number, indicating formation of Q^1 and Q^2 units, for lower concentrations of BaO. The transmission band near 705 cm^{-1} in BCBSA glasses represents both Al-O and B-O vibrations, but for the BCBS glasses they represent only B-O stretching vibrations (Sasmal et al. 2014; Hong et al. 2008). That is why the band is sharper in Figure 4.3a which contains Al_2O_3. Further reduction of BaO leads to even lesser transmission as observed for 20B, 10B and 00B. Presence of Al_2O_3 in the network causes formation of AlO_4 units which in the presence of other modifiers like alkaline earths form localized bonds with the cation, which is stronger than the bond between cation and NBO (Ashutosh Goel et al. 2009). Hence transmission of the Al_2O_3 free BCBS samples, were found to be weaker than the BCBSA glass system. The wide band centred at 985 cm^{-1}, representing the SiO_4 tetrahedron was found to exhibit very low transmission for 20B, 10B and 00B with low BaO concentrations. The bands near 1245

cm^{-1} and 1405 cm^{-1} representing B-O-B vibrations show consistent transmission as seen in the BCBSA system. FTIR spectra confirmed the existence of all the vibration bands expected to be present in BCAS glass.
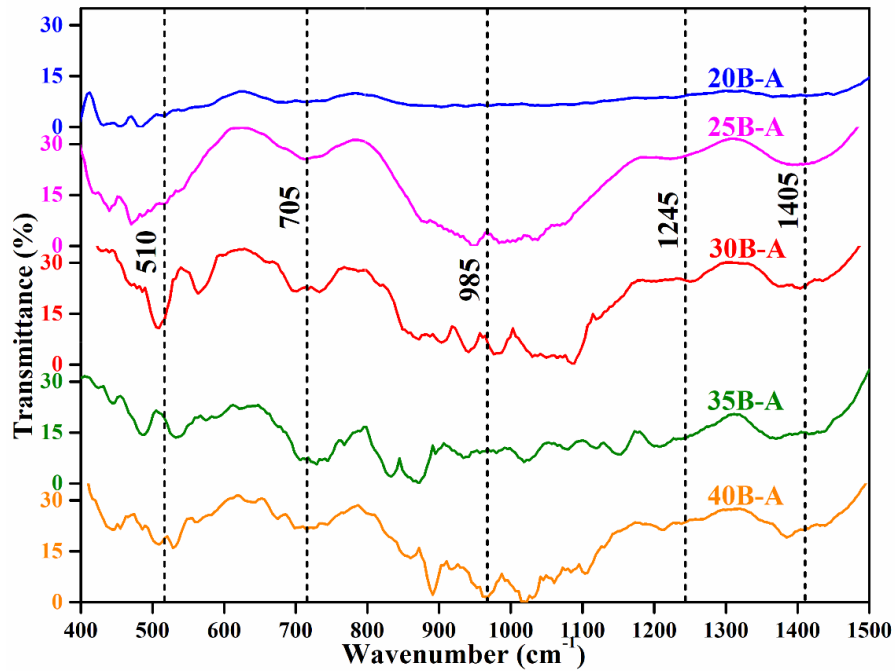
Figure 4.3a. FTIR data of BCBSA glasses
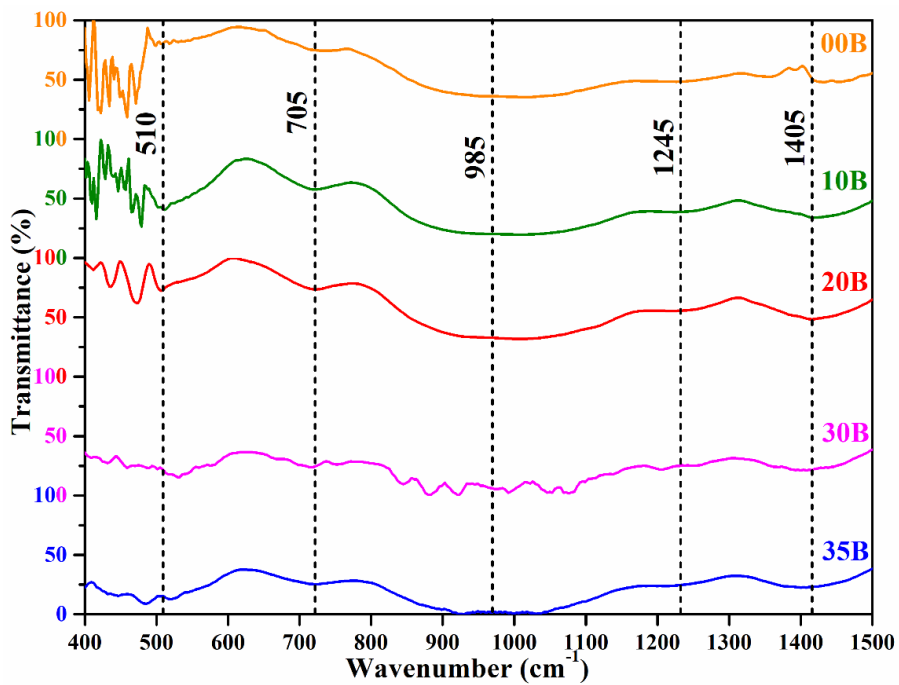
Figure 4.3b. FTIR data of BCBS glasses

4.5. Optical Properties

4.5.1. U V Visible Spectroscopy

Figure 4.4a and 4.4b represent the absorption spectra of BCBSA and BCBS glass series. The UV Visible spectra shows that both the glass series are transparent to visible range and absorbs the UV spectra. Absorption edge in the BCBSA series does not show much shift with reduction of BaO content from 40 mol% in 40B-A to 20 mol% in 20B-A, as observed from figure 4a. From the BCBS series, shown in figure 4b, it is observed that 30B, 35B and 20B exhibit the absorption edge in the range, same as BCBSA series in the range of 345 – 348 nm. Among these three samples 20B bears the lowest BaO content respectively, of 20 mol%. But 10B and 00B, with 10 mol% BaO and without BaO content exhibit absorption edge at a higher wavelength, near 353 nm. This leads to the conclusion that since the samples of the BCBSA series and 30B, 35B and 20B of BCBS series show absorption edge in the same range, the content of Al_2O_3 has minimum effect on the shift of the band edge. Absorption of UV spectrum shifts to higher wavelengths below 20 mol% of BaO content in the BCBS glasses.
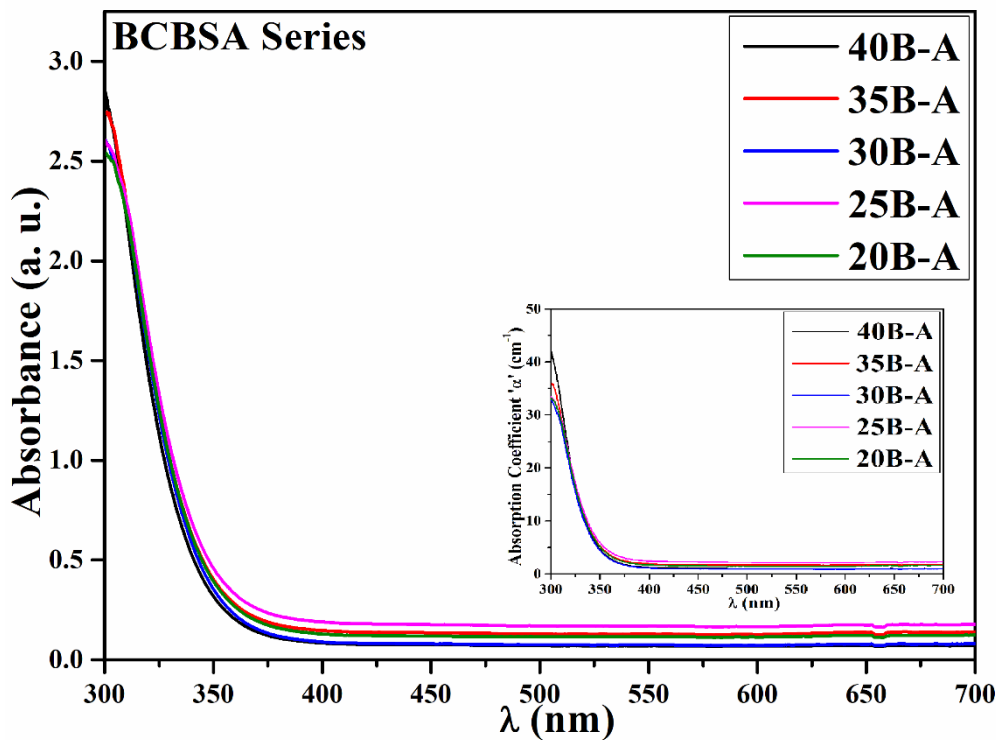
Figure 4.4a. Absorption Spectra of BCBSA Glass, inset shows variation of α with wavelength
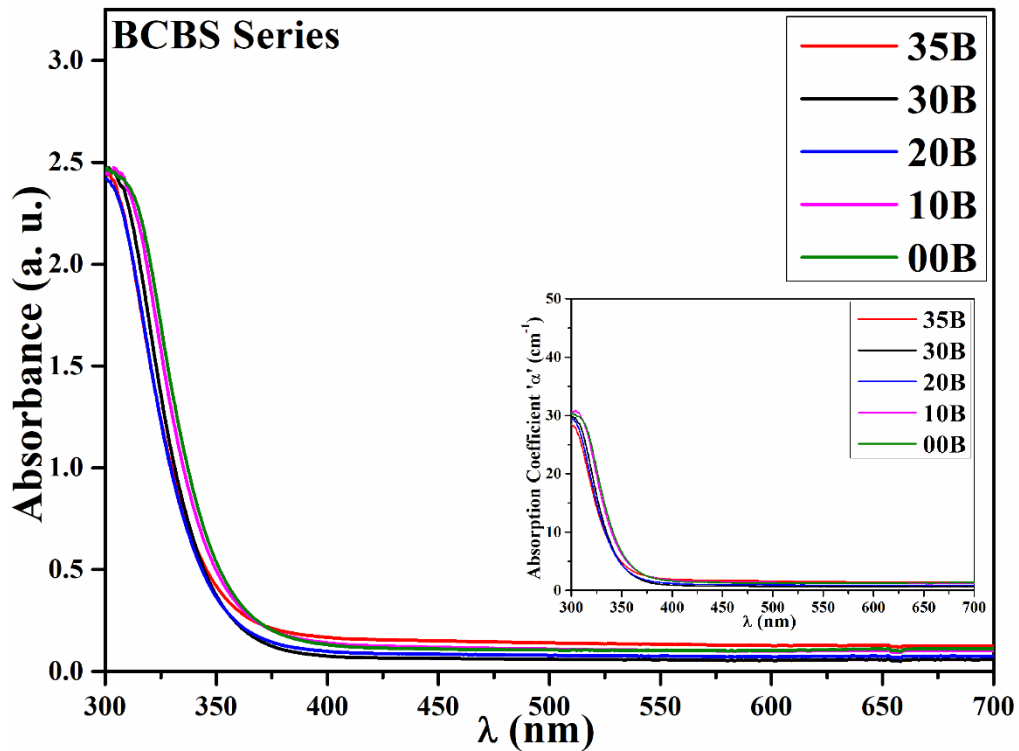
Figure 4.4b. Absorption Spectra of BCBS Glass, inset shows variation of α with wavelength

Similar observations were made from the wavelength versus absorption coefficient 'α' graphs inset in figure 4.4a and 4.4b. No shift in α was observed in the samples 40B-A to 20B but shift to higher wavelengths was observed in sample 10B and 00B. This is because BaO being a heavy cation with large radius increases the number of non-bridging oxygens (NBOs) in the glass matrix, which increases the disorder in the structure of the sample. Reduction of BaO reduces the number of NBOs in glass. Shift of the absorption edge towards the longer wavelength of the UV spectra, which is also called the red shift, corresponds to the reduction of NBOs in the glass matrix (Gautam and Yadav 2013). The reduction of BaO in the composition also reduces the ionic nature of the network bonds and establishes a stronger covalent type bonding. Covalent bonds have lower energies as compared to the ionic bonds and hence the transmission corresponds to longer wavelengths according to the formula $E_g = h\upsilon = hc/\lambda$. This explains the shift of the band gap towards higher wavelength with reduction of BaO in the composition.

Figure 4.5a and 4.5b show the $(\alpha h\upsilon)^{1/2}$ vs $h\upsilon$ diagram for BCBSA and BCBS glass series. This is derived from the Davis-Mott formula given in equation 2.4.
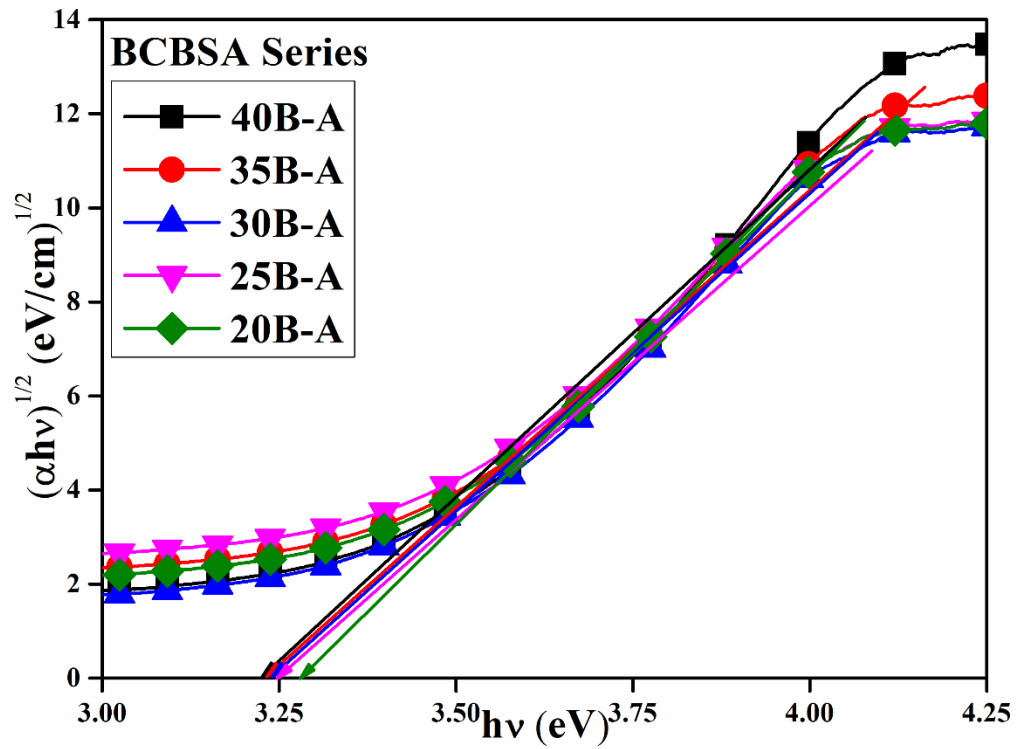
Figure 4.5a. $(\alpha h\upsilon)^{1/2}$ vs $h\upsilon$ plot for BCBSA glass series
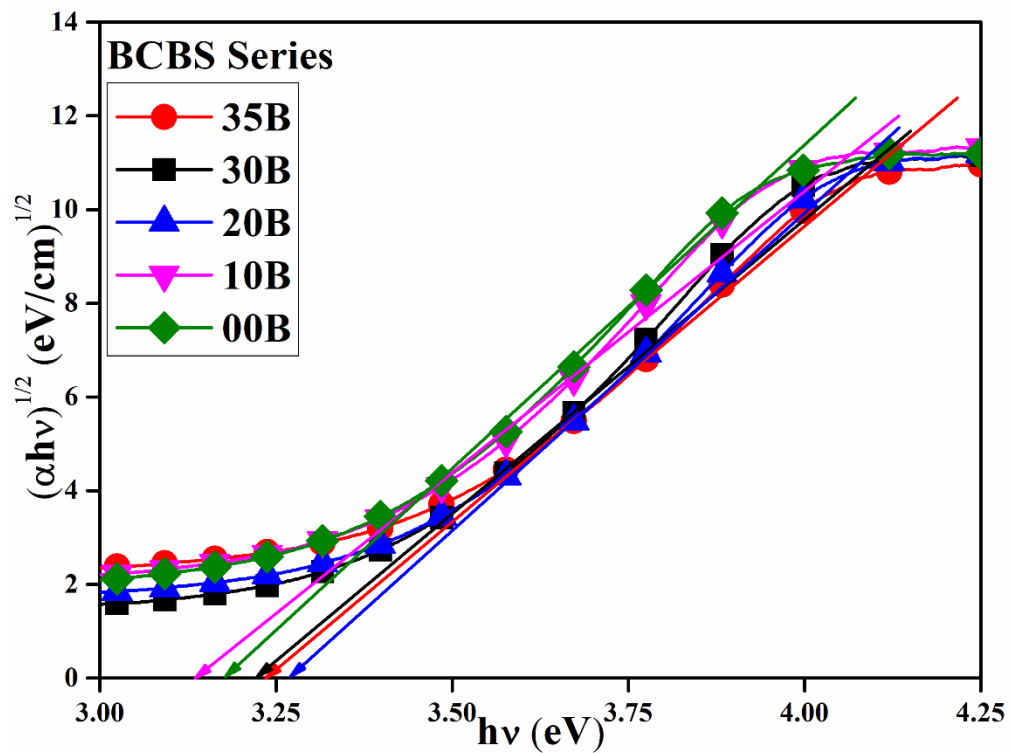
Figure 4.5b. $(\alpha h\upsilon)^{1/2}$ vs $h\upsilon$ plot for BCBS glass series

The band gap energies of all the samples are listed in table 4.2. Samples 10B and 00B with BaO content less than 20 mol% were found to exhibit minimum band gap energy. This is in agreement with the reduction of density of the samples and absorption curve where red shifted absorption edge for 10B and 00B indicates increase in number of bridging oxygens and low energy covalent bonding in the matrix (Gautam and Yadav 2013).

Figure 4.6a and 4.6b represents the ln α versus hv graph drawn in accordance to equation 2.6. The values of Urbach energy for all samples are also listed in table 4.2. Though the E_u for all samples lies in a very close range, the samples 10B and 00B exhibit the lowest value, which is in agreement with the argument of having lowest disorder in the matrix in case of samples below 20 mol% BaO content. This data supports the reduction of density, reduction of the number of NBOs and red shift of the absorption spectra of the samples 10B and 00B.

Table 4.2. Band Gap Energy and Urbach Energy of BCBSA and BCBS glasses

BCBSA Series				BCBS Series			
Sample	Sample Thickness (mm)	E_g (eV)	E_u (eV)	Sample	Sample Thickness (mm)	E_g (eV)	E_u (eV)
40B-A	1.566	3.22	0.26	**35B**	1.914	3.23	0.26
35B-A	1.760	3.23	0.26	**30B**	1.980	3.25	0.26
30B-A	1.843	3.23	0.26	**20B**	1.888	3.27	0.25
25B-A	1.796	3.25	0.26	**10B**	1.844	3.17	0.24
20B-A	1.770	3.27	0.25	**00B**	1.872	3.15	0.24
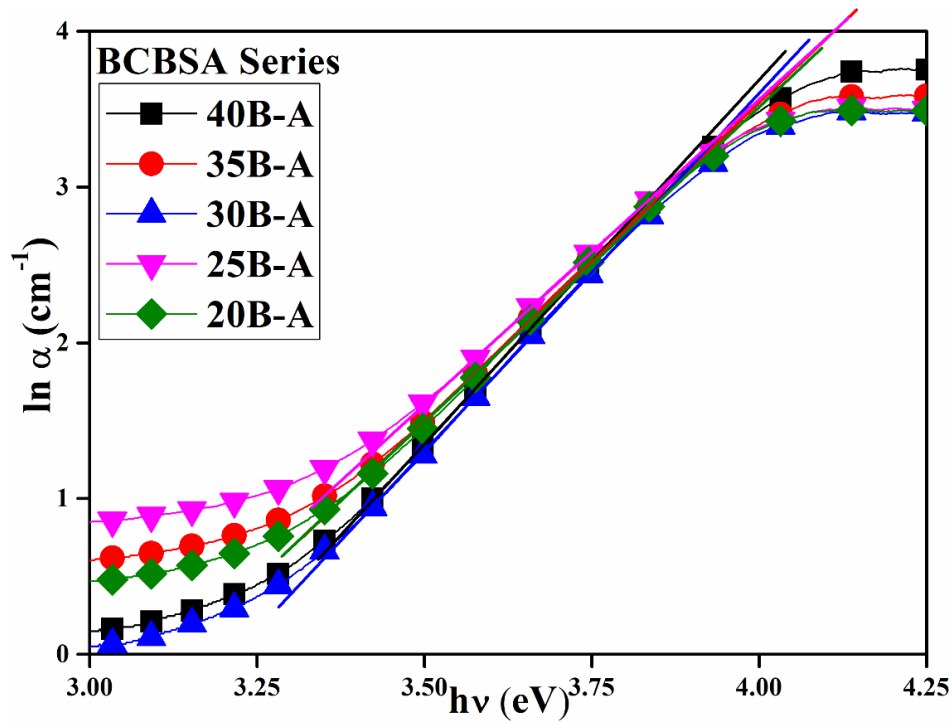
Figure 4.6a. Variation Urbach Energy w.r.t. Photon Energy
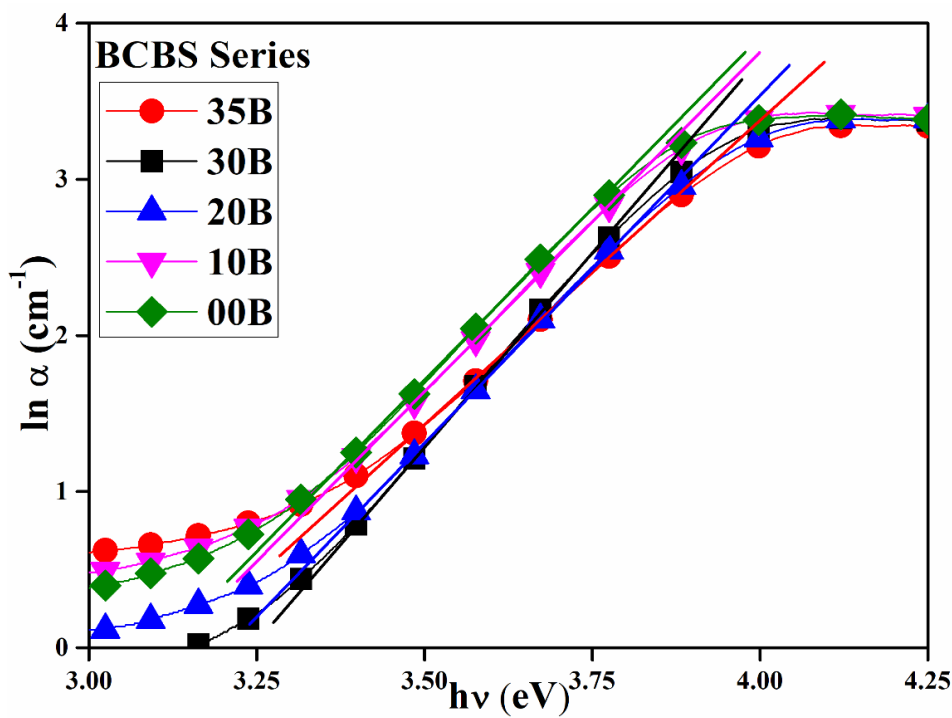
Figure 4.6b. Variation of Urbach Energy w.r.t. Photon Energy

The variation of E_g and E_u with the BaO content for both BCBS and BCBSA glasses are shown in figure 4.7. Shadia et. al. in 2013 reported that E_g increases as E_u reduces (J Shadia and Ahmad-bitar 2013). In the present investigation not much variation in E_g and E_u was observed for compositions above 30 mol% of BaO content. In samples with 20 mol% BaO the E_g was observed to increase and E_u was observed to reduce as compared with the samples with 30 mol% BaO and above. Below 20 mol% BaO content i.e. for samples 10B and 00B both E_g and E_u were observed to reduce, though the reduction in E_u value is very small. This may be due to removal of the large cation from the matrix, leading to a sudden rise of bridging oxygen, and hence reducing the band gap energy (Gautam and Yadav 2013). At the same time reduction of density and disorder in the material cause the reduction of the Urbach energy of the other compositions.
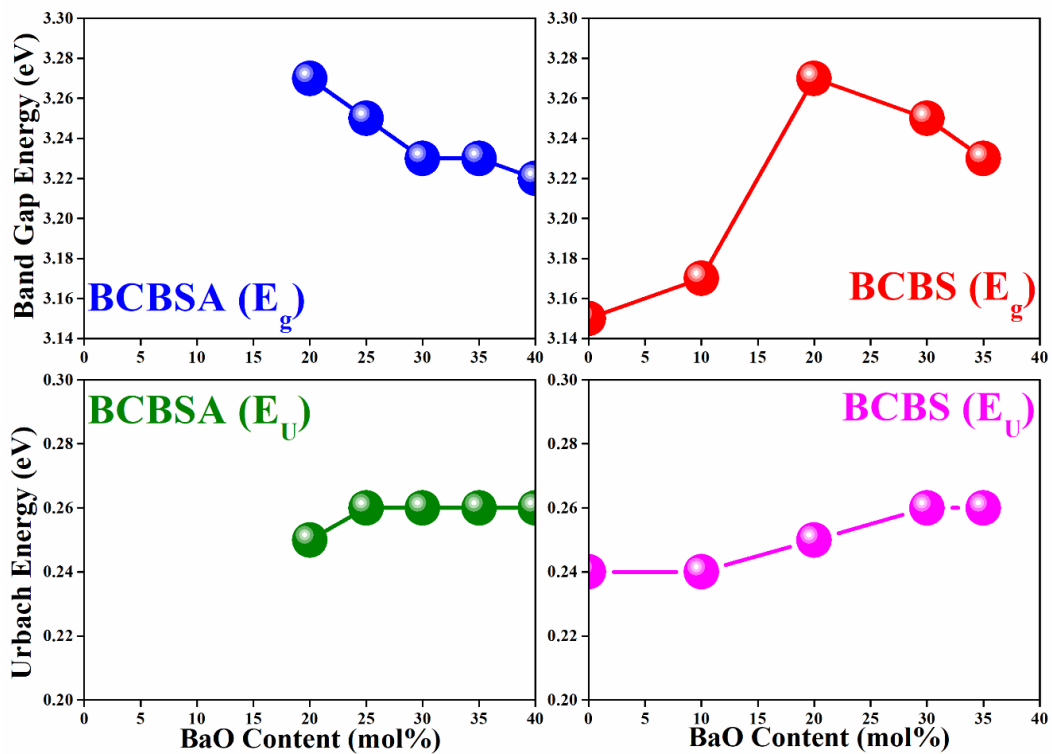
Figure 4.7. Relation between E_g and E_u for all samples

Table 4.3. Optical Properties of BCBS and BCBSA glasses

	BCBSA Series				BCBS Series		
	Refractive Index (n)	R_m/V_m	$M = 1 - (R_m/V_m)$		Refractive Index (n)	R_m/V_m	$M = 1 - (R_m/V_m)$
40BA	1.6932	0.3836	0.6164	**35B**	1.6933	0.3836	0.6164
35BA	1.6928	0.3834	0.6166	**30B**	1.6945	0.3842	0.6158
30BA	1.6933	0.3836	0.6164	**20B**	1.6922	0.3832	0.6168
25BA	1.6923	0.3832	0.6168	**10B**	1.6920	0.3831	0.6169
20BA	1.6932	0.3836	0.6164	**00B**	1.6937	0.3838	0.6162

4.5.2. Refractive index and Metallization Criterion

The refractive indices 'n' of all the samples, measured using Abbe Refractometer, is listed in table 4.3. All the samples were found to exhibit the refractive indices in a very narrow range of values near 1.69. in order to evaluate the metallization tendency of the samples the Lorentz Lorenz equation (Dimitrov and Komatsu 2010) given as equation 2.7, in chapter 2 of this thesis was used.

The calculated values of R_m/V_m are listed in table 4.3. On the basis of this theory an estimation of metallic or insulating behaviour of the material can be drawn using equation 2.8. The values of M are also listed in table 4.3. All samples exhibit value of M more than 0.61. This confirms that all samples are perfect insulators, which is in agreement with the band gap of each sample listed in table 4.2, as they lie in the typical range of insulators.

4.6. Isothermal Heat Treatment and crystallization studies

All synthesized bulk samples were ground to fine powder and were subjected to heat treatments at elevated temperatures to study their crystallization kinetics. Samples were found to crystallize partially at 700 °C in the preliminary work on heat treatment of these glasses (figure not shown). The diffraction peaks corresponding to crystallization phases observed were well defined for the samples heat treated at 800 °C for 50 hours. Appearance of a few extra peaks on heat treating the samples at 900

$^\text{O}$C suggests that crystallization is not complete at 800 $^\text{O}$C. X-ray diffractograms for the samples heated at 800 $^\text{O}$C for 50 hours are shown in figure 4.8a.
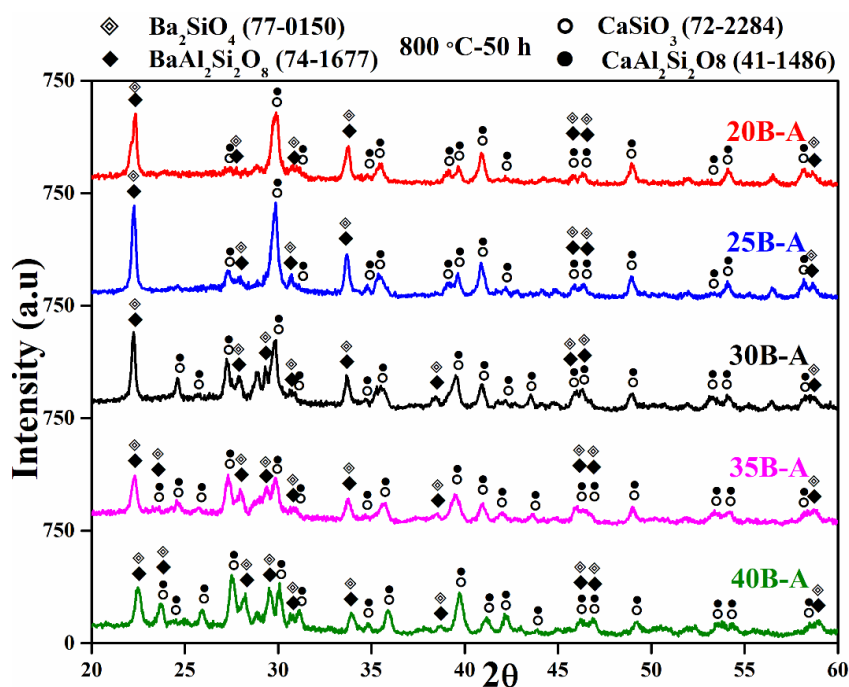
Figure 4.8a. XRD of BCBSA glasses heated at 800 $^\text{O}$C for 50 hours
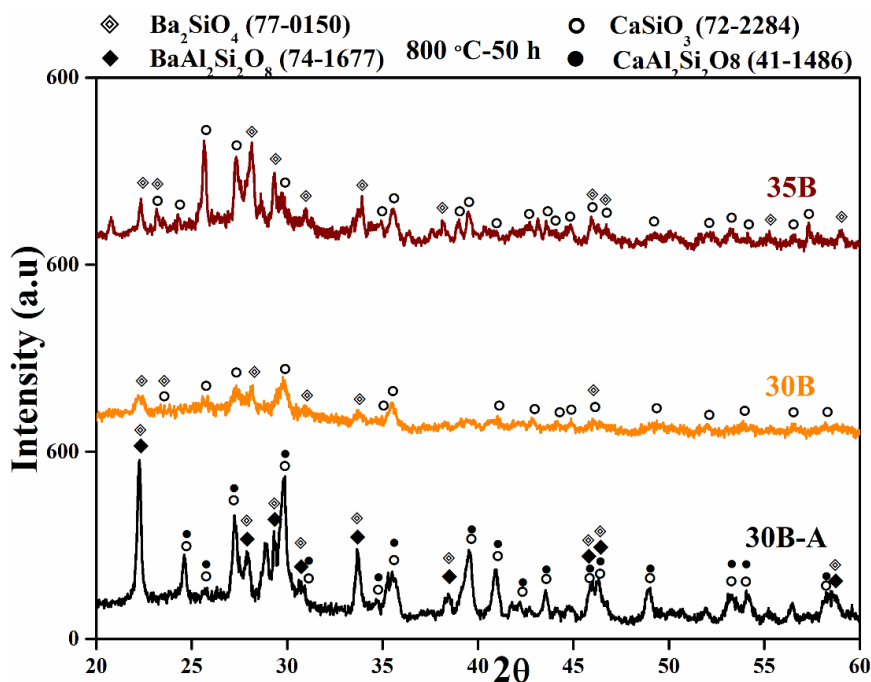
Figure 4.8b. XRD of BCBS glasses and 30B-A heated at 800 $^\text{O}$C for 50 hours

Wollastonite ($CaSiO_3$; ICDD 72-2284) and Anorthite ($CaAl_2Si_2O_8$; ICDD 41-1486) phases were found to be the major phases present in the compositions involving Al_2O_3 and wollastonite was found to be the predominant phase in the two Al_2O_3 free compositions, 30B and 35B. The crystalline structure of the Al_2O_3 free samples are compared with the base composition 30B-A at 800 °C as shown in Figure 4.8b. Barium silicate ($BaSiO_3$; ICDD 77-0150) and mono celsian phases ($BaAl_2Si_2O_8$; ICDD 74-1677) are also found to exist as minor phases in the samples containing Al_2O_3. The diffraction peaks of silicate and alumina-silicate of calcium and barium species are found to overlap. These silicate and alumina-silicate phases were distinguished through comparison between the diffractograms of glasses with and without Al_2O_3. The diffractograms of Al_2O_3 free glasses showed only silicate phases of calcium and barium species with relatively lower intensity. On removal of Al_2O_3 from the composition the samples showed a glassy nature which can be seen as a broad hump appearing near 30° in sample 30B and 35B, which are not observed in rest of the samples heated at 800 °C for 50 hours. On removal of Al_2O_3, the glass network may break giving rise to amorphous nature (Kim, Choi, and Yang 2015), which is responsible for appearance of the hump near 30° in samples 30B and 35B (figure 4.8b).
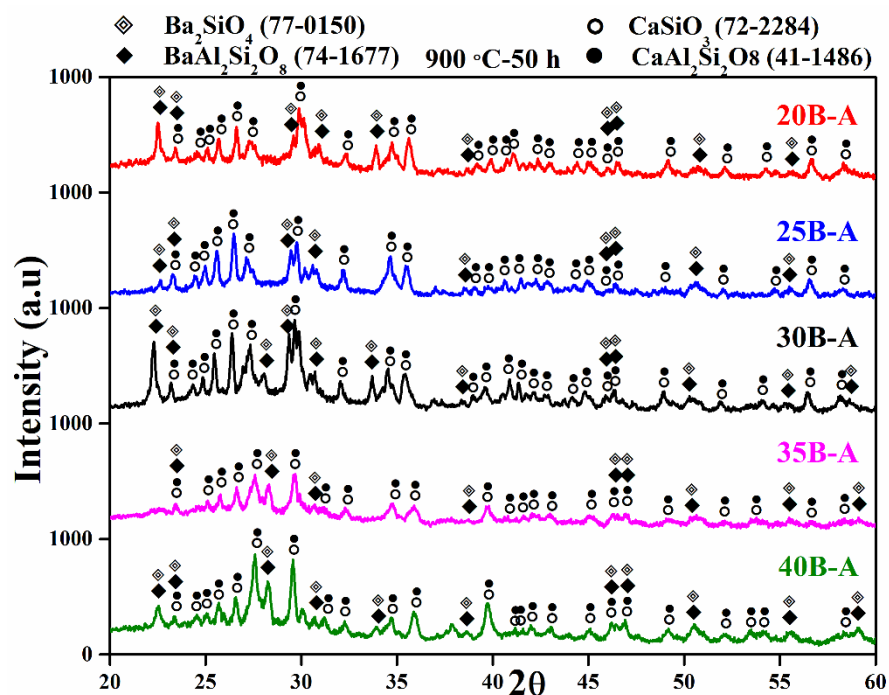
Figure 4.9a. XRD of BCBSA glasses heated at 900 °C for 50 hours
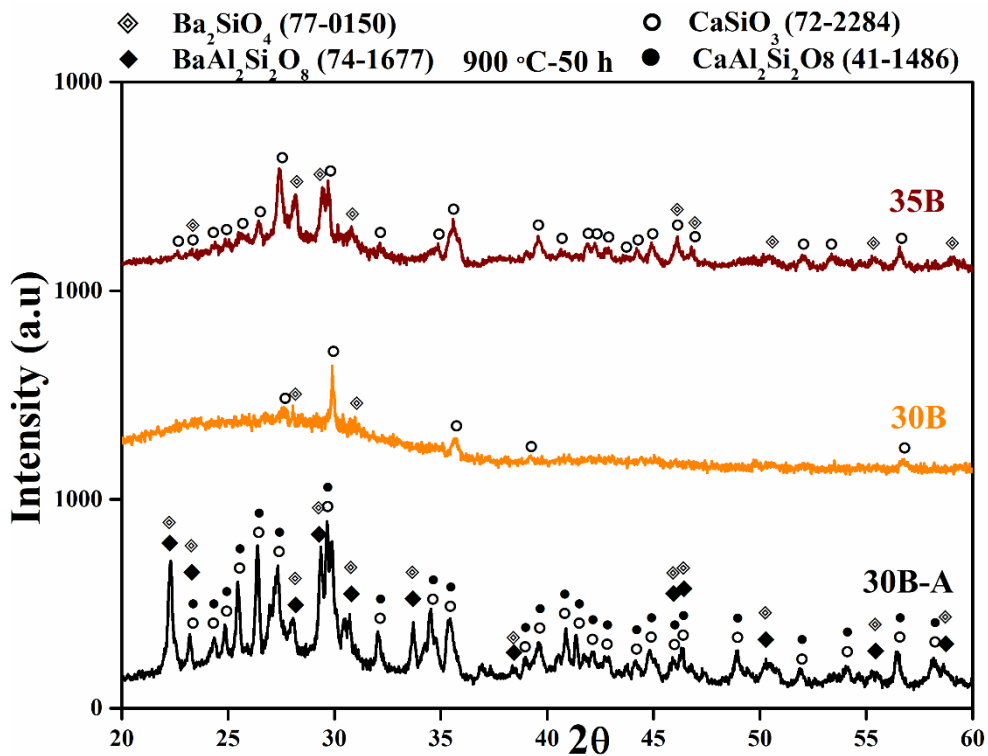
Figure 4.9b. XRD of BCBS glasses and 30B-A heated at 900 °C for 50 hours

The samples heat treated at 900 °C for 50 hours are shown in Figure 4.9a and 4.9b. These graphs show a number of additional peaks that are not present at 800 °C. Wang et. al. (2016) reported that content of crystalline phases increases with increasing temperature, for strontium based glasses (X. Wang et al. 2016). Similarly in this case additional peaks corresponding to Ba and Ca containing phases, were observed. Most of the extra peaks were identified as anorthite and wollastonite phases. This shows devitrification of these Ba and Ca containing phases are accelerated at 900 °C, as in agreement with Wang et al. (2016) (X. Wang et al. 2016). Though barium silicate and mono celsian were found in the samples containing Al_2O_3 as minor phases, the intensity of the barium phases below 30 mol% concentration of BaO were observed to be very low. This is in agreement with Ghosh et. al. (2010) who reported that 30 mol% BaO in the composition reduces the activation energy of crystallization (E_a) that helps in devitrification (Ghosh, Sharma, et al. 2008). Below 30 mol% concentration barium phases are expected to crystallize poorly. Intensities of the crystalline peaks exhibited by glasses 20B-A and 25B-A were hence observed to reduce. The glassy hump observed near 30° for the samples heated at 800 °C, were also found to exist in the

diffractograms of samples heated at 900 ^{O}C for 50 hours. They are more prominent for the samples with low BaO concentration because these compositions below 30 mol% BaO content have high activation energy of crystallization (Ghosh, Sharma, et al. 2008). It is clearly observed from Figure 4.9b, that on removal of Al_2O_3, the glassy hump becomes prominent in 35B and even more prominent for 30B which has lower BaO content than 35B.
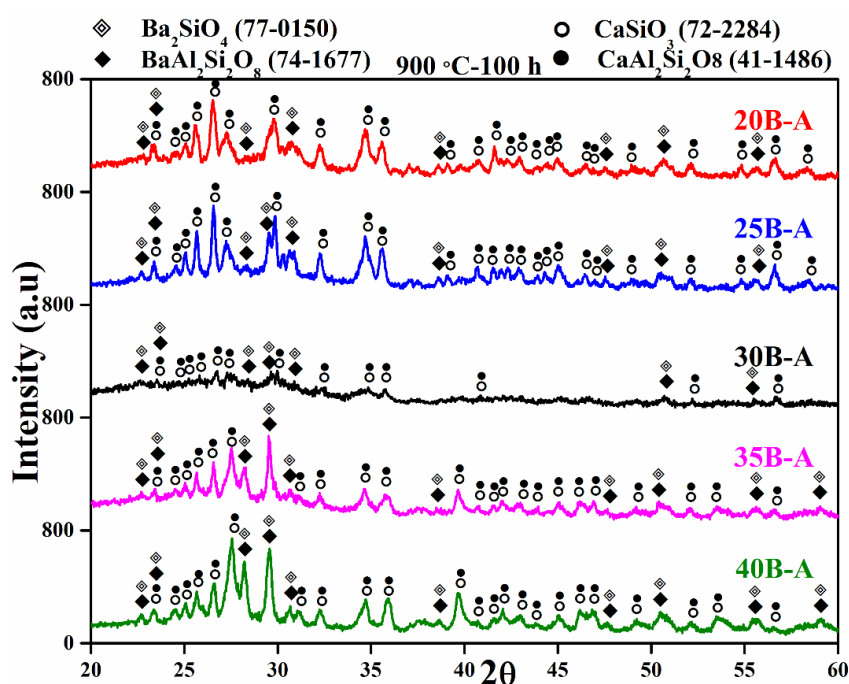
Figure 4.10a. XRD of BCBSA glasses heated at 900 ^{O}C for 100 hours

When the samples were heated at 900 ^{O}C for 100 hours, the intensity of the different barium phases were found to reduce drastically. 30B that appears to be almost amorphous when heated for 50 hours at 900 ^{O}C (figure 4.9b), shows crystalline peaks with better intensities when heated for 100 hours at the same temperature. The glassy hump was also found to be less prominent when heated for 100 hours at 900 ^{O}C (figure 4.10b). This shows that crystallization especially that of the calcium phase improves after longer duration of heating inspite of removal of Al_2O_3 and reduction in BaO content. Sabato et. al. (2016) reported that calcium phases became sharper due to prolonged heat treatment, which is in agreement with the results obtained in the present work (Sabato et al. 2016).
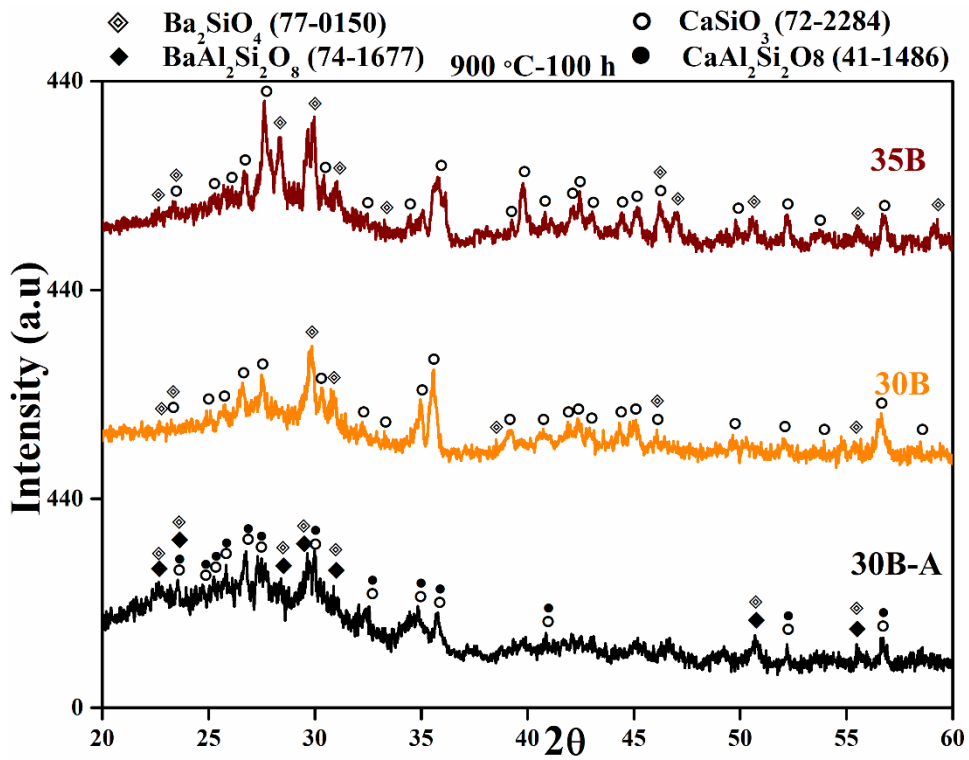
Figure 4.10b. XRD of BCBS glasses and 30B-A heated at 900 $^{\circ}$C for 100 hours
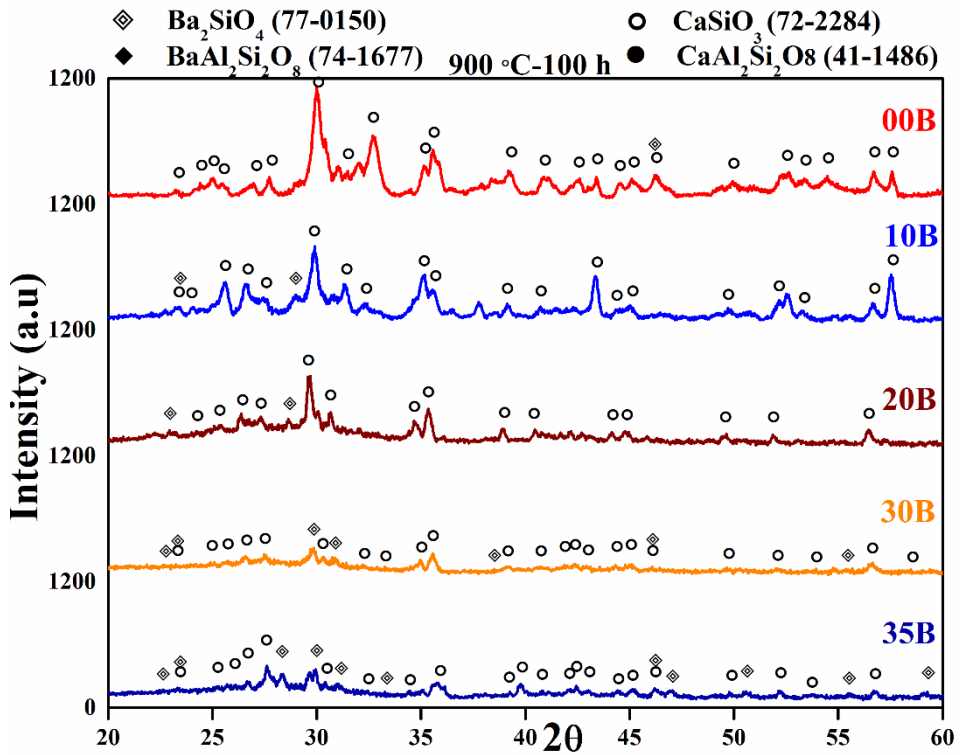
Figure 4.10c. XRD for all Al$_2$O$_3$ free samples heated at 900 $^{\circ}$C for 100 hours

Samples 20B, 10B and 00B were heated at 900 ^{O}C for 100 hours and their X-ray diffractographs are shown in figure 4.10c. Among the Al_2O_3 free samples, 20B with lowest CaO content was found to crystallize the least. 20B also exhibits the glassy hump near 30°. This hump was not observed in 10B and 00B, instead sharp and intense peaks were observed. $BaSiO_3$ was found to precipitate as a minor phase and in very low intensities in sample 20B and 10B.

4.7.Summary

BaO-CaO-B_2O_3-SiO_2 (BCBS) and BaO-CaO-B_2O_3-SiO_2-Al_2O_3 (BCBSA) glasses could be melted at 1300 ^{O}C with ZnO and MgO added as flux. The samples were found to show densities in the acceptable range required for SOFC application. The density of these glasses can be altered by varying BaO and CaO concentrations. FTIR transmission spectra confirmed the presence of the important structural vibration bands. Optical absorption studies indicated the band gap energies of the glasses to lie in the range of 3.00 eV to 3.25 eV. This along with the refractive index studies confirmed the insulating nature of all the glasses. Samples with BaO content lower than 20 mol% exhibit a red shift in the absorption spectra and minimum values of density and band gap energy.

Devitrification of glasses was found to be incomplete at 800 ^{O}C. Wollastonite was found to grow predominantly in all glasses at both 800 ^{O}C and 900 ^{O}C. Growth of celsian phase was avoided by removing Al_2O_3 from glass matrix. Samples 30B to 00B are devoid of celsian phase. 20B, 10B and 00B i.e. the samples with less than 30 mol% BaO concentration show excellent devitrification at 900 ^{O}C and develop a stable glass ceramic phase. Samples 30B to 00B show suitable structural phases required for SOFC sealant application. The BaO free sample 00B was used further for screen printing on Crofer22APU substrates and the results are discussed in chapter 6.

Effect of concentration of BaO was observed to be more than Al_2O_3 on optical properties of the synthesized glasses. It can be concluded from the isothermal heat treatment studies that the detrimental celsian phase can be avoided in alumina free samples with 30 mol% BaO and also without BaO.

CHAPTER 5

THERMAL AND MECHANICAL PROPERTIES OF BCBS GLASS SYSTEM WITH AND WITHOUT ALUMINA

BaO-CaO-Al$_2$O$_3$-SiO$_2$ (BCAS) glass and their derivatives have gained extreme importance for their high endurance to elevated temperatures and being suitable for various electrochemical applications. The thermal and mechanical properties of these two glass systems mentioned in table 2.1, (Chapter 2) are discussed in this chapter. Reduction of BaO concentration improves the coefficient of thermal expansion (CTE/α) and other characteristic temperatures of glasses. Compacted pellets made of the water quenched frits show maximum shrinkage at 700°C. Dilatometric analysis is conducted on the compacts that show maximum shrinkage. CTE of these pellets are more than that of the bulk glasses. Glasses with low BaO concentrations exhibit high hardness and Young's modulus. Glasses with BaO content below or equal to 20mol% meet the thermal and mechanical properties required for high temperature sealing applications.

5.1. Results and Discussion

Effect of BaO on thermal and mechanical properties of the prepared glasses were investigated and the details of the analysis are discussed in this chapter.

5.2. Thermal Property

5.2.1. Dilatometric investigations on bulk glasses

The dilatometric data (ΔL/L) for BCBSA and BCBS glasses are shown in figure 5.1. The values of thermal expansion coefficient (α), determined from dilatometric studies of all samples from room temperature to 700 °C are listed in table 5.1. The glass transition temperature T_g and softening temperature T_d were evaluated from the dilatometric data as shown in figure 5.1. The T_g and T_d were found to reduce on addition of BaO in the glass matrix. This trend is clearly exhibited by both BCBSA and BCBS glasses as shown in figures 5.1a and 5.1b and in table 5.1. Figure 5.2 shows the behaviour of T_g and T_d, with variation in BaO content for BCBSA and BCBS glasses respectively. 40 B-A in the BCBSA glass system, has the maximum BaO content and lowest T_g value of 624 °C while 20B-A with 20 mol% BaO has the value of 640 °C.

This indicates that BaO in affecting the T_g of BCBSA glasses. Similarly in the BCBS glasses too, increasing BaO from 0 to 40 mol% reduced the T_g from 644 °C to 620 °C indicating the influence of BaO. These values are suitable for high temperature sealing applications and are also in agreement with those reported by Ghosh et al. (2008) for BCAS glasses with added La_2O_3 and ZnO and BAS glasses with added La_2O_3 and B_2O_3 and Ojha et. al. (2011) for Sr-La-Al-B-Si based system (Ghosh, Das Sharma, et al. 2008; Ghosh, Kundu, et al. 2008; Ojha et al. 2011).
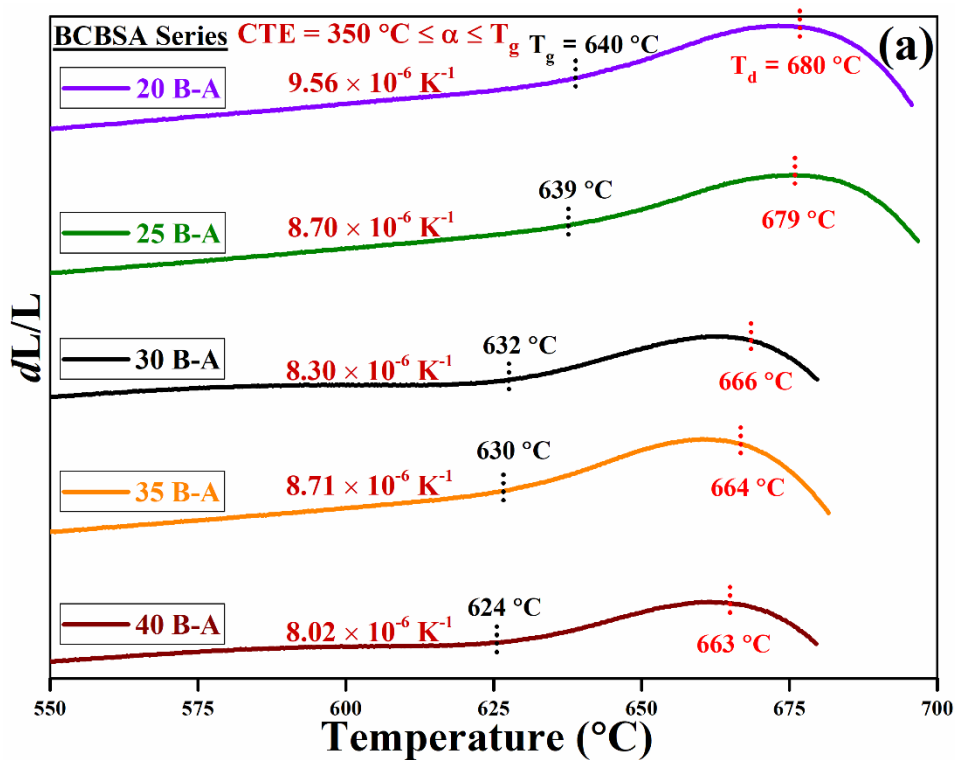
Figure 5.1a. Dilatometer data from RT to 700°C at 5°C/min for BCBSA glasses
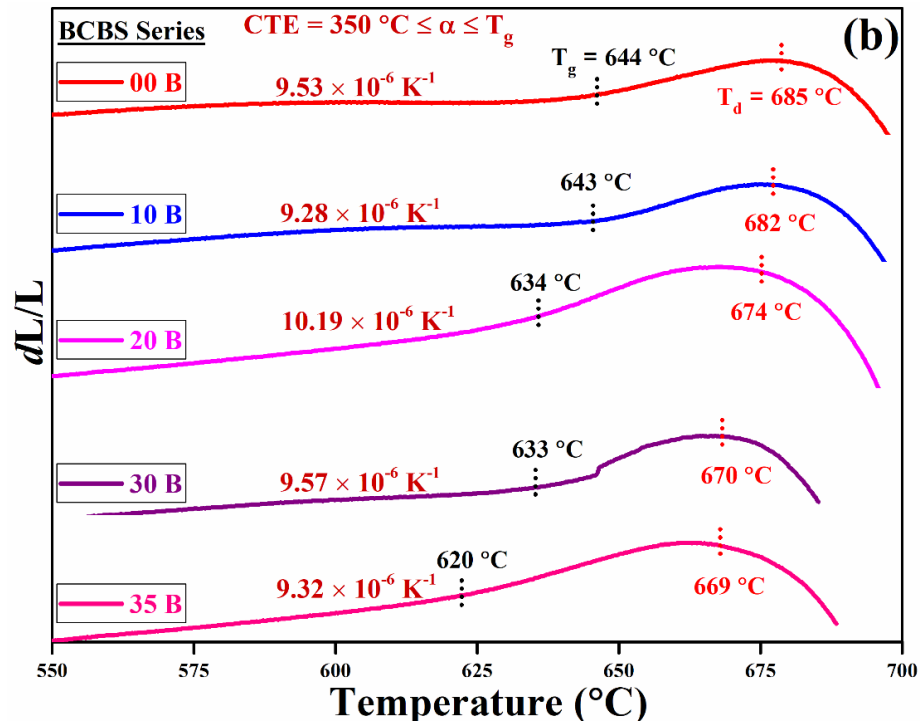
Figure 5.1b. Dilatometer data from RT to 700°C at 5°C/min for BCBS glasses

Similar dependence of T_d on BaO content has beem observed for both BCBSA and BCBS glass systems as shown in figure 5.2.
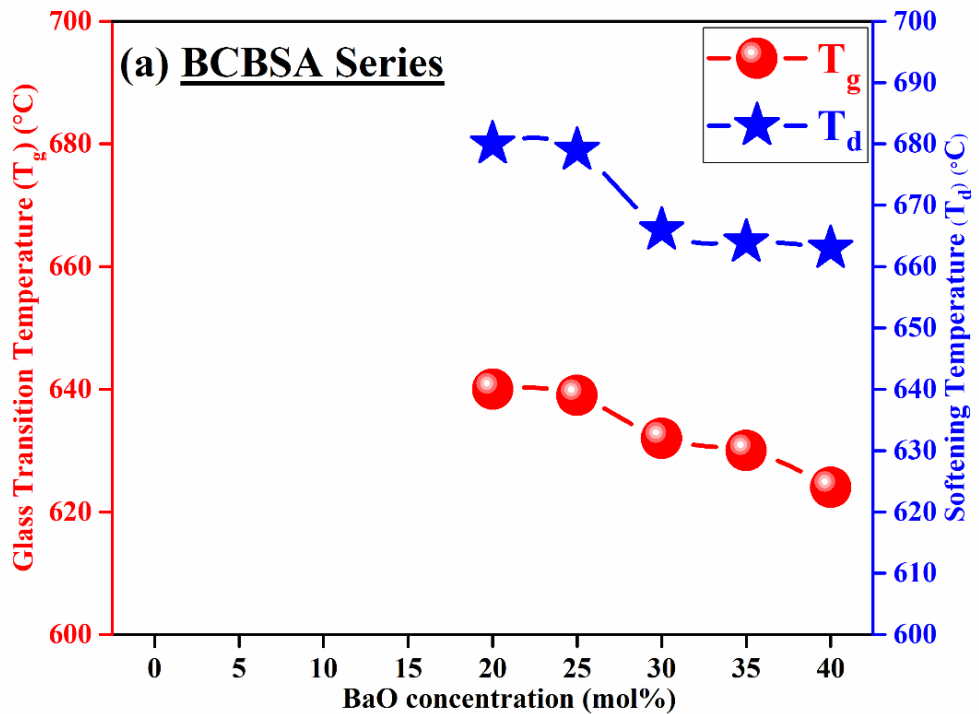
Figure 5.2a. Behaviour of T_g and T_d with rising BaO concentrations for BCBSA glasses
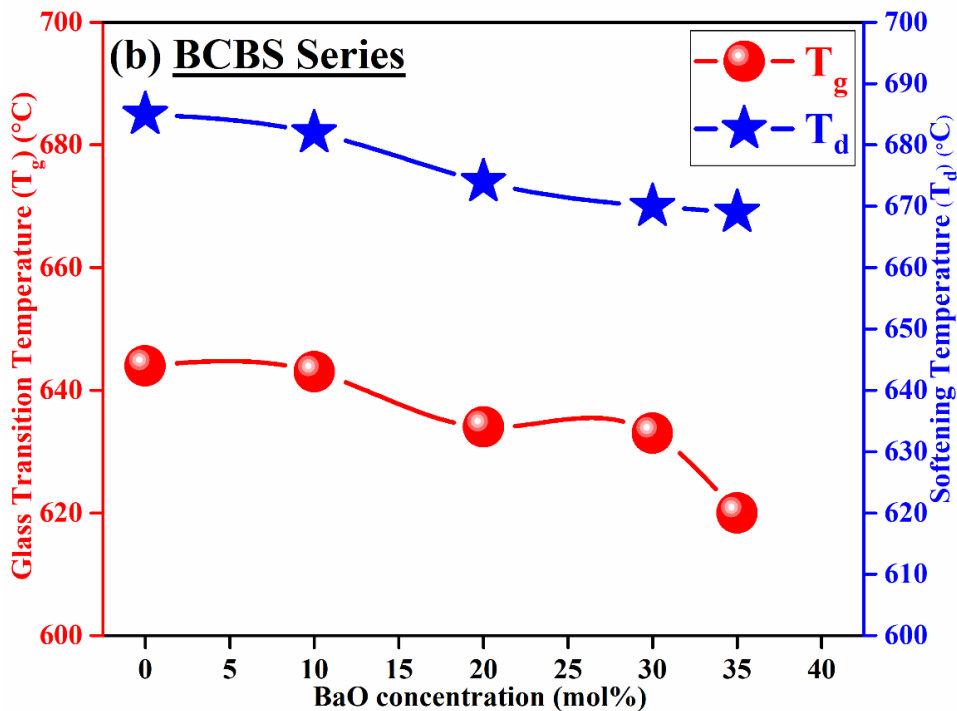
Figure 5.2b. Behaviour of T_g and T_d with rising BaO concentrations for BCBS Glasses

Glass transition temperature (T_g) is the onset temperature at which the glass shows visco-elastic behaviour and softening temperature (T_d) of any glass is the temperature at which the glass starts deformation under the load equivalent to its own weight (J E Shelby 2005). BaO and CaO are both alkaline earth metal oxides that have divalent ions. Introducing these ions in the glass network would lead to breaking of network releasing two NBOs per alkaline earth ion forming weaker ionic bonds (J E Shelby 2005; Varshneya K 1994; Mukhopadhyay et al. 2009). Additionally, introducing Ba^{2+} and Ca^{2+} ions in the matrix leads to filling up of the interstitial spaces. Filling up interstices, on heating the glass, affects the internal stretching or bending phenomenon of bonds, leading to faster disintegration of the sample, which causes reduction of T_g and T_d (Ghosh, Sharma, et al. 2008). In fact addition of any modifier would lead to reduction of the characteristic temperatures. It is expected that increasing the BaO content at the cost of CaO would cause faster disintegration of bonds since Ba^{2+} has much higher ionic radius than that of Ca^{2+} ions (Ghosh, Sharma, et al. 2008; Mukhopadhyay et al. 2009). As a result glass transition would occur at lower

temperature and T_g must reduce with increase in the BaO content in the glass matrix, as found in the present study.

Figure 5.3 compares T_g and T_d of BCBSA and BCBS glasses at different compositions of BaO. Removal of Al_2O_3 resulted in reduction of T_g as shown in figure 5.3a. This is in agreement with Sun et al. (2010) (Sun et al. 2010). Although Al_2O_3 has considerable effect on the T_g of the glasses, the behaviour of thermal characteristic temperatures, T_g and T_d were found to be dominated by alkaline earth metals. When Al_2O_3 is introduced in the glass matrix, it may behave as a modifier or a glass former depending on its total concentration and Al_2O_3/MO ratio (Sun et al. 2010; Varshneya K 1994). If $Al_2O_3/MO < 1$ or for Al_2O_3 content ≤ 5 mol%, then it goes into the matrix as a network former (Sun et al. 2010; Varshneya K 1994). Under such circumstances, it was found that $[AlO_4]^{-1}$ units are created with unit negative charge, which is satisfied by an alkaline earth ion (Varshneya K 1994). Further addition of Al_2O_3, where $Al_2O_3/MO > 1$, Al^{3+} ions enter the matrix as modifiers and behave as regular modifiers do, reducing T_g and increasing CTE (Varshneya K 1994). In the present work, maximum 5 mol% Al_2O_3 is used ($Al_2O_3/MO = 0.1$), in BCBSA series and is hence expected to contribute as a glass former in the matrix. Formation of $[AlO_4]^{-1}$ units was observed for the reported glasses and confirmed by Fourier Transformed Infra-Red (FTIR) spectroscopy, which is explained in chapter 4 (Bhattacharya and Shashikala 2018). So, there would be no creation of additional NBOs. In that case addition of Al_2O_3 must result in raising T_g and all such characteristic temperatures. CTE and density must reduce and crystallization of the material should be improved. Reduction in density and better crystallization on addition of Al_2O_3 is already shown in chapter 4 (Bhattacharya and Shashikala 2018). Comparison between the samples with and without alumina, but having equal BaO concentrations, can help in understanding the effect of Al_2O_3, independent of the influence of BaO. T_d for samples with concentrations greater than 20 mol% BaO, was apparently found to increase on removal of Al_2O_3, but that is because the 5 mol% Al_2O_3 was compensated with another alkaline earth, CaO.

The coefficient of thermal expansion (CTE) is defined as the fractional increase in the length per unit rise in temperature (J E Shelby 2005). Heating a material causes

increase in the bond length and hence expansion of the whole material. In a loosely packed network, like that of glass, phenomenon like bond bending and rotation is observed. This hinders the stretching of bonds and thus thermal expansion. Introduction of modifiers results in formation of a denser network by filling up the interstices and by creation of more NBOs. This restricts bending or rotation of bonds allowing it to expand. Thus introduction of any modifiers leads to increase in number of NBOs and hence the CTE of the glass (Varshneya K 1994).

The thermal expansion values for all the samples are listed in table 5.1. Figure 5.3b demonstrates the variation of CTE (α) with the change of BaO concentration for both BCBSA and BCBS glasses. For both the system of glasses the CTE was observed to lie in a narrow range, showing an overall trend of reduction with increasing BaO content. The samples with equal to 20 mol% BaO or even lower concentrations, show a high CTE in both cases, i.e. with or without Al_2O_3. Variation of CTE with change of BaO content is less because the BaO is substituted by another alkaline earth, CaO. Irrespective of addition of Al_2O_3 in BCBSA glasses the CTE was observed to depend mainly on the composition of alkaline earth metals, which may be due to its large concentration and bigger ionic radii, as compared to Al_2O_3. Similar behaviour of CTE with variation of BaO in BCAS glasses, was also reported by Ghosh et. al. (2008) (Ghosh, Das Sharma, et al. 2008).

CTE of the glasses were found to increase on removal of Al_2O_3 for constant BaO concentrations, fixed at 20, 30 and 35 mol%, as evident from figure 5.3b. Irrespective of addition of Al_2O_3, in the BCBSA series, the variation of T_g, T_d and CTE are mostly dominated by alkaline earth oxide composition. This is because with only 5 mol% Al_2O_3 in the composition, it does not act as a modifier. This observation is in agreement with the work done by Sun et. al. (2010) on CaO free $BaO-Al_2O_3-B_2O_3-SiO_2$ glasses (Sun et al. 2010).
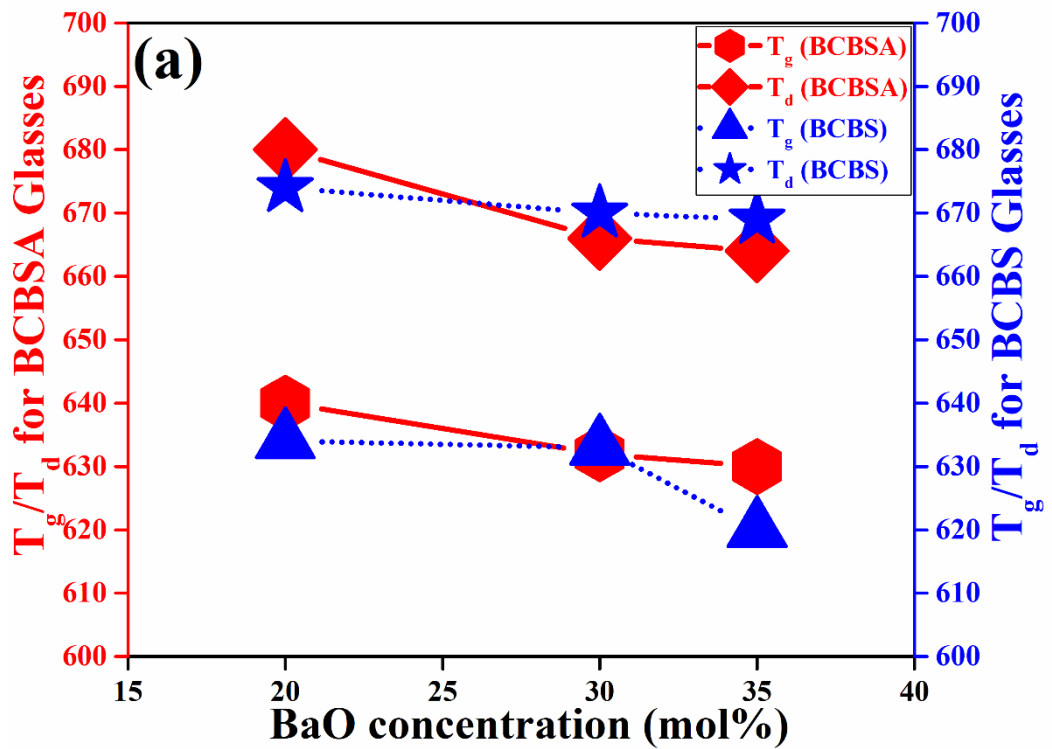
Figure 5.3a. Variation of T_g & T_d with increasing BaO content for BCBSA and BCBS glasses
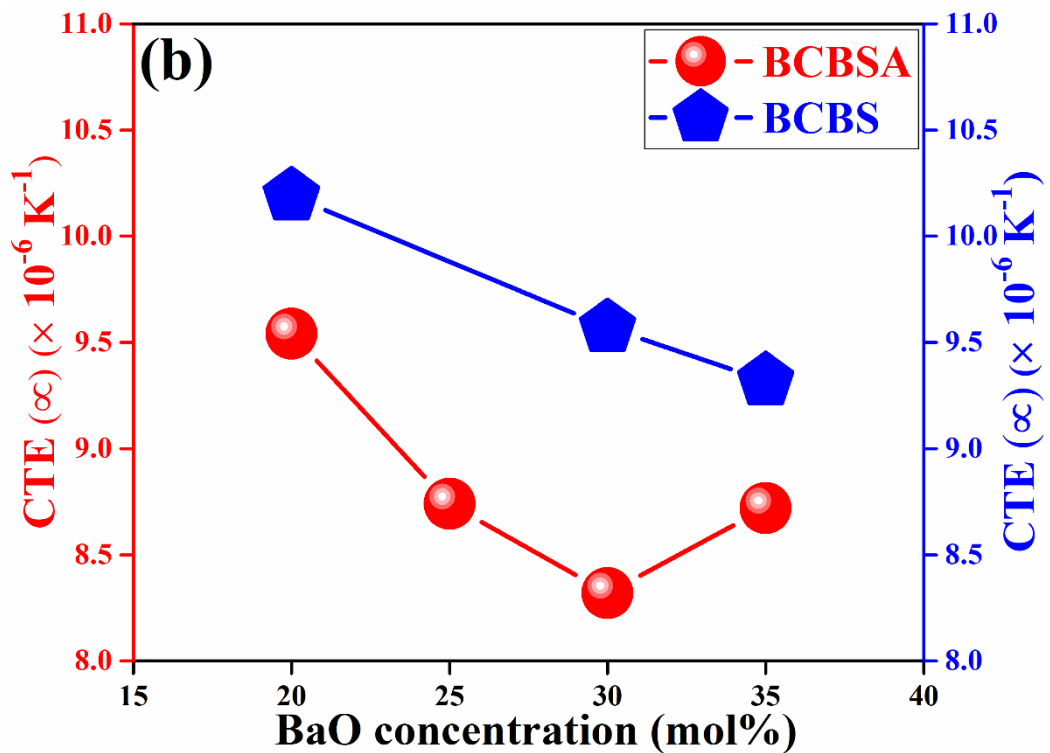
Figure 5.3b. Variation of CTE (α) with increasing BaO content for BCBSA and BCBS glasses

Table 5.1. Thermal Properties (Dilatometer Data)

Samples			T_g (°C)	T_d (°C)	CTE (α) ($\times 10^{-6}$ K^{-1})
Cubic Bulk Glasses (10 mm × 10 mm × 5 mm)	BCBSA	20 B-A	640	680	9.54
		25 B-A	639	679	8.74
		30 B-A	632	666	8.32
		35 B-A	630	664	8.72
		40 B-A	624	663	8.28
	BCBS	00 B	644	685	9.53
		10 B	643	682	9.28
		20 B	634	674	10.19
		30 B	633	670	9.57
		35 B	620	669	9.32
Max. Shrunk Pellets		00 B	643	683	11.79
		10 B	642	678	13.90
		30 B-A	626	659	8.41

5.2.2. Shrinkage behaviour of glasses

Sample 30B-A is the reference sample used in this work from the beginning. Sample 10B and 00B have sufficiently high CTE and low BaO content. Due to this reason samples 10B and 00B along with sample 30B-A containing 5 mol% Al_2O_3, were chosen to study their shrinkage behaviour. The linear and volume shrinkage percentages, calculated using equation 2.13 and 2.14 are listed in table 5.2 along with the densities of the samples after sintering. It is evident from the data that for all the three samples subjected to sintering, shrinkage starts at 650 °C and all the three samples show maximum linear shrinkage at 700 °C on heating for one hour. This means the

temperature of first shrinkage (T_{FS}), is 650 ˚C and the temperature of maximum shrinkage, (T_{MS}), is 700 ˚C for all tested samples. Samples 30B-A and 00B show maximum volume shrinkage at 700 ˚C, but 10B shows maximum volume shrinkage at 800 ˚C as shown in figure 5.4. Figure 5.4 shows the linear and volume shrinkages exhibited by the samples after sintering. Densities of the samples sintered at 700 ˚C were found to match to the densities of their bulk glass counterparts, presented in figure 4.1 in chapter 4 (Bhattacharya and Shashikala 2018). Sample 00B shows both linear and volume shrinkages to be positive at 900 ˚C, which is actually expansion of the glasses.
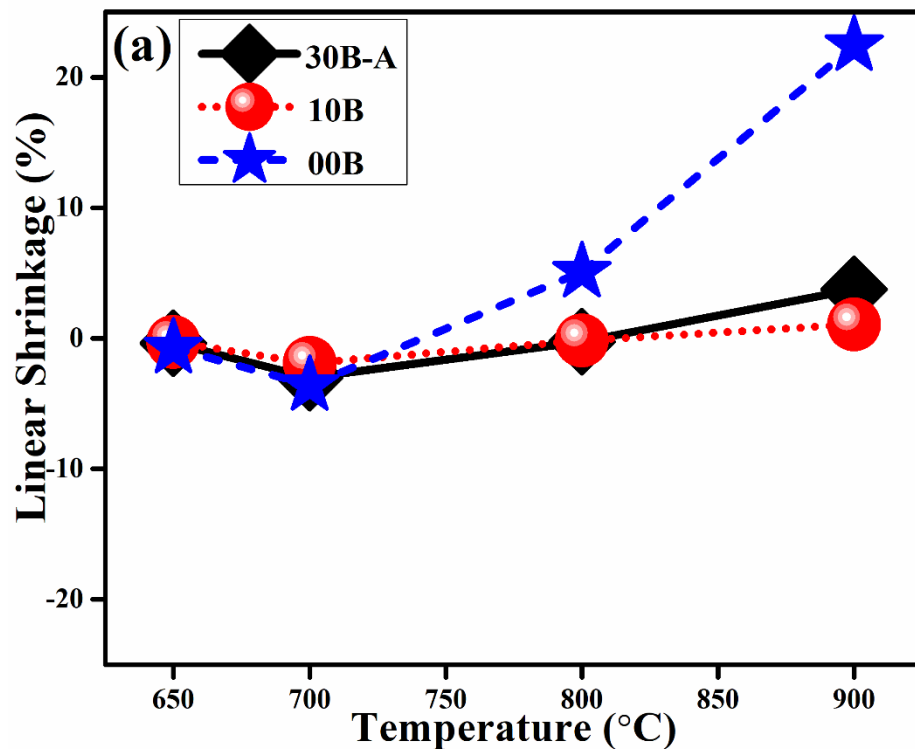
Figure 5.4a. Linear shrinkage of glasses with increasing temperature

The glass pellets show the maximum linear and volume shrinkage, mostly at 700 ˚C as exhibited in table 5.2. Hence one can conclude that 700 ˚C is the most suitable operation temperature for these glasses. Though densities of the glasses sintered at 800 ˚C do not match very closely to the densities of the bulk glasses, they still show acceptable volume shrinkage (Bhattacharya and Shashikala 2018).
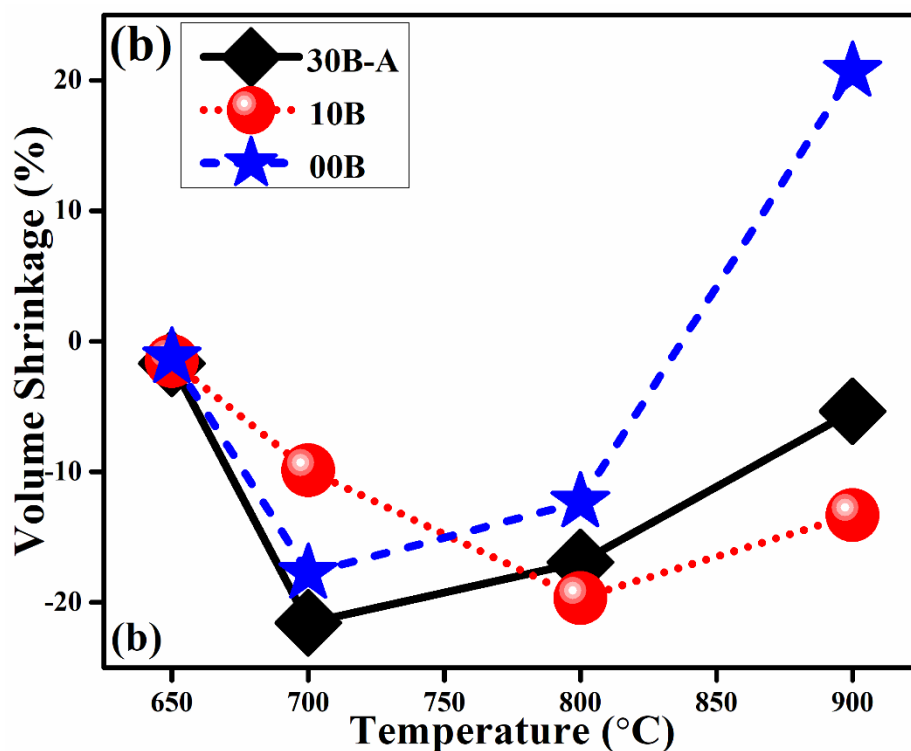
Figure 5.4b. Volume shrinkage of glasses with increasing temperature

The glasses sintered at 700 ˚C for one hour were again subjected to a second cycle of heat treatment for one more hour at the same temperature and heating rates. All samples were found to exhibit both linear and volume shrinkages after second cycle as shown in table 5.2. At 800 ˚C, the glasses are undergoing through densification under the action of shrinkage, but crystallization studies in chapter 4, revealed that these glasses also crystallizes at 800 ˚C (Bhattacharya and Shashikala 2018). Therefore, at this temperature both densification and crystallization occur simultaneously. This may be a reason for reduction of shrinkage at 800 ˚C. Though shrinkage is less, the samples show volume shrinkage of 12% to 19%, which lies in the acceptable range for shrinkage of sealant glasses, as reported by Silva et. al. and Bakal et. al. in 2016 (M. J. Da Silva et al. 2016; Ozgur Colpan, Ibrahim, and Feridun 2008). The isothermal heat treatment studies mentioned in chapter 4 have also shown that these glasses do not show good devitrification at 700 ˚C (Bhattacharya and Shashikala 2018), and now they exhibit maximum shrinkage at the same temperature. Hence, these glasses are most suitable to work with, at 700 ˚C, and can also be worked with at 800 ˚C. At 900 ˚C however, all

glasses show linear expansion. This indicates that at 900 ˚C or more the glass softens and is not suitable to work at that temperature.

Table 5.2. Linear Shrinkage, Volume Shrinkage and Density of Sintered Glasses (with calculated standard deviation of mean)

	Parameter	Sintering Temperatures				
		650 ˚C	700 ˚C	800 ˚C	900 ˚C	700 ˚C (2nd Cycle)
30B-A	Linear Shrinkage (%)	-0.44	-3.01	-0.27	+3.74	-1.78
	Volume Shrinkage (%)	-1.76	-21.57	-16.92	-5.35	-3.07
	Density after Sintering (g cm^{-3})	2.6408 (±0.1724)	3.1331 (±0.0230)	2.8730 (±0.1055)	2.5186 (±0.0815)	3.1195 (±0.0920)
10B	Linear Shrinkage (%)	-0.30	-1.90	-0.17	+1.05	-1.76
	Volume Shrinkage (%)	-1.51	-9.88	-19.67	-13.31	-7.35
	Density after Sintering (g cm^{-3})	2.3118 (±0.1128)	2.7203 (±0.0054)	2.6751 (±0.0351)	2.5736 (±0.0341)	2.6231 (±0.0695)
00B	Linear Shrinkage (%)	-0.73	-3.60	+5.09	+22.44	-2.87
	Volume Shrinkage (%)	-1.29	-17.78	-4.99	+20.69	-9.89
	Density after Sintering (g cm^{-3})	2.5881 (±0.0939)	2.9036 (±0.0063)	2.2285 (±0.0990)	2.1293 (±0.0669)	2.8434 (±0.0617)

5.2.3. *Dilatometric investigations on sintered glass pellets*

Figure 5.5 exhibits the dilatometric data for the sintered samples. The T_g, T_d and CTE values of the glasses are listed in table 5.1. These dilatometric studies were carried out on sintered pellets to check the suitability of CTE, T_g and T_d of these glasses for SOFC sealant applications.
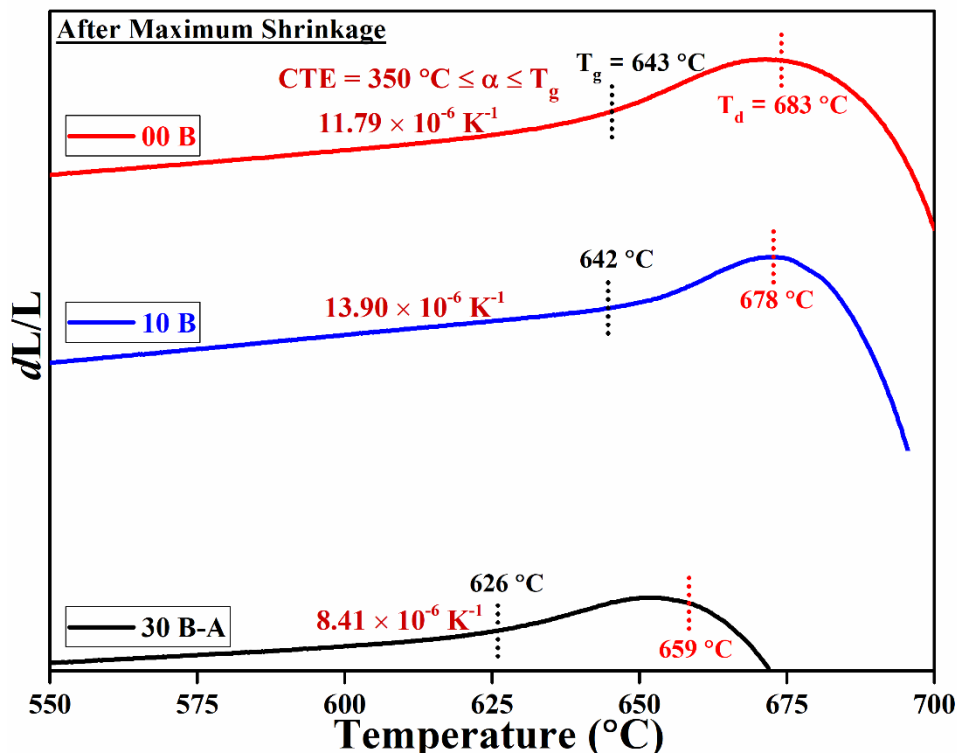
Figure 5.5. Dilatometer data of 00B, 10B and 30B-A after maximum shrinkage

The T_g and T_d of 00B, 10B and 30B-A, observed after sintering were found to match very closely to their bulk counterpart. Sample 30 B-A with 5 mol% Al_2O_3 shows less T_g and T_d than samples 10 B and 00 B. Samples 10 B and 00 B show T_g 644 °C and 643 °C respectively for bulk glasses and 644 °C and 643 °C respectively, after sintering. Similarly not much variation in T_d was observed due to sintering as evident from table 5.1. However CTE of the sintered samples were found to be higher as compared to the bulk glasses. This is expected and is mainly due to crystallization and formation of a modified structure during the sintering process (Kurama and Saydam 2017; G. Kaur et al. 2013). The sample 30B-A contains both Al_2O_3 and BaO and thus

supports formation of the celsian phase which due to prolonged heating reduces the CTE. However sample 10B develops Ba_2SiO_4 and $CaSiO_3$ phases bearing CTE around 15.6 and 13.4 ($\times 10^{-6}$) K^{-1}, respectively (Kerstan and Rüssel 2011; Conradt et al. 2013). Sample 00B develops only the $CaSiO_3$ phase as it does not contain BaO. Hence the CTE of these two samples were found to be increase due to the development of high CTE phases as compared to 30B-A. The sample 30B-A, containing Al_2O_3 also showed an increase in CTE with respect to its bulk counterpart, but its overall CTE was found to be less compared to the remaining two samples. Samples 10 B and 00 B have CTE values of 13.90 and 11.79 ($\times 10^{-6}$) K^{-1} respectively. These CTE values are suitable to work with, in high temperature sealing applications in SOFCs, using chromium based steel interconnects like Crofer22APU and yattria stabilized zirconia (YSZ) based electrolytes having CTE in the range of 12-14 ($\times 10^{-6}$) K^{-1} and 10-12 ($\times 10^{-6}$) K^{-1} respectively (Hao et al. 2012; Heydari et al. 2013; M. Kaur et al. 2017).
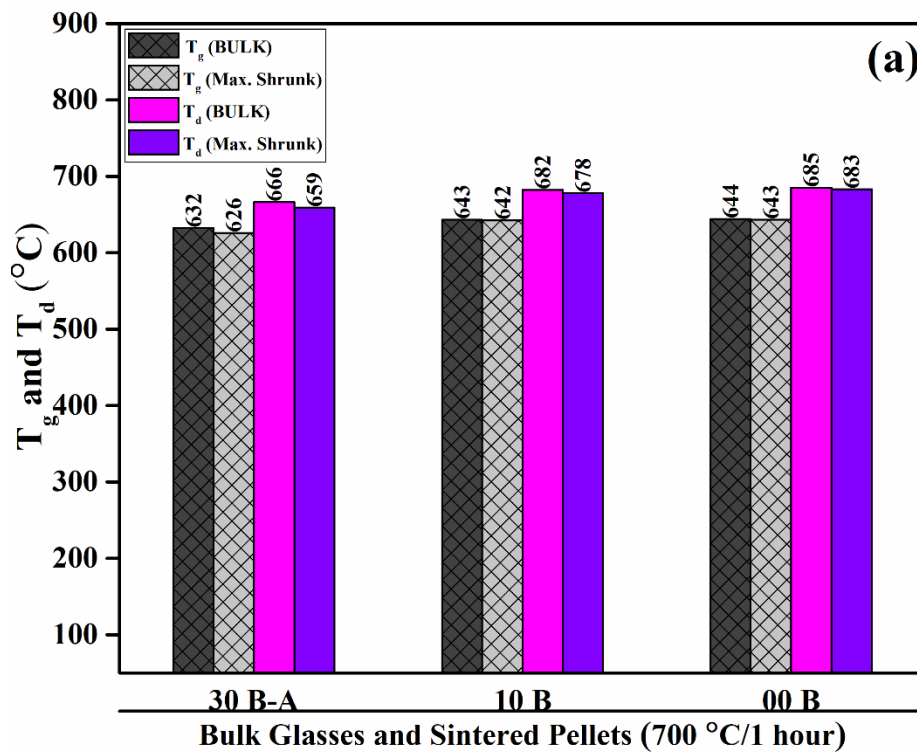
Figure 5.6a. Variation of T_g and T_d for bulk glasses and sintered pellets

Figure 5.6 shows the variation of T_g, T_d and CTE for bulk glasses and compacted glass pellets sintered at 700 °C. It is clearly evident that both bulk glasses

and sintered pellets have same T_g and T_d whereas CTE of the sintered pellets is more as compared to the bulk forms. This result is in agreement with Mukhapadhyay et. al. (2009) and Kurama et. al. (2017) (Mukhopadhyay et al. 2009; Kurama and Saydam 2017).
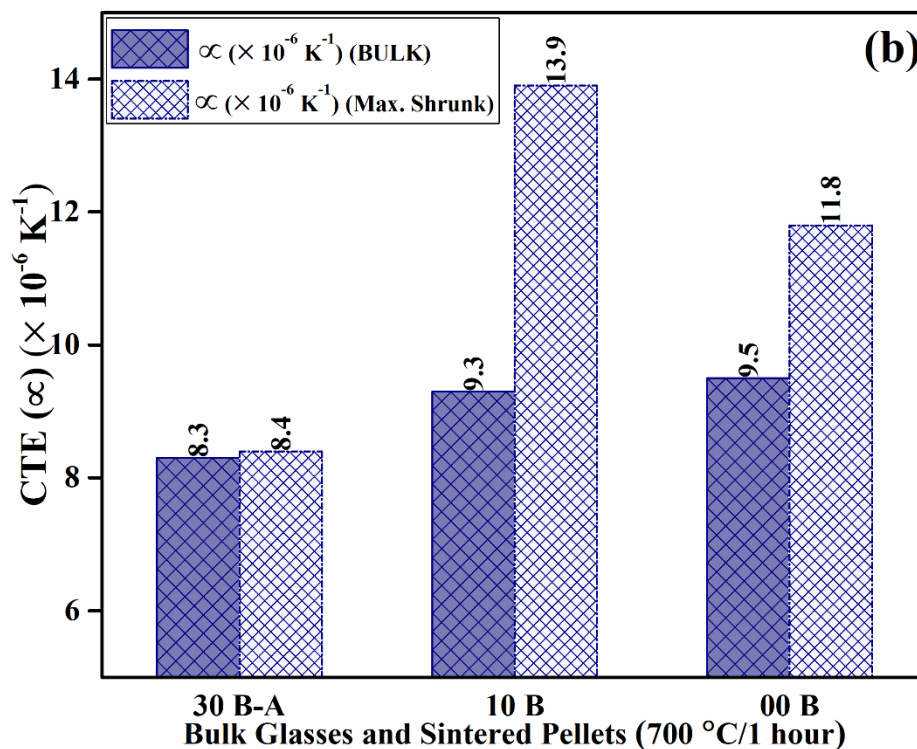
Figure 5.6b. Variation of CTE for bulk glasses and sintered pellets

5.3. *Mechanical Properties*

Hardness is the measure of the resistance of the material, to being penetrated or eroded by another material's sharp projections (Varshneya K 1994). The Vickers hardness (H_v) for all samples were conducted under different loads of 0.25 N, 0.49 N, 0.98 N and 1.96 N. The hardness values for all glasses, under different applied loads were not found to exhibit much variation. Figure 5.7a show variation of microhardness with BaO concentration for both BCBSA and BCBS glasses under applied load of 0.98 N. In the BCBS series, the hardness was observed to reduce consistently with increase in BaO content. The hardness values for BCBSA series, under the applied loads 0.98 N was not found to exhibit much variation. This helps us to conclude that addition of BaO leads to reduction of microhardness of glasses at least in the BCBS series. This is in

agreement with S R Lopez et. al. who reported that BaO containing samples show lesser hardness than other dopants like SrO (Rodríguez-López et al. 2017). Samples without Al_2O_3, with low BaO content, i.e. samples 10B and 00B exhibit highest values for Vicker's hardness than all other samples in BCBSA glasses.

Figures 5.7b and 5.7c show the dependence of hardness on applied load for BCBSA and BCBS glasses respectively. Hardness was observed to reduce as expected with increasing load for all samples. Under 1 N load, sealant glasses used in SOFCs are reported to have hardness in the range of 7.1 GPa to 7.7 GPa for better functioning (Rodríguez-López et al. 2017). It is evident from figure 5.7c that samples 10B and 00B have shown better microhardness values than the other compositions with more BaO content, for all applied loads. In figures 5.7b and 5.7c the microhardness values of all samples appear to stabilize under the load of 0.98 N. All the calculations of mechanical properties are hence done by considering the microhardness values exhibited by glasses under the load of 0.98 N.
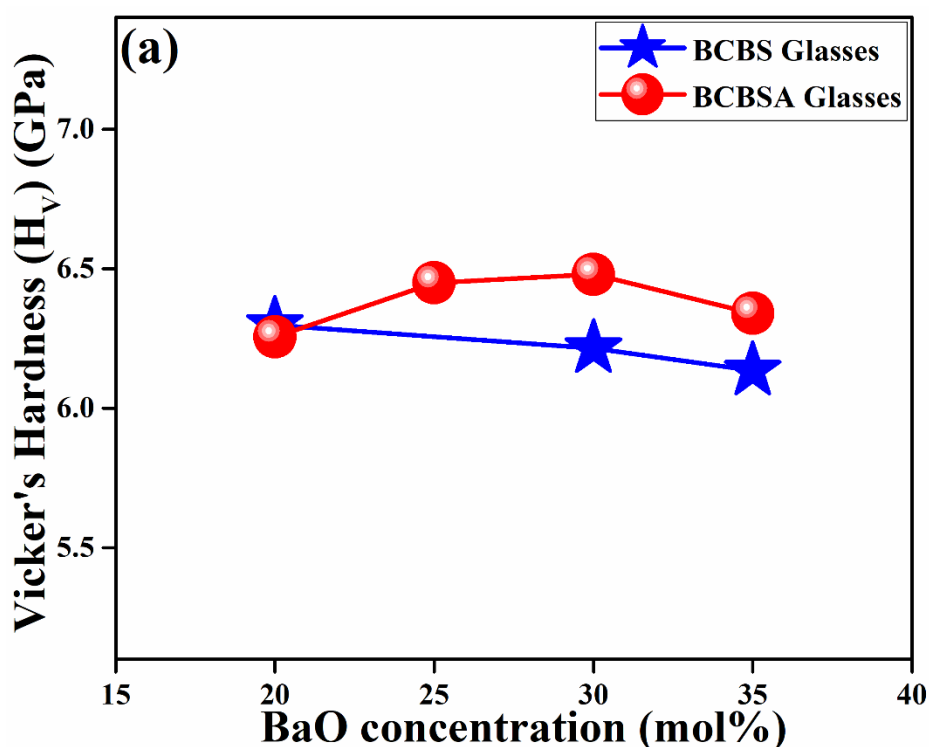
Figure 5.7a. Behaviour of Vicker's Hardness with variation of BaO concentration
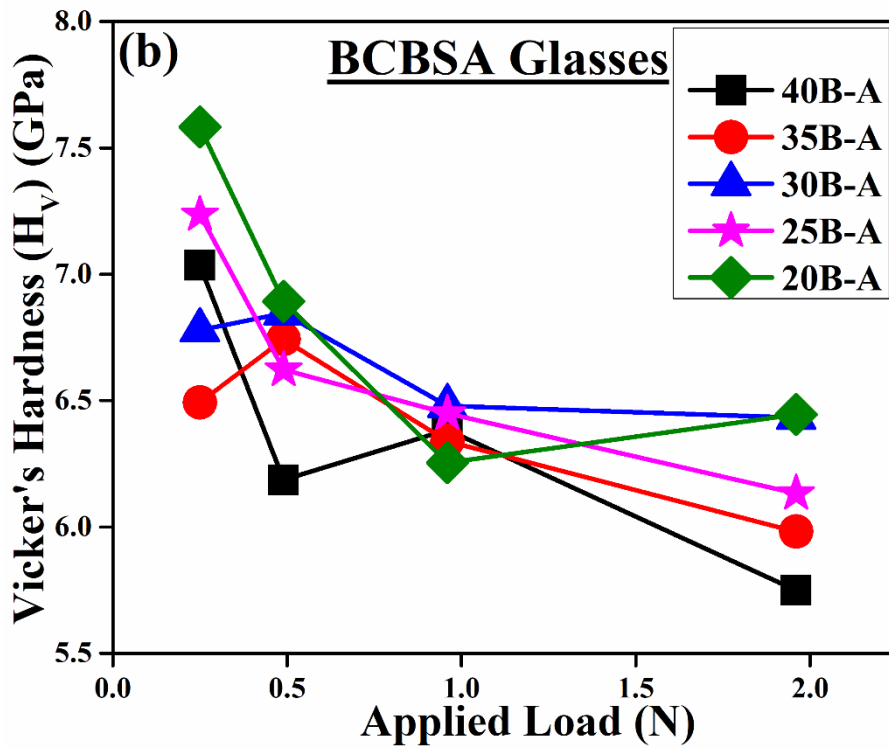
Figure 5.7b. Behaviour of Vicker's Hardness with different loads for BCBSA glasses
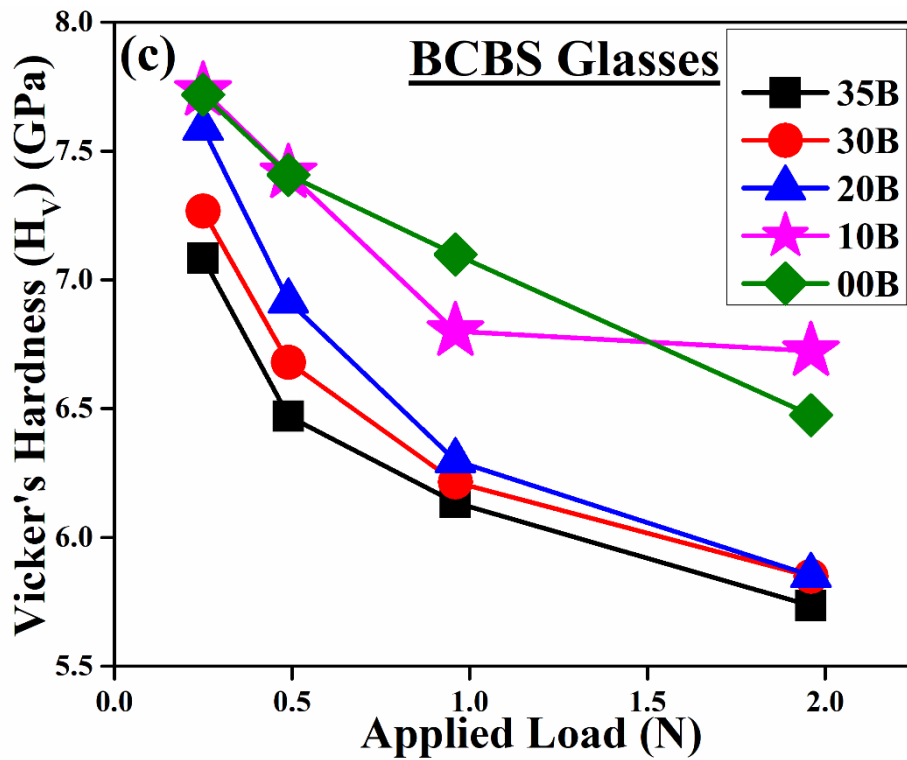
Figure 5.7c. Behaviour of Vicker's Hardness with different loads for BCBSA glasses

Samples containing Al_2O_3, have more hardness than their Al_2O_3 free counterparts with same BaO content as shown in figure 5.7a. Though the samples show only marginal increase in hardness on addition of Al_2O_3, the increment is evident, at least for samples higher than 20 mol% BaO. This trend is exhibited in the comparative graphs shown in figure 5.8a. However micro-hardness exhibited by samples 10B and 00B are higher than these, and lie in acceptable range for high temperature sealant applications (Rodríguez-López et al. 2017).
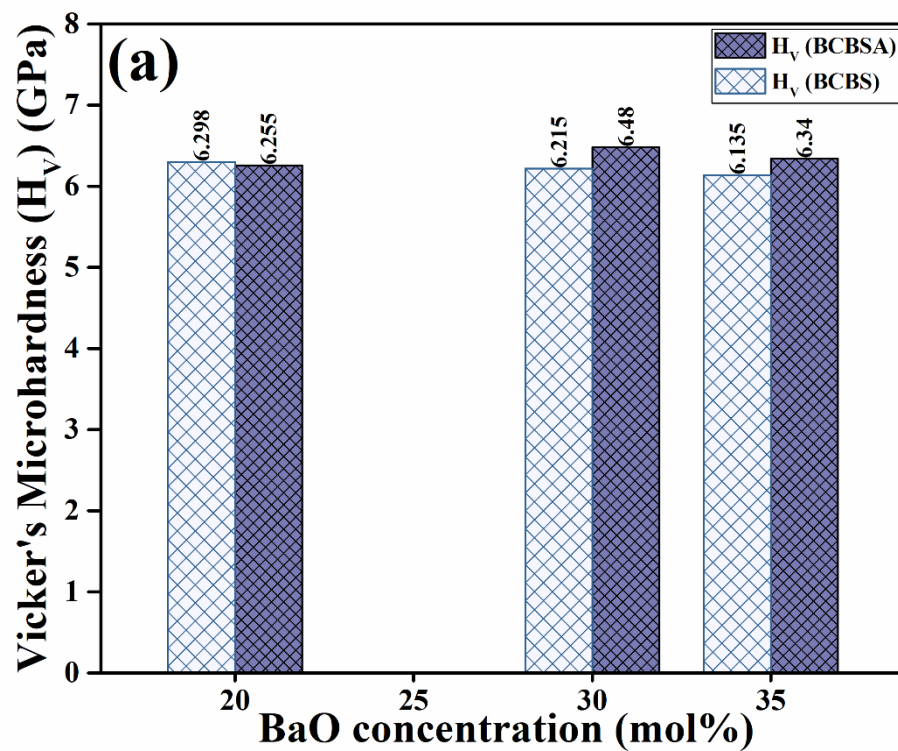
Figure 5.8a. Variation of H_V of BCBSA and BCBS glasses for 0.98 N applied load
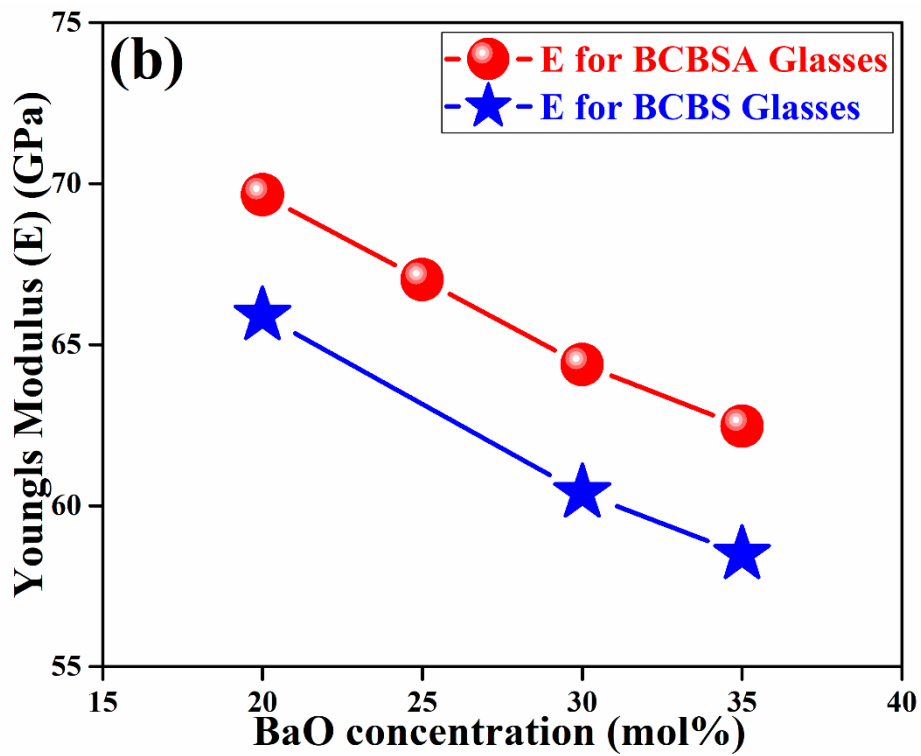
Figure 5.8b. Variation of E of BCBSA and BCBS glasses for 0.98 N applied load
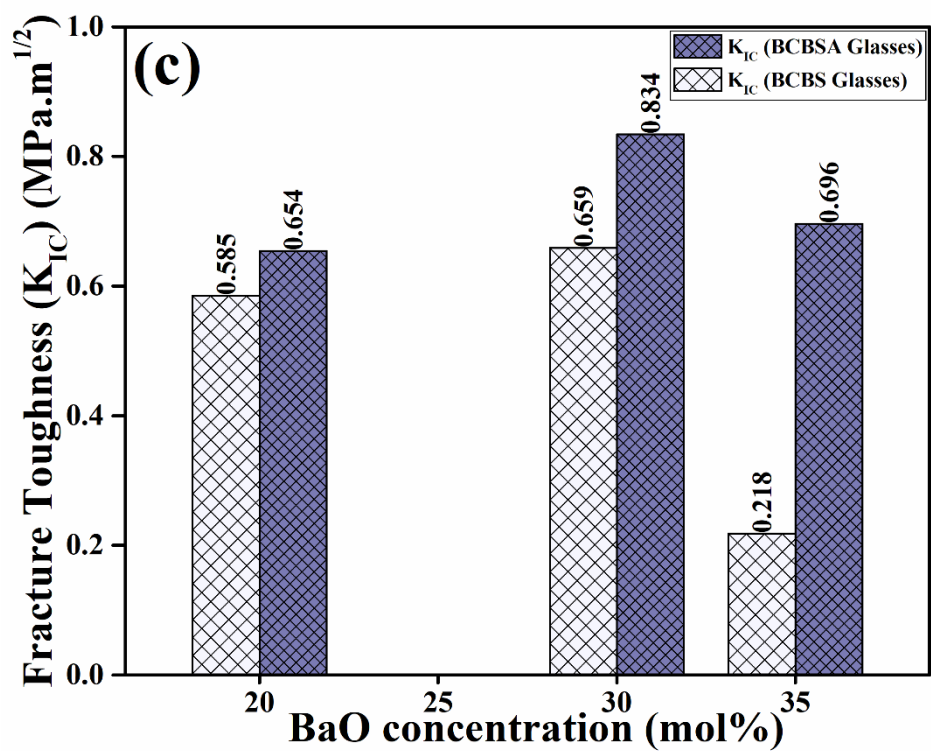
Figure 5.8c. Variation of K_{IC} of BCBSA and BCBS glasses for 0.98 N applied load

Addition of alkaline earth metals in the matrix breaks the connectivity of the glass. However addition of ≤ 5 mol% Al_2O_3 in the matrix, acts as a network former and improves the connectivity, as discussed in the thermal property section. The samples with this improved connectivity is expected to have higher microhardness.

Young's Modulus (E), for all samples were calculated using Makishima-Mackenzie method (Makishima and Mackenzie 1973). The Young's modulus, fracture toughness (K_{IC}) and Brittleness (B) are calculated using equation 2.9, 2.11 and 2.12 respectively, and the measured H_v values under the applied load of 0.98 N, are listed in table 5.3. From figure 5.8b, Young's modulus was observed to decrease consistently with increase in BaO content in the glass matrix or more appropriately as content of CaO increases in the matrix for both BCBSA and BCBS glasses. This observation is similar to what was reported by S R Lopez et. al. (2017) who mentioned that E is higher for SrO and CaO containing glasses as compared to BaO containing glasses (Rodríguez-López et al. 2017). Young's modulus for samples containing Al_2O_3 were found to be more than their Al_2O_3 free counterparts with same BaO concentrations, as can be seen from figure 5.8b. This means Al_2O_3 helps in increasing Young's modulus. So BCBS and BCBSA glasses show similar trend in variation of Young's modulus with Al_2O_3 content as reported by Ghosh et al. (2010) for BCAS glasses (Mukhopadhyay et al. 2009). Materials with Young's modulus (E) between 60 GPa to 65 GPa are good candidates for high temperature sealing applications (Mukhopadhyay et al. 2009). All samples under investigations were found to exhibit E in the approximate range of 60 GPa to 80 GPa from table 5.3. Hence all the glasses with and without Al_2O_3 in the matrix, can be considered as good candidates to be high temperature sealants. However the more appropriate glasses suitable for sealant applications can be decided from the thermal, mechanical and structural properties.

The crack lengths of indentation for all the samples were measured by SEM. The half crack lengths (C), which is the half of the average of two diagonals of the indent, is presented in table 5.3, for all samples tested under an applied load of 0.98 N. With the help of these crack lengths, micro-hardness and Young's modulus, fracture toughness were calculated using equation 2.11. Fracture toughness for the glasses with Al_2O_3 were observed to be higher than the glasses without Al_2O_3. Fracture toughness

for silicate glasses are typically near 0.7 MPa.m$^{1/2}$. With addition of various dopants it may increase up to 1 MPa.m$^{1/2}$ (Rodríguez-López et al. 2017). In the present work, removal of Al_2O_3 reduces the fracture toughness, as evident from figure 5.8c. The effect was observed to be more prominent in sample containing 35 mol% BaO.

Glass ceramics are generally known to be highly brittle. Brittleness listed in table 5.3 shows that Al_2O_3 containing glasses are comparatively less brittle than those with Al_2O_3. This is expected because Al_2O_3 reduces the discontinuity of the system by acting like a glass former. This helps in stronger bonding and reduces brittle behaviour. However, samples 10B and 00B without alumina, show considerably low brittleness as shown in table 5.3. All mechanical parameters for samples 10B and 00B, listed in table 5.3, are in the acceptable range for high temperature sealant applications (Rodríguez-López et al. 2017; Mukhopadhyay et al. 2009).

Table 5.3. Mechanical properties of BCBS and BCBSA glasses

Sample	Micro-Hardness (H_v) (Load 0.98 N) (GPa)	Young's Modulus (E) (GPa)	Crack Length (C) (Load 0.98 N) (µm)	Fracture Toughness (K_{IC}) (MPa m$^{1/2}$)	Brittleness (B) (µm$^{1/2}$)
BCBSA GLASSES					
40 B-A	6.385±0.002	60.391±0.059	11.53±0.04	1.207±0.023	5.288±0.142
35 B-A	6.340±0.002	62.471±0.098	16.87±0.05	0.696±0.012	9.107±0.227
30 B-A	6.480±0.012	64.377±0.091	14.99±0.04	0.834±0.036	7.768±0.472
25 B-A	6.449±0.009	67.021±0.072	9.75±0.02	1.628±0.060	3.962±0.207
20 B-A	6.255±0.007	69.654±0.090	18.31±0.06	0.654±0.022	9.557±0.457
BCBS GLASSES					
35 B	6.135±0.004	58.484±0.061	36.13±0.09	0.218±0.006	28.094±1.045
30 B	6.215±0.002	60.399±0.039	17.42±0.11	0.659±0.013	9.437±0.260
20 B	6.298±0.010	65.904±0.051	19.32±0.10	0.585±0.024	10.760±0.621
10 B	6.801±0.006	71.986±0.002	16.32±0.10	0.758±0.023	8.969±0.385
00 B	7.099±0.004	79.987±0.008	14.35±0.05	0.949±0.023	7.481±0.256

Among the glasses without Al_2O_3, 00B and 10B show fracture toughness near 0.76 and 0.95 $MPam^{1/2}$ respectively, the values of which are in the range acceptable for high temperature sealant applications (Rodríguez-López et al. 2017). Their thermal expansion coefficient values are comparable with the components used in SOFCs. Comparative CTE of sealant and interconnect provide better bonding between them. Apart from that since the 10B and 00B glasses do not contain alumina, the formation of the detrimental monocelsian phase can be avoided at SOFC operating temperatures. Among these two glasses 00B does not contain BaO. The advantage of the glass without BaO is that there will not be any danger of barium chromate phase formation, when coated on Crofer22APU interconnect at high operating temperatures.

5.4. Summary

Thermal and mechanical properties of BCBS based glasses were evaluated in this chapter. Reduction of BaO was found to improve the T_g, T_d and CTE of all glasses. Glasses with low BaO concentrations, especially below 20 mol% like 10B and 00B proved to be better candidates for high temperature sealing. Sintering studies revealed that these glasses two show acceptable shrinkage at 700 °C and 800 °C but starts expanding at 900 °C. Samples that show maximum shrinkage at 700 °C show increase in CTE which matches with the CTE of chromium based steel interconnects. Investigation of the mechanical properties revealed that glasses 10B and 00B are sufficiently hard, have acceptable young's modulus and resistance to fracture. Thus sample 10B and 00B can be concluded to be most suitable candidates for high temperature sealing applications among the investigated glasses in the present work, as they show the required thermal and mechanical properties. They are still devoid of detrimental mono-celsian phase as observed earlier (Bhattacharya and Shashikala 2018). Among these two glasses 00B without BaO poses no danger of reacting with Crofer22APU leading to formation of $BaCrO_4$, during high temperature operations in solid oxide fuel cells.

CHAPTER 6

STRUCTURAL AND ELECTRICAL BEHAVIOUR OF GLASS CERAMIC 00B UNDER SANDWICHED CONDITION BETWEEN TWO METALLIC SUBSTRATES

Obtaining high temperature glass and glass ceramic based seals is one of the biggest challenge in the present day fabrication of Solid Oxide Fuel Cell (SOFC) stacks. Formation of $BaCrO_4$ phase in BCAS glasses leads to degradation of cell performance. This work focusses on one glass composition derived from a BCAS species named 00B which is free of BaO, Al_2O_3 contents and $BaCrO_4$ phase. 00B was sandwiched between two Crofer22APU plates forming CGC sandwiches and heated for repeated thermal cycles from RT to 800 °C to check their compatibility with the metal. Microscopic images of the CGC interface, XRD analysis of the internal surface of the broken sandwich were recorded to observe the structural properties of the prepared sandwich. DC resistivity measurements of the glass under sandwiched conditions between two Crofer22APU plates, at RT and at elevated temperatures were carried out, to determine its resistivity in air, at high temperatures, similar to SOFC operating conditions. The CGC sandwiches prepared using sample 00B show good structural properties after repeated thermal cycles and sufficiently high specific resistance at room and elevated temperatures, and are potentially promising candidates for SOFC sealant applications.

6.1. Results and Discussion

The compatibility between the prepared BaO and Al_2O_3 free glass composition 00B, with Crofer22APU was verified in this chapter.

6.2. Microscopic investigations on CGC interface

Figures 6.1a, b and c represent the optical microscopic images of the CGC00B sandwiches which were heat treated for one, three and five cycles respectively at 800 °C taken at 400X zoom. It is evident form the figures that all samples have a well-defined interface boundary, which shows the glass to be uniformly sandwiched. The thicknesses of the sandwiched glass layer were measured and the recorded thickness

are listed in table 6.1. 1CGC00B exhibited a thickness around 120 μm. But for 3CGC00B the thickness was found to reduce to 76 μm. This implies that the sandwiched glass underwent shrinkage. This is expected and is consistent with the shrinkage studies discussed in chapter 5. After five cycles of heat treatment shrinkage is complete and now thermal expansion is likely to take place, and hence the width increases to around 173 μm. It was observed that in spite of enlargement than the original thickness, after five thermal cycles the metal and glass joint was strong. This must be due to the glasses having matching CTE with that of Crofer22APU, which is in agreement with the thermal expansion studies discussed earlier in chapter 5. After five heating cycles at 800 °C, when thermal expansion has already taken place the quality of the metal – glass – metal seal was uncompromised.
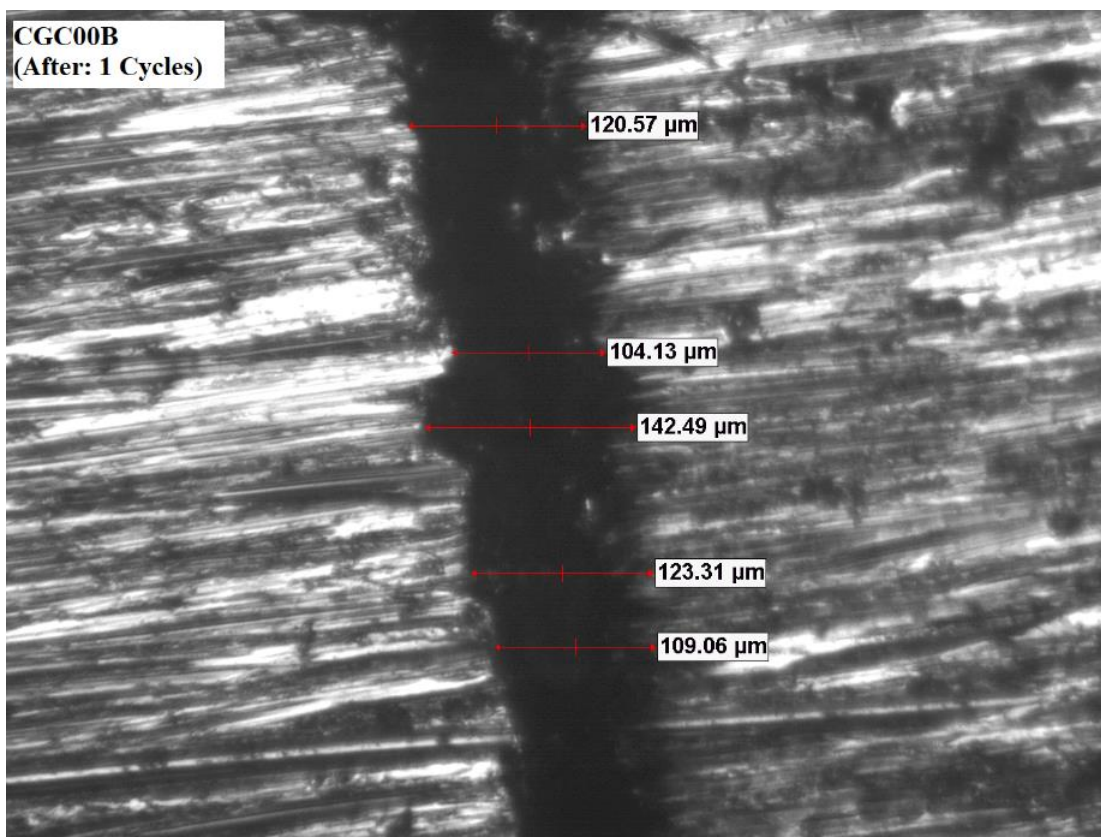
Figure 6.1a: Microscopic image of CGC interface after one thermal cycle
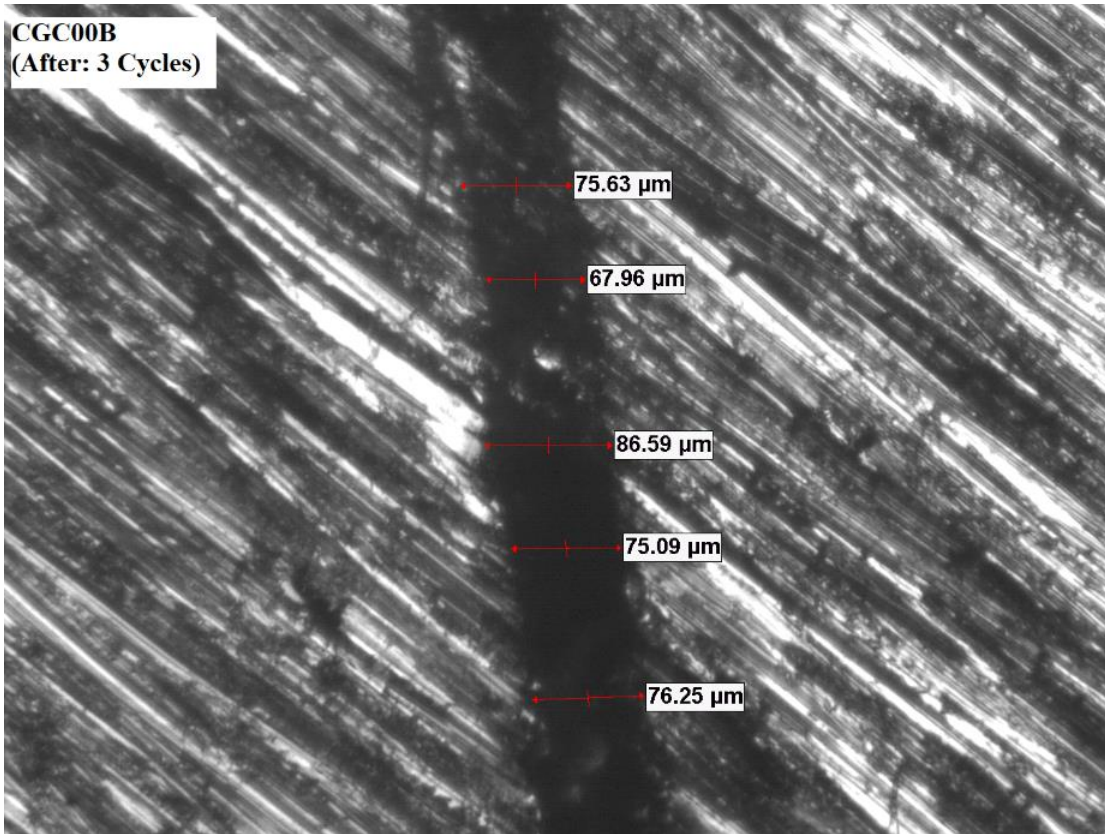
Figure 6.1b: Microscopic image of CGC interface after three thermal cycle

Table 6.1: Resistivity of 00B at different temperatures and thicknesses of the sandwiched layer after different cycles.

Temperature (°C)	Resistivity (Ω-cm)	No of cycles at 800 °C	Sandwich Code	Thickness (μm)
RT	4.2×10^8	1	*1CGC00B*	119.91 (±5.96)
650	4.8×10^8	3	*3CGC00B*	76.10
700	6.3×10^7			(±2.51)
750	8.2×10^6	5	*5CGC00B*	173.30
800	8.1×10^5			(±7.79)
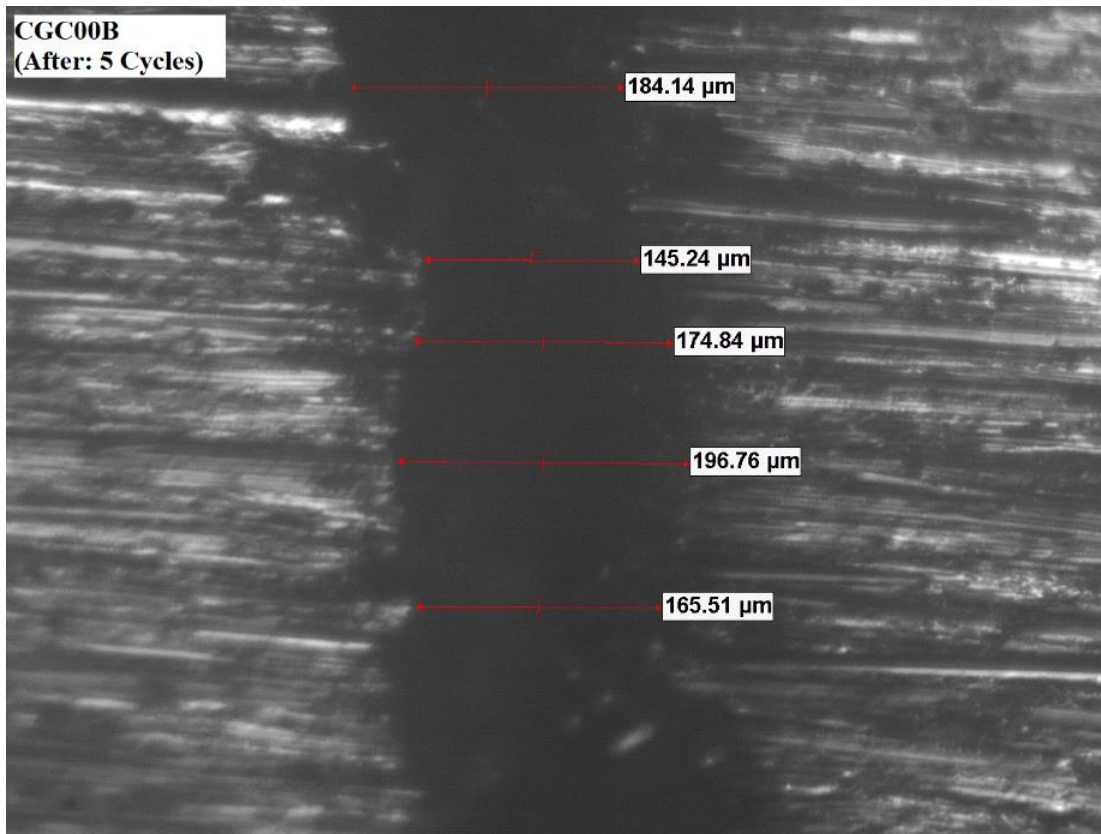
Figure 6.1c: Microscopic image of CGC interface after five thermal cycle

6.3. X-Ray Diffraction (XRD)

Figure 6.2 shows the XRD data for the CGC sandwiches after one three and five cycles of heating. All samples were found to be crystalline. The sharp peaks found near the 2θ of $44.3°$ and $64.6°$ were assigned to the Crofer22APU steel substrate (ICDD File No.: 87-0721). Five different peaks found in the $25°$ to $40°$ region, were all assigned to calcium silicate crystal (ICDD File No.: 72-2284) (Bhattacharya and Shashikala 2018). The crystallization was found to be more profound in 3CGC00B as compared to 1CGC00B. The peak appearing near $56°$ in 3CGC00B, does not appear in 1CGC00B. This shows that crystallization is not complete after one thermal cycle. However not much additional devitrification was observed to occur between the 3CGC00B and 5CGC00B. This indicates that crystallization process is completed after three heating cycles. After five heating cycles of the glass, which has now turned in to a ceramic material was found to exhibit a stable structure and high quality joining strength with Crofer22APU metallic interconnect.
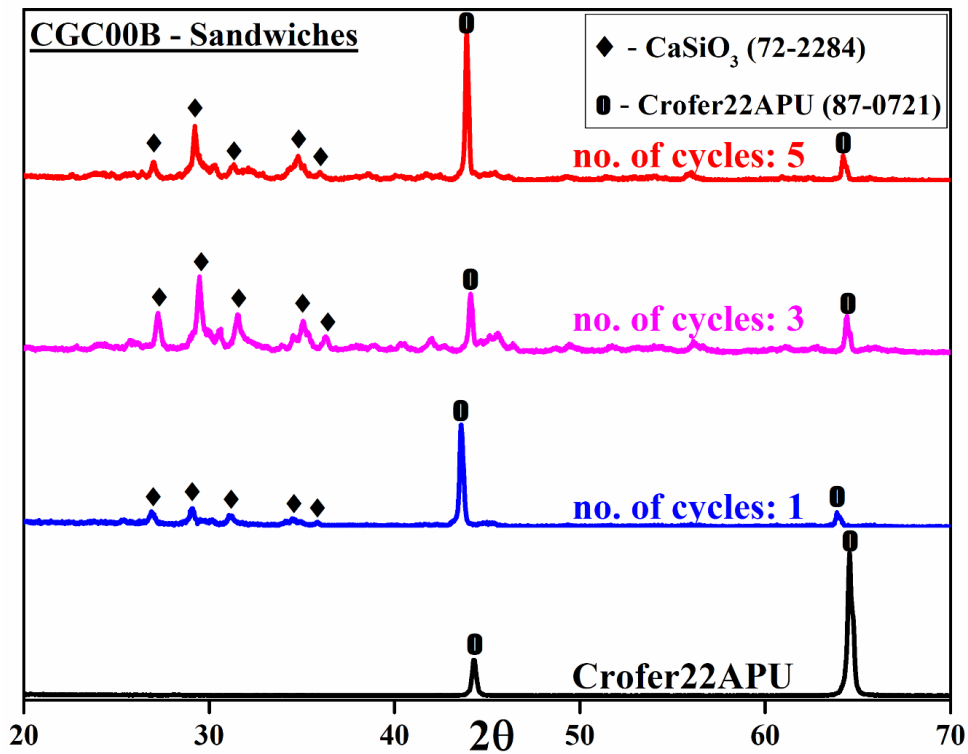
Figure 6.2: XRD patterns of CGC sandwiches after different heating cycles and Crofer22APU

6.4. DC resistivity measurements

DC electrical resistivity measurements were conducted on 1CGC00B, at room temperature and at elevated temperatures from 650 °C to 800 °C. Figure 6.3 shows the ln(R) versus 1/T plot of the glass in the sandwiched condition between two Crofer22APU plates at elevated temperatures. The measured resistivity of the glass at all temperatures are listed in table 6.1. The glass ceramic 00B was found to exhibit a very high resistivity of 4.2×10^8 Ω.cm at room temperature. The resistivity was found to be nearly the same as RT value, at 650 °C, which is just after glass transition. At higher temperatures beyond glass transition temperature resistivity of the samples are generally expected to reduce, which is evidently observed in the present case. The samples were still found to have resistivity more than 10^4 Ω.cm at 700 °C and 800 °C, which is essential for high temperature sealant applications (Grema 2018). The activation energy (E_a) for the sample 00B was calculated and found to be 183 kJ/mol or 1.9 eV, which is appropriate for high temperature sealing applications, and are in

agreement with Goel et al. (2010) and Lara et al. (2006) reported for other compositions of glasses used as SOFC sealants (Ashutosh Goel et al. 2009; Lara et al. 2006).
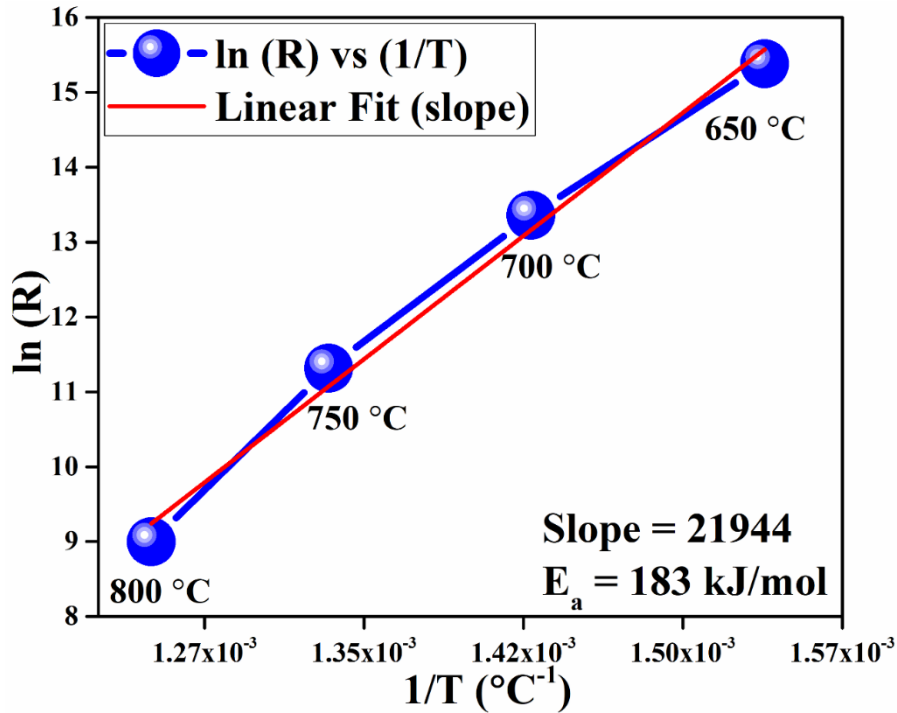
Figure 6.3: Determination of Activation Energy (E_a) for CGC sandwiched sample

6.5. Summary

A CaO – B_2O_3 – SiO_2 glass composition termed as 00B was screen printed on Crofer22APU, a metallic interconnect, used commonly in high temperature sealing. Crofer22APU – Glass – Crofer22APU sandwich with approximately 100 μm glass thickness could be assembled by applying 100 g load and under the load heat treatment at 800 °C. The glass – metal joint was strong and sustainable after five thermal cycles, during which it clearly underwent both expansion and shrinkage. Crystallization is complete within three heating cycles and the glass turns into a completely ceramic material with a stable structure and high thermal expansion coefficient. This ceramic material also offers a high activation energy of 183 kJ/mol for conduction under CGC sandwiched condition and sufficiently high resistance, $>10^5$ Ω.cm at 700 °C and 800 °C, which are operating temperatures of SOFC. The glass ceramic 00B offers a very strong and efficient high temperature metal-glass-metal sealing that exhibits long term stability at both 700 °C and 800 °C.

CHAPTER 7

SUMMARY AND CONCLUSIONS

This chapter summarises the important findings of the present work along with the conclusions. This chapter also discusses the scope of the future work.

7.1. Summary

From the results and discussions presented in chapters 3, 4, 5 and 6 the following can be summarized:

Chapter 3: This chapter explains that 350 °C is the optimum calcination temperature, while the TGA studies confirms the calcination duration of 7 hours at 350 °C for complete conversion of H_3BO_3 to B_2O_3.

Chapter 4: BaO-CaO-B_2O_3-SiO_2 (BCBS) and BaO-CaO-B_2O_3-SiO_2-Al_2O_3 (BCBSA) glasses melted at 1300 °C with ZnO and MgO added as flux, show densities in the acceptable range required for SOFC application (S. F. Wang et al. 2009, 2017; M. Kaur et al. 2017). The density of these glasses can be altered by varying the concentrations of BaO and CaO. The optical band gap energies of the glasses to lie in the range of 3.00 eV to 3.25 eV. This along with the refractive index studies confirmed the insulating nature of all the glasses. Samples with BaO content lower than 20 mol% exhibited a red shift in the absorption spectra and minimum values of density and band gap energy. Wollastonite was found to grow predominantly in all glasses at both 800 °C and 900 °C. Growth of celsian phase was avoided by removing Al_2O_3 from glass matrix. Samples 30B to 00B are devoid of celsian phase. 20B, 10B and 00B i.e. the samples with less than 30 mol% BaO concentration showed excellent devitrification at 900 °C and developed a stable glass ceramic phase.

Chapter 5: Reduction of BaO was found to improve the T_g, T_d and CTE of all glasses. Glasses with low BaO concentrations, especially below 20 mol% like 10B and 00B proved to be better candidates for high temperature sealing. Sintering studies revealed that these glasses have acceptable shrinkage at both 700 °C and 800 °C but started expanding at 900 °C. Samples that show maximum shrinkage at 700 °C show increase in CTE which matches with the CTE of Crofer22APU interconnect. Glasses 10B and 00B were found to be sufficiently hard, having acceptable young's modulus and resistance to fracture (Rodríguez-López et al. 2017; Mukhopadhyay et al. 2009).

Chapter 6: The CaO – B_2O_3 – SiO_2 glass composition termed as 00B, which is free of both BaO and Al_2O_3 was screen printed on Crofer22APU. Crofer22APU – Glass – Crofer22APU joint was observed to be strong and sustainable after five thermal cycles, after it underwent both expansion and shrinkage. Crystallization is complete within three heating cycles and the glass turns into a completely ceramic material. This ceramic material also offers a CTE, a high activation energy of 183 kJ/mol for conduction and sufficiently high resistance, $>10^5$ $\Omega.cm$ at 800 °C, under CGC sandwiched condition.

7.2. Conclusions

In general it can be concluded that all the synthesized glasses are insulators in nature. The isothermal heat treatment studies indicate that the detrimental celsian phase can be avoided in alumina free samples and in samples with below 30 mol% BaO concentrations. Sample 10B and 00B, which are devoid of detrimental mono-celsian phase poses no danger of reacting with Crofer22APU leading to formation of $BaCrO_4$, during high temperature operations in solid oxide fuel cells. This ceramic material, 00B offers a high activation energy for conduction and sufficiently high resistance, $>10^5$ $\Omega.cm$ at 700 °C and 800 °C, under CGC sandwiched condition. The glass ceramic 00B, bearing composition 50mol% $CaO-10B_2O_3-40SiO_2$ is a novel glass, which was never reported for this application to the best of the knowledge of the author and it offers a very strong and efficient high temperature metal-glass-metal sealing that exhibits long term stability at both 700 °C and 800 °C.

7.3. Scope of future work

Development of a usable and efficient high temperature glass as a sealant material for SOFC or similar electrochemical devices are highly important to meet the ever growing demands of energy. It is highly recommended to focus on the production of energy that involves no emission of hydrocarbons as in the case of SOFCs. The work presented here in this thesis concludes that low BaO containing borosilicate glasses or BaO free glasses are best suitable materials for high temperature sealant applications. This still leaves us with a scope to further investigate:

- more compositions of BaO and Al_2O_3 free glasses for SOFC sealant applications.
- achieving better control over the coating, thickness of coatings.
- preparation of CGC sandwiches of optimum thickness and dimensions.
- performing gas leakage tests to understand efficiency of the glass under CGC condition at elevated temperatures.
- development of multiple SOFC stacks for high temperature operation using the recommended composition of glass, to check actual usability.

BIBLIOGRAPHY

A A Reddy, Tulyaganov, Dilshat U. 2013. "Study of Calcium – Magnesium – Aluminum – Silicate (CMAS) Glass and Glass-Ceramic Sealant for Solid Oxide Fuel Cells," no. 2013. https://doi.org/10.1016/j.jpowsour.2012.12.055.

Amarnath, Allu, Neda Eghtesadi, Dilshat U Tulyaganov, Maria J Pascual, Luis F Santos, Surendran Rajesh, Fernando M B Marques, and José M F Ferreira. 2014. "Bi-Layer Glass-Ceramic Sealant for Solid Oxide Fuel Cells." *Journal of the European Ceramic Society* 34 (5): 1449–55. https://doi.org/10.1016/j.jeurceramsoc.2013.11.012.

Bhattacharya, Soumalya, and H. D. Shashikala. 2018. "Optical and Structural Properties of BCBS Glass System with and without Alumina." *Physica B: Condensed Matter* 548 (April): 10–19. https://doi.org/10.1016/j.physb.2018.08.013.

Bhattacharya, Soumalya, and H D Shashikala. 2019. "Physica B : Condensed Matter Effect of BaO on Thermal and Mechanical Properties of Alkaline Earth Borosilicate Glasses with and without Al$_2$O$_3$." *Physica B: Physics of Condensed Matter* 571 (April): 76–86. https://doi.org/10.1016/j.physb.2019.06.065.

Cao, Can, Zhuo-bin Li, Xiao-liang Wang, Xin-bing Zhao, and Wei-qiang Han. 2014. "Recent Advances in Inorganic Solid Electrolytes for Lithium Batteries" 2 (June): 1–10. https://doi.org/10.3389/fenrg.2014.00025.

Conradt, R, A Schusser, M J Pascual, A Prange, and A Dura. 2013. "Characterization of a Soldering System Consisting of a Glass from The" 39: 3753–58. https://doi.org/10.1016/j.ceramint.2012.10.213.

Dimitrov, V, and T Komatsu. 2010. "An interpretation of optical properties of oxides and oxide glasses in terms of the electronic ion polarizability and average single bond strength (review)," 219–50.

El-nahass, M M, M Dongol, M Abou-zied, and A El-denglawey. 2005. "The Compositional Dependence of the Structural and Optical Properties of Amorphous As 20 Se 80 À x Tl x Films" 368: 179–87. https://doi.org/10.1016/j.physb.2005.07.014.

Ferrari, Anna Maria, José M. F. Ferreira, Andreas Prange, Federica Bondioli, Dilshat U. Tulyaganov, Ashutosh Goel, and Essam R. Shaaban. 2010. "Structure, Sintering, and Crystallization Kinetics of Alkaline-Earth Aluminosilicate Glass-Ceramic Sealants for Solid Oxide Fuel Cells." *Journal of the American Ceramic Society* 93 (3): 830–37. https://doi.org/10.1111/j.1551-2916.2009.03503.x.

Ferreira, José M.F., Vladislav V. Kharton, Aleksey A. Yaremchenko, Dilshat U. Tulyaganov, and Ashutosh Goel. 2008. "The Effect of Cr$_2$O$_3$ Addition on Crystallization and Properties of La$_2$O$_3$-Containing Diopside Glass-Ceramics." *Acta Materialia* 56 (13): 3065–76. https://doi.org/10.1016/j.actamat.2008.02.036.

Fu, Anna I, and John C Mauro. 2013. "Topology of Alkali Phosphate Glass Networks." *Journal of Non-Crystalline Solids* 361:

57–62. https://doi.org/10.1016/j.jnoncrysol.2012.11.001.

Gaddam, Anuraag, Hugo R Fernandes, Maria J Pascual, and M F Ferreira. 2016. "Influence of Al_2O_3 and B_2O_3 on Sintering and Crystallization of Lithium Silicate Glass System" 840 (37546): 833–40. https://doi.org/10.1111/jace.14040.

Gautam, CR, and Avadhesh Kumar Yadav. 2013. "Synthesis and Optical Investigations on (Ba,Sr) TiO_3 Borosilicate Glasses Doped with La_2O_3" 2013 (August): 1–7.

Ghosh, Saswati, P. Kundu, A. Das Sharma, R. N. Basu, and H. S. Maiti. 2008. "Microstructure and Property Evaluation of Barium Aluminosilicate Glass-Ceramic Sealant for Anode-Supported Solid Oxide Fuel Cell." *Journal of the European Ceramic Society* 28 (1): 69–76. https://doi.org/10.1016/j.jeurceramsoc.2007.05.008.

Ghosh, Saswati, A. Das Sharma, P. Kundu, S. Mahanty, and R. N. Basu. 2008. "Development and Characterizations of BaO-CaO-Al_2O_3-SiO_2 Glass-Ceramic Sealants for Intermediate Temperature Solid Oxide Fuel Cell Application." *Journal of Non-Crystalline Solids* 354 (34):4081–88. https://doi.org/10.1016/j.jnoncrysol.2008.05.036.

Ghosh, Saswati, A Das Sharma, P Kundu, and R N Basu. 2008. "Glass-Ceramic Sealants for Planar IT-SOFC : A Bilayered Approach for Joining Electrolyte and Metallic Interconnect," no. 3: 473–78. https://doi.org/10.1149/1.2883732.

Goel, A., D. U. Tulyaganov, S. Agathopoulos, and J. M.F. Ferreira. 2008. "The Effect of Al_2O_3 on Sintering and Crystallization of $MgSiO_3$-Based Glass-Powder Compacts." *Ceramics International* 34 (3):505–10. https://doi.org/10.1016/j.ceramint.2006.11.006.

Goel, Ashutosh, and Maria J Pascual. 2010. "Stable Glass-Ceramic Sealants for Solid Oxide Fuel Cells : Influence of Bi_2O_3 Doping"
5. https://doi.org/10.1016/j.ijhydene.2010.04.106.

Goel, Ashutosh, Dilshat U Tulyaganov, Vladislav V Kharton, Aleksey A Yaremchenko, Sten Eriksson, and José M F Ferreira. 2009. "Optimization of La_2O_3 - Containing Diopside Based Glass-Ceramic Sealants for Fuel Cell Applications" 189: 1032–43. https://doi.org/10.1016/j.jpowsour.2009.01.013.

Grema, L U. 2018. "The Effects of Composition on the Thermal , Mechanical and Electrical Properties of Alumino-Borosilicate Sealing Glasses for Solid Oxide Fuel Cell (SOFC) Applications . By Lawan Umar Grema A Thesis Submitted for the Degree of Doctor of Philosophy The Un."

Hao, Jie, Qingfeng Zan, Desheng Ai, Jingtao Ma, Changsheng Deng, and Jingming Xu. 2012. "Structure and High Temperature Physical Properties of Glass Seal Materials in Solid Oxide Electrolysis Cell." *Journal of Power Sources* 214: 75–83. https://doi.org/10.1016/j.jpowsour.2012.03.087.

Hassanien, Ahmed Saeed, and Alaa Ahmed Akl. 2015. "Influence of Composition on Optical and Dispersion Parameters of Thermally Evaporated Non-Crystalline Cd50 S50-XSex Thin Films," no. September. https://doi.org/10.1016/j.jallcom.2015.06.231.

Herzfeld, K F. 1927. "On Atomic Properties Which Make an Element a Metal" 2 (2).

Heydari, Fatemeh, Amir Maghsoudipour, Zohreh Hamnabard, and Sajad Farhangdoust. 2013. "Evaluation on Properties of $CaO-BaO-B_2O_3-Al_2O_3-SiO_2$ Glass-Ceramic Sealants for Intermediate Temperature Solid Oxide Fuel Cells." *Journal of Materials Science and Technology* 29 (1): 49–54. https://doi.org/10.1016/j.jmst.2012.11.011.

Hong, Seung Kwon, Dae Soo Jung, Jung Sang Cho, and Yun Chan Kang. 2008. "Characteristics of $ZnO-B_2O_3-CaO-Na_2O-P_2O_5$ Glass Powders Prepared by Spray Pyrolysis" 354: 3012–18. https://doi.org/10.1016/j.jnoncrysol.2007.12.014.

J E Shelby. 2005. *Introduction to Glass Science and Technology (2nd Edition)*. 2nd ed.

J Shadia, Shadia, and Riyad N Ahmad-bitar. 2013. "Original Article A Study of the Optical Bandgap Energy and Urbach Tail of Spray-Deposited CdS : In Thin Films." *Integrative Medicine Research* 2 (3):
221–27. https://doi.org/10.1016/j.jmrt.2013.02.012.

Jain, Himani. 1996. "Correlation between Dielectric Constant and Chemical Structure of Sodium Silicate Glasses Correlation between Dielectric Constant and Chemical Structure of Sodium Silicate Glasses," no.
September. https://doi.org/10.1063/1.363824.

Javed, Hassan, Antonio Gianfranco Sabato, Kai Herbrig, Domenico Ferrero, Christian Walter, Milena Salvo, and Federico Smeacetto. 2018. "Design and Characterization of Novel Glass-Ceramic Sealants for Solid Oxide Electrolysis Cell (SOEC) Applications." *International Journal of Applied Ceramic Technology* 15 (4): 999–1010. https://doi.org/10.1111/ijac.12889.

Kaur, Gurbinder, K. Singh, O. P. Pandey, D. Homa, B. Scott, and G. Pickrell. 2013. "Structural and Thermal Properties of Glass Composite Seals and Their Chemical Compatibility with Crofer 22APU for Solid Oxide Fuel Cells Applications." *Journal of Power Sources* 240: 458–70. https://doi.org/10.1016/j.jpowsour.2013.03.142.

Kaur, Mandeep, Gurbinder Kaur, O. P. Pandey, K. Singh, and V. Kumar. 2017. "Influence of CaO/MgO Ratio on the Crystallization Kinetics and Interfacial Compatibility with Crofer 22APU and YSZ of Strontium Based Alumino-Borosilicate Glasses for SOFC Applications." *International Journal of Hydrogen Energy* 42 (25): 16244–57. https://doi.org/10.1016/j.ijhydene.2017.05.026.

Kerstan, Marita, and Christian Rüssel. 2011. "Barium Silicates as High Thermal Expansion Seals for Solid Oxide Fuel Cells Studied by High-Temperature X-Ray Diffraction (HT-XRD)." *Journal of Power Sources* 196 (18): 7578–84. https://doi.org/10.1016/j.jpowsour.2011.04.035.

Kim, E A, H W Choi, and Y S Yang. 2015. "Effects of Al_2O_3 on (1 À x)[$SrO-SiO_2-B_2O_3$] – x Al_2O_3 Glass Sealant for Intermediate Temperature Solid Oxide Fuel Cell." *Ceramics International* 41 (10):
14621–26. https://doi.org/10.1016/j.ceramint.2015.07.182.

Kožušníková, Alena. 2009. "Determination of Microhardness and Elastic Modulus of Coal Components by Using Indentation Method." *GeoLines* 22: 40–43.

Kruzic, J. J., D. K. Kim, K. J. Koester, and R. O. Ritchie. 2009. "Indentation Techniques for Evaluating the Fracture Toughness of Biomaterials and Hard Tissues." *Journal of the Mechanical Behavior of Biomedical Materials* 2 (4): 384–95. https://doi.org/10.1016/j.jmbbm.2008.10.008.

Kurama, Semra, and Gamze Saydam. 2017. "Investigation Properties of BaO/RO-Al_2O_3-R_2O_3-B_2O_3-SiO_2 glass-Ceramic Sealants for Solid Oxide Fuel Cell." *Journal of the Australian Ceramic Society* 53 (2): 293–98. https://doi.org/10.1007/s41779-017-0036-8.

Lara, C, M J Pascual, R Keding, and A Dur. 2006. "Electrical Behaviour of Glass – Ceramics in the Systems RO – BaO – SiO_2 (R = Mg , Zn) for Sealing SOFCs" 157: 377–84. https://doi.org/10.1016/j.jpowsour.2005.07.084.

Lara, C, M J Pascual, M O Prado, and A Dura. 2004. "Sintering of Glasses in the System RO – Al_2O_3 – BaO – SiO_2 (R = Ca , Mg , Zn) Studied by Hot-Stage Microscopy" 170: 201–8. https://doi.org/10.1016/j.ssi.2004.03.009.

Li, Z. X., H. J. Mao, Y. W. Zhang, and W. J. Zhang. 2018. "Influences of Glass Content on the Microstructure and Properties of BaO-CaO-Al_2O_3-SiO_2 Glass/Alumina Composite for LTCC Applications." *IOP Conference Series: Materials Science and Engineering* 292 (1). https://doi.org/10.1088/1757-899X/292/1/012082.

Mafra, Luis, Maria J Pascual, Vladislav V Kharton, and Ekaterina V Tsipis. 2014. "Thermal and Mechanical Stability of Lanthanide- Containing Glass – Ceramic Sealants for Solid Oxide," no. i: 1834–46. https://doi.org/10.1039/c3ta13196c.

Makishima, A., and J. D. Mackenzie. 1973. "Direct Calculation of Young's Moidulus of Glass." *Journal of Non-Crystalline Solids* 12 (1): 35–45. https://doi.org/10.1016/0022-3093(73)90053-7.

Meinhardt, K. D., D. S. Kim, Y. S. Chou, and K. S. Weil. 2008. "Synthesis and Properties of a Barium Aluminosilicate Solid Oxide Fuel Cell Glass-Ceramic Sealant." *Journal of Power Sources* 182 (1): 188–96. https://doi.org/10.1016/j.jpowsour.2008.03.079.

Meinhardt K D Morin, P, T H Applebaum, R Bowman, Y Zhao, Compact Multilingual, Word Recog, P Morin, et al. 2002. "(12) United States Patent" 1 (12): 1–5.

Mukhopadhyay, A.K., R.N. Basu, A. Das Sharma, P. Kundu, and Saswati Ghosh. 2009. "Effect of BaO Addition on Magnesium Lanthanum Alumino Borosilicate-Based Glass-Ceramic Sealant for Anode-Supported Solid Oxide Fuel Cell." *International Journal of Hydrogen Energy* 35 (1): 272–83. https://doi.org/10.1016/j.ijhydene.2009.10.006.

Ojha, Prasanta Kumar, S. K. Rath, T. K. Chongdar, N. M. Gokhale, and A. R. Kulkarni.

2011. "Physical and Thermal Behaviour of Sr-La-Al-B-Si Based SOFC Glass Sealants as Function of SrO Content and B_2O_3/SiO_2 Ratio in the Matrix." *Journal of Power Sources* 196 (10): 4594–98. https://doi.org/10.1016/j.jpowsour.2011.01.021.

Ozgur Colpan, C., Dincer Ibrahim, and Hamdullahpur Feridun. 2008. "A Review on Macro-Level Modeling of Planar Solid Oxide Fuel Cells C." *International Journal of Energy Research* 32 (32): 336–55. https://doi.org/10.1002/er.

Puig, J., F. Ansart, P. Lenormand, R. Conradt, and S. M. Gross-Barsnick. 2016. "Development of Barium Boron Aluminosilicate Glass Sealants Using a Sol–Gel Route for Solid Oxide Fuel Cell Applications." *Journal of Materials Science* 51 (2): 979–88. https://doi.org/10.1007/s10853-015-9428-8.

Puig, J., A. Prange, B. Arati, C. Laime, P. Lenormand, and F. Ansart. 2017. "Optimization of the Synthesis Route of a Barium Boron Aluminosilicate Sealing Glass for SOFC Applications." *Ceramics International* 43 (13): 9753–58. https://doi.org/10.1016/j.ceramint.2017.04.151.

Rao, K. J. 2002. *Structural Chemistry of Glasses*.

Reddy, Allu Amarnath, Dilshat U Tulyaganov, Ashutosh Goel, Mariana Sardo, Paul V Wiper, Maria J Pascual, Vladislav V Kharton, Vladislav A Kolotygin, and Ekaterina V Tsipis. 2013. "Effects of ZrO_2 Additions Assessed by Microscopy ," 6471–80. https://doi.org/10.1039/c3ta10789b.

Reis, S. T., M. J. Pascual, R. K. Brow, C. S. Ray, and T. Zhang. 2010. "Crystallization and Processing of SOFC Sealing Glasses." *Journal of Non-Crystalline Solids* 356 (52–54): 3009–12. https://doi.org/10.1016/j.jnoncrysol.2010.02.028.

Rodríguez-López, S., J. Wei, K. C. Laurenti, I. Mathias, V. M. Justo, F. C. Serbena, C. Baudín, J. Malzbender, and M. J. Pascual. 2017. "Mechanical Properties of Solid Oxide Fuel Cell Glass-Ceramic Sealants in the System BaO/SrO-MgO-B_2O_3-SiO_2." *Journal of the European Ceramic Society* 37 (11): 3579–94. https://doi.org/10.1016/j.jeurceramsoc.2017.03.054.

Sabato, A G, G Cempura, D Montinaro, A Chrysanthou, M Salvo, E Bernardo, M Secco, and F Smeacetto. 2016. "Glass-Ceramic Sealant for Solid Oxide Fuel Cells Application : Characterization and Performance in Dual Atmosphere." *Journal of Power Sources* 328: 262–70. https://doi.org/10.1016/j.jpowsour.2016.08.010.

Sasmal, Nibedita, Mrinmoy Garai, Atiar Rahman Molla, Anal Tarafder, Shiv Prakash Singh, and Basudeb Karmakar. 2014. "Effects of Lanthanum Oxide on the Properties of Barium-Free Alkaline-Earth Borosilicate Sealant Glass." *Journal of Non-Crystalline Solids* 387: 62–70. https://doi.org/10.1016/j.jnoncrysol.2013.12.030.

Schilm, Jochen, Axel Rost, Mihails Kusnezoff, Stefan Megel, and Alexander Michaelis. 2018. "Glass Ceramics Sealants for SOFC Interconnects Based on a High Chromium Sinter Alloy." *International Journal of Applied Ceramic Technology* 15 (2): 239–54. https://doi.org/10.1111/ijac.12811.

Science, Materials, Ashutosh Goel Rutgers, and Pascual Spanish. 2013. "Sintering and Devitrification of Glass-Powder Compacts in the Akermanite-Gehlenite System," no. June 2016. https://doi.org/10.1007/s10853-013-7225-9.

Sevim, Fatih, Fatih Demir, Murat Bilen, and Hüseyin Okur. 2006. "Kinetic Analysis of Thermal Decomposition of Boric Acid from Thermogravimetric Data" 23 (5): 736–40.

Shao, Haibin, Tingwei Wang, and Qitu Zhang. 2009. "Preparation and Properties of CaO – SiO$_2$ – B$_2$O$_3$ Glass-Ceramic at Low Temperature" 484: 2–5. https://doi.org/10.1016/j.jallcom.2009.03.186.

Silva, Laís D., Alisson M. Rodrigues, Ana Candida M. Rodrigues, María J. Pascual, Alicia Durán, and Aluísio A. Cabral. 2017. "Sintering and Crystallization of SrO-CaO-B$_2$O$_3$-SiO$_2$ Glass-Ceramics with Different TiO$_2$ Contents." *Journal of Non-Crystalline Solids* 473 (July): 33–40. https://doi.org/10.1016/j.jnoncrysol.2017.07.021.

Silva, Maviael J. Da, José F. Bartolomé, Antonio H. De Aza, and Sonia Mello-Castanho. 2016. "Glass Ceramic Sealants Belonging to BAS (BaO-Al$_2$O$_3$-SiO$_2$) Ternary System Modified with B$_2$O$_3$ Addition: A Different Approach to Access the SOFC Seal Issue." *Journal of the European Ceramic Society* 36 (3): 631–44. https://doi.org/10.1016/j.jeurceramsoc.2015.10.005.

Soares, Priscilla Barbosa Ferreira, Sarah Arantes Nunes, Sinesio Domingues Franco, Raphael Rezende Pires, Darceny Zanetta-Barbosa, and Carlos Jose Soares. 2014. "Measurement of Elastic Modulus and Vickers Hardness of Surround Bone Implant Using Dynamic Microindentation-Parameters Definition." *Brazilian Dental Journal* 25 (5): 385–90. https://doi.org/10.1590/0103-6440201300169.

Sun, Tao, Hanning Xiao, Wenming Guo, and Xiucheng Hong. 2010. "Effect of Al$_2$O$_3$ Content on BaO-Al$_2$O$_3$-B$_2$O$_3$-SiO$_2$ Glass Sealant for Solid Oxide Fuel Cell." *Ceramics International* 36 (2): 821–26. https://doi.org/10.1016/j.ceramint.2009.09.045.

Tulyaganov, Dilshat U. 2016. "Effect of BaO Addition on Crystallization , Microstructure , and Properties of Diopside – Ca - Tschermak Clinopyroxene - Based Glass – Ceramics," no. May. https://doi.org/10.1111/j.1551-2916.2007.01743.x.

Varshneya K, Varshneya. 1994. *Fundamentals of Inorganic Glasses*. Vol. 170. https://doi.org/10.1016/0022-3093(94)90112-0.

Venkateswara Rao, G., and H. D. Shashikala. 2014. "Structural, Optical and Mechanical Properties of Ternary CaO-CaF$_2$-P$_2$O$_5$ Glasses." *Journal of Advanced Ceramics* 3 (2): 109–16. https://doi.org/10.1007/s40145-014-0099-8.

Wang, Sea Fue, His Chuan Lu, Yi Xin Liu, Yung Fu Hsu, and Zu You Liu. 2017. "Characteristics of Glass Sealants for Intermediate-Temperature Solid Oxide Fuel Cell Applications." *Ceramics International* 43 (May): S613–20. https://doi.org/10.1016/j.ceramint.2017.05.211.

Wang, Sea Fue, Yuh Ruey Wang, Yung Fu Hsu, and Ching Chin Chuang. 2009. "Effect

of Additives on the Thermal Properties and Sealing Characteristic of BaO-Al$_2$O$_3$-B$_2$O$_3$-SiO$_2$ Glass-Ceramic for Solid Oxide Fuel Cell Application." *International Journal of Hydrogen Energy* 34 (19): 8235–44. https://doi.org/10.1016/j.ijhydene.2009.07.094.

Wang, Xiuling, Ding Rong, Zhe Zhao, and Mojie Cheng. 2016. "Stability of SrO – La$_2$O$_3$ – Al$_2$O$_3$ – SiO$_2$ Glass Sealants in High-Temperature Air and Steam." *Ceramics International* 42 (6): 7514–23. https://doi.org/10.1016/j.ceramint.2016.01.158.

Wu, Yefan, Jijun Shi, ZuZhi Huang, Liang Cheng, Youchen Lin, Linghong Luo, and Liangliang Sun. 2015. "Application of BaO–CaO–Al$_2$O$_3$–B$_2$O$_3$–SiO$_2$ Glass–Ceramic Seals in Large Size Planar IT-SOFC." *Ceramics International* 41 (8): 9239–43. https://doi.org/10.1016/j.ceramint.2015.01.091.

Xu, Qiutong, and Li Xu. 2018. "A Novel High-Performance Ti / ATONPs-MWCNTs Electrode Based on Screen Printing Technique for Degradation of C . I . Acid Red 73" 13: 119–35. https://doi.org/10.20964/2018.01.06.

Xu, Xu, Leying Wang, Yefan Wu, Linghong Luo, Liang Cheng, Liangguang Liu, and Zuzhi Huang. 2018. "Effect of Al$_2$O$_3$ Addition on the Non-Isothermal Crystallization Kinetics and Long-Term Stability of BCABS Sealing Glass for IT-SOFCs." *Journal of Advanced Ceramics* 7 (4): 380–87. https://doi.org/10.1007/s40145-018-0294-0.

Zhang, Qi, Lihua Fang, Jie Shen, Maria J Pascual, and Teng Zhang. 2015. "Tuning the Interfacial Reaction Between Bismuth-Containing Sealing Glasses and Cr-Containing Interconnect: Effect of ZnO" 3806. https://doi.org/10.1111/jace.13779.

RESEARCH OUTPUTS

1. PEER REVIEWED RESEARCH

- Bhattacharya S., Shashikala H. D. (2018). "*Effect of Calcination Temperature and Time on Synthesis of BaO-CaO-Al$_2$O$_3$ -SiO$_2$Glass.*" Materials Today: Proceedings. 5(8), pp. 16863-16868. doi.org/10.1016/j.matpr.2018.05.105

- Bhattacharya S., Shashikala H. D. (2018). "*Optical and structural properties of BCBS glass system with and without alumina.*" Physica B: Condensed Matter. 548, pp. 10-19. doi.org/10.1016/j.physb.2018.08.013

- Bhattacharya S., Shashikala H. D. (2019). "*Effect of BaO on thermal and mechanical properties of alkaline earth borosilicate glasses with and without Al$_2$O$_3$*" Physica B: Condensed Matter. 571, pp. 76-86. doi.org/10.1016/j.physb.2019.06.065.

- Bhattacharya S., Shashikala H. D. "*Structural and electrical behaviour of glass ceramic 00B under sandwiched condition between two metallic substrates.*" Materials Today: Proceedings. **(Accepted – 27th May 2020)**

- Subhashini, Bhattacharya S., Shashikala H. D. (2014). "Synthesis and studies on microhardness of alkali zinc borate glasses." AIP Proceedings. 1591, pp. 749-750. doi.org/10.1063/1.4872742

- Rajat Ramteke, Kalpana K., Bhattacharya S., Rahman M. R., (2019). "Synthesis and characterization of zinc oxide incorporated iron borate glass ceramic." Journal of Alloys and compounds. 151876. doi.org/10.1016/j.jallcom.2019.151876

2. CONFERENCES ATTENDED

- "Synthesis and studies on microhardness of alkali zinc borate glasses." The 58th DAE – Solid State Physics Symposium (DAE-SSPS 2013) held at Thapar University, Patiala, Punjab, during 17-21 December 2013. The full-length paper was published in AIP: Proceedings listed in *Peer Reviewed Research* section.

- "Effect of temperature on certain physical and mechanical properties of alkali zinc borate glasses." International Union of Materials Research Societies (IUMRS – ICA 2013) held at Indian Institute of Science, Bangalore during 16-20 December 2013.

- "Effect of incorporation of Fly Ash on physical and mechanical properties of Calcium Phosphate glass." National Conference on Condensed Matter Physics and Applications (CMPA 2013) held at Manipal Institute of Technology, Manipal during 27-28 December 2013.

- "Effect of soaking temperature on properties of 50.8 wt% BaO- 9.3 wt% CaO- 5.6 wt% Al_2O_3- 7.7 wt% B_2O_3- 26.6 wt% SiO_2 glass." First International Conference on Emerging Materials: Characterization and Application (EMCA 2014) held at CSIR – Central Glass and Ceramic Research Institute, Kolkata during 4-6 December 2014.

- "Effect of calcination temperature and time on synthesis of BCAS glass." International Conference on Advanced Materials (SCICON 2016) held at Amrita Vishwa Vidyapeetham, Coimbatore during 19-21 December 2016. The full-length paper was published in Materials Today: Proceedings listed in *Peer Reviewed Research* section.

3. WORKSHOPS ATTENDED

- Experimental Physics for high school teachers - Presented a talk of "Radar" on 19th January 2013, held at NITK.

- Three day workshop on "Frontiers of Astronomy" – Attended during 1-3 February 2013, held at NITK.

- Three day workshop on "Application of Statistical and Soft Computing Techniques in Engineering Research" – Participated during 29-31 July 2013, held at Canara Engineering College, Mangalore.

- National Seminar on Advances in Materials Science (SAMS 2013) – Participated during 22nd November 2013, held in Mangalore University.

Soumalya Bhattacharya

Father's Name: Mr. Samarendra Bhattacharyya
Mother's Name: Mrs. Rinku Bhattacharyya
Date of Birth: 06th July 1988.
Address: 64/20, Khudiram Bose Sarani,
    Duttabagan Milk Colony,
    Kolkata, West Bengal.
    Pin: 700037, India.
E-mail: bhattacharya.6788@gmail.com

Phone: +91-8050303887

EDUCATION

Name of Degree	Discipline	Institution	Year of Passing	Marks Obtained
Bachelor of Science (B.Sc.)	Physics	D G Ruparel College of Arts, Commerce and Science	2010	63.88 %
Master of Science (M.Sc.)	Solid State Physics	Institute of Science, University of Mumbai	2012	64.60 %
Doctor of Philosophy (Ph.D.)	Physics	National Institute of Technology Karnataka	2012 - ongoing	75.00% (C. Work)

ACADEMIC THESIS

- **M.Sc. Dissertation:** Synthesis and characterization of TiO_2 nano powders.
  Doctor of Philosophy: Synthesis and characterization of alkaline earth oxide added borosilicate glasses for high temperature sealant application.

PEER REVIEWED RESEARCH

1. Subhashini, Bhattacharya S., Shashikala H. D. (2014). "Synthesis and studies on microhardness of alkali zinc borate glasses." AIP Proceedings. 1591, pp. 749-750. doi.org/10.1063/1.4872742
2. Bhattacharya S., Shashikala H. D. (2018). "Effect of Calcination Temperature and Time on Synthesis of $BaO-CaO-Al_2O_3$ -SiO_2Glass." Materials Today: Proceedings. 5(8), pp. 16863-16868. doi.org/10.1016/j.matpr.2018.05.105

3. Bhattacharya S., Shashikala H. D. (2018). "Optical and structural properties of BCBS glass system with and without alumina." Physica B: Condensed Matter. 548, pp. 10-19. doi.org/10.1016/j.physb.2018.08.013

4. Bhattacharya S., Shashikala H. D. (2019). "Effect of BaO on thermal and mechanical properties of alkaline earth borosilicate glasses with and without Al_2O_3" Physica B: Condensed Matter. 571, pp. 76-86. doi.org/10.1016/j.physb.2019.06.065.

5. Rajat Ramteke, Kalpana K., Bhattacharya S., Rahman M. R., (2019). "Synthesis and characterization of zinc oxide incorporated iron borate glass ceramic." Journal of Alloys and compounds. 151876. doi.org/10.1016/j.jallcom.2019.151876.

6. Bhattacharya S., Shashikala H. D. "*Structural and electrical behaviour of glass ceramic 00B under sandwiched condition between two metallic substrates.*" Materials Today: Proceedings. **(Accepted – 27th May 2020)**

POSTERS PRESENTED AT CONFERENCES

1. "Synthesis and studies on microhardness of alkali zinc borate glasses." The 58th DAE – Solid State Physics Symposium (DAE-SSPS 2013) held at Thapar University, Patiala, Punjab, during 17-21 December 2013. The full-length paper was published in AIP: Proceedings listed in *Peer Reviewed Research* section.

2. "Effect of temperature on certain physical and mechanical properties of alkali zinc borate glasses." International Union of Materials Research Societies (IUMRS – ICA 2013) held at Indian Institute of Science, Bangalore during 16-20 December 2013.

3. "Effect of incorporation of Fly Ash on physical and mechanical properties of Calcium Phosphate glass." National Conference on Condensed Matter Physics and Applications (CMPA 2013) held at Manipal Institute of Technology, Manipal during 27-28 December 2013.

4. "Effect of soaking temperature on properties of 50.8 wt% BaO- 9.3 wt% CaO- 5.6 wt% Al_2O_3- 7.7 wt% B_2O_3- 26.6 wt% SiO_2 glass." First International Conference on Emerging Materials: Characterization and Application (EMCA 2014) held at CSIR – Central Glass and Ceramic Research Institute, Kolkata during 4-6 December 2014.

5. "Effect of calcination temperature and time on synthesis of BCAS glass." International Conference on Advanced Materials (SCICON 2016) held at Amrita Vishwa Vidyapeetham, Coimbatore during 19-21 December 2016. The full-length paper was published in Materials Today: Proceedings listed in *Peer Reviewed Research* section.

WORKSHOPS ATTENDED

- Experimental Physics for high school teachers - Presented a talk of "Radar" on 19th January 2013, held at NITK.
- Three day workshop on "Frontiers of Astronomy" – Attended during 1-3 February 2013, held at NITK.

- Three day workshop on "Application of Statistical and Soft Computing Techniques in Engineering Research" – Participated during 29-31 July 2013, held at Canara Engineering College, Mangalore.
- National Seminar on Advances in Materials Science (SAMS 2013) – Participated during 22nd November 2013, held in Mangalore University.

TEACHING AND LABORATORY EXPERIENCE

- Conducted First Year Physics – Undergraduate Laboratory Course sessions for B.Tech. students at NITK.
- Conducted First and Second Year Physics – Postgraduate Laboratory Course sessions for M.Sc. students at NITK.
- Conducted First Year Physics – Postgraduate Tutorial Course: Classical Mechanics for M.Sc. students at NITK.
- Assisted in Postgraduate (M.Sc. Major Project) Dissertation work for *eight* final year M.Sc. Students during 2014 – 2018 at NITK.

CURRENTLY WORKING AS

Senior Research Fellow (Post-Doctoral, Employee Code: 60001187)

Project:

- GAP0158 – Laser Glass
- Glass Division, Central Glass and Ceramic Research Institute, Kolkata.
- PI: Dr. K Annapurna.

REFERENCE

Dr. H D Shashikala, *Professor,*
Research Supervisor,
Department of Physics, NITK,
e-mail: sasiholavana@gmail.com

I HEREBY DECLARE THAT THE INFORMATION FURNISHED ABOVE IS TRUE TO THE BEST OF MY KNOWLEDGE.

Yours faithfully,

Place: *Kolkata.*
Date: *05th June 2020.*

(SOUMALYA BHATTACHARYA)